Performance and applications of satellite remote sensing data for water quality in Norwegian lakes. Evaluation of MERIS, Sentinel-2 and Sentinel-3 products

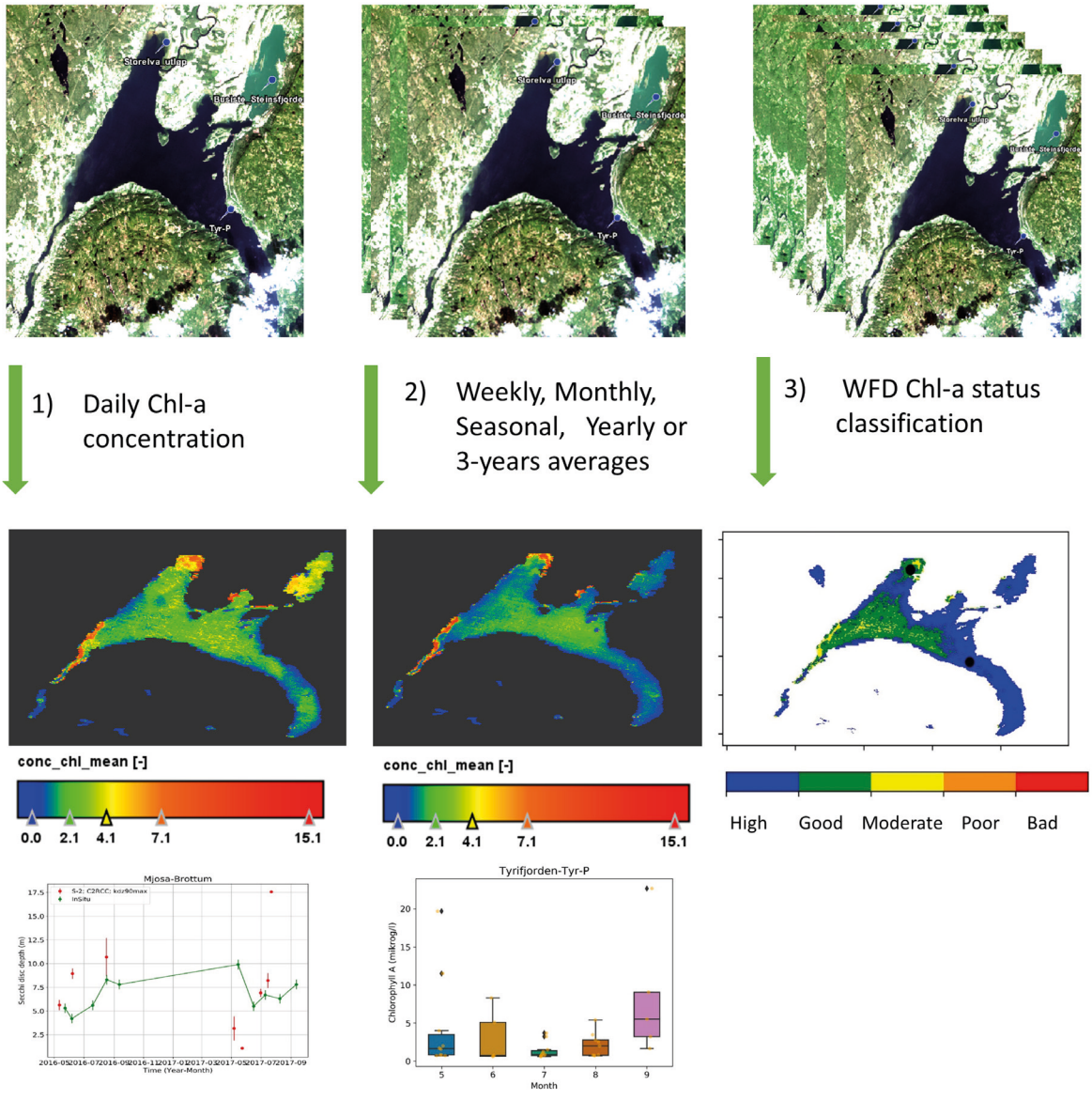

Norwegian Institute for Water Research

REPORT

Main Office
Gaustadalléen 21
NO-0349 Oslo, Norway
Phone (47) 22 18 51 00

NIVA Region South
Jon Lilletuns vei 3
NO-4879 Grimstad, Norway
Phone (47) 22 18 51 00

NIVA Region East
Sandvikaveien 59
NO-2312 Ottestad, Norway
Phone (47) 22 18 51 00

NIVA Region West
Thormøhlensgate 53 D
NO-5006 Bergen Norway
Phone (47) 22 18 51 00

NIVA Denmark
Njalsgade 76, 4th floor
DK 2300 Copenhagen S, Denmark
Phone (45) 39 17 97 33

Internet: www.niva.no

Title	Serial number	Date
Performance and applications of satellite remote sensing data for water quality in Norwegian lakes. Evaluation of MERIS, Sentinel-2 and Sentinel-3 products	7443-2019	11.12.2019
Author(s) Anna Birgitta Ledang, Therese Harvey and Sabine Marty	Topic group Environmental monitoring	Distribution Open
	Geographical area Southeast Noway	Pages 63 + Appendix

Client(s)	Client's reference
Norwegian Environment Agency	Steinar Sandøy
Client's publication: Miljødirektoratet rapport M-1579|2019	Printed NIVA Project number 17277

Summary

In this work, five lakes have been evaluated for the purpose of including satellite remote sensing products in water quality monitoring. Atmospheric correction has been performed and in-water products have been calculated, and the results are analysed in comparison with in situ data. The work shows that additional optical measurements are needed for a proper validation and for sound development of the remote sensing water quality products e.g. Chlorophyll-a (Chl-a). Still, Case2Regional CoastColour (C2RCC) products show promising results for the lakes investigated. A pixel-based average product of Chl-a, for example, shows the spatial variation within a lake which is a great add-on to the in situ classification and would otherwise be unavailable through conventional monitoring approaches. Challenges with dissolved organic matter absorbing in the same blue green spectra as chlorophyll needs careful consideration, and Chl-a products such as mean and yearly maps can be produced if the development of regional conversion factors are secured through additional sampling of the necessary parameters.

Four keywords	Fire emneord
1. Lakes	1. Innsjøer
2. Remote sensing	2. Fjernmåling
3. Water quality	3. Vannkvalitet
4. Monitoring	4. Overvåking

This report is quality assured in accordance with NIVA's quality system and approved by:

Anna Birgitta Ledang	*Trond Kristiansen*	*Andrew Luke King*
Project Manager	Quality Assurance	Research Manager

ISBN 978-82-577-7178-2
NIVA-report ISSN 1894-7948

Performance and applications of satellite remote sensing data for water quality in Norwegian lakes

Evaluation of MERIS, Sentinel-2 and Sentinel-3 products

Preface

This project is one of several Research and Development projects financed by the Norwegian Environment Agency (NEA) and the Norwegian Space Agency. In this project the contract has been between NIVA and NEA. The project has lasted from April 2017 to December 2019 and this report is the final deliverable. The purpose of the project has been to test the use of remote sensing data in lakes monitored by the NEA. The focus has been on MEdium Resolution Imaging Spectrometer (MERIS), Sentinel-2 (S-2) and Sentinel-3 (S-3) data. In addition, there have been in situ measurements from a certain number of lakes and an international workshop on the use of remote sensing on lakes, inland and coastal waters as well as water quality work related to the Water Framework Directive was arranged by NIVA.

Anna Birgitta Ledang was responsible for downloading and processing of the MERIS, S-2 and S-3 data. Øyvind Garmo, Jarl Eivind Løvik and Anna Birgitta Ledang conducted field sampling in 2017. Therese Harvey, Sabine Marty, Kai Sørensen and Anna Birgitta Ledang conducted optical field sampling in 2019. Additional sampling was performed by Jonas Persson in Tyrifjorden and Jan Erik Thrane in Mjøsa during 2019. Jan Karud developed the lake polygons. Anna Birgitta Ledang, Therese Harvey and Kai Sørensen arranged and hosted the remote sensing workshop in Oslo in September 2019. Sabine Marty has processed and visualized the ac9 and bb6 data. Therese Harvey and Anna Birgitta were responsible for visualisation, analysis and writing of the report. Trond Kristiansen and Kai Sørensen have performed the QA of the report. Contact persons at Norwegian Environment Agency were Steinar Sandøy and Agnès Moquet-Stenback.

Oslo, 10th of December 2019

Anna Birgitta Ledang

Content

Summary

The purpose of the project was to evaluate the use of satellite remote sensing data in the lake monitoring program run by the Norwegian Environment Agency. Monitoring of water quality as part of the Water Framework Directive (WFD) of Norwegian lakes is challenging due to the large number of lakes and the remote location of some of these. Use of cost-effective methods such as remote sensing can supplement in situ monitoring. Today, the lakes are mainly assessed either by in situ monitoring, grouping and extrapolation to similar lakes or based on expert judgment. With the resources provided through the European Commission Copernicus programme including several satellite sensors adapted for water quality data, the use of remote sensing data as part of regular monitoring can be operational. We have conducted case studies to test this in five different lakes: Lake Mjøsa, Tyrifjorden, Steinsfjorden, Lake Vansjø and Hemnessjøen. There are several steps that need to be developed for an operational system to be in place. In this project, initial tests of the performance of different algorithms for the satellite sensors MEdium Resolution Imaging Spectrometer (MERIS), Sentinel-2 (S-2) and Sentinel-3 (S-3) were done, and provided, in general, good results for Chlorophyll-a (Chl-a), total suspended matter (TSM) and Secchi disc depth. The remote sensing reflectance showed in general expected results for the Free University of Berlin (FUB) and Case2Regional CoastColour (C2RCC) atmospheric corrections, indicating good performance of the atmospheric correction algorithms. However, the spectra looked different when comparing lakes and sometimes also across stations within the same lake, which can be explained by natural variation in the water quality parameters, i.e. Chl-a, TSM, and coloured dissolved organic matter (cDOM). However, additional in situ reflectance measurements are needed to confirm this hypothesis. Time series of MERIS data showed good agreement with the monitoring dataset, and the quality of the retrieved water quality parameters from 2016-2018 from S-2 showed very promising results. The temporal variability for remote sensing Chl-a for the most part followed the in situ data, although there was a discrepancy between the timing of the observations. The TSM data from S-2 sometimes identified river plumes of particles from melting events during the spring which the in situ monitoring was not able to detect. The monthly means were overall coherent across remote sensing and in situ observations, although there were some differences across stations and months. The S-3 data performed well for both Chl-a and TSM. A big advantage with remote sensing data is the higher degree of spatial resolution and temporal coverage, which can be advantageous for the study of spatio-temporal variability in lakes as well as for assessing the water quality and classification levels accordance to the Water Framework Directive for the waterbody. We show the results of Chl-a classification for the case studies where the assessment was based on all pixels within the whole water body instead of a single in situ data point. The results showed spatial patterns for Chl-a over the last 3 years in most of the lakes. The amount of data, in terms of days of observations, was also much higher for remote sensing data, especially if one can use S-2 and S-3 data simultaneously, which together with in situ data provide a much broader and more detailed information of the water quality of the lake between seasons and years. To be able to make the best use of the remote sensing data in an operational manner for environmental monitoring and assessment monitoring of water bodies; downloading, processing, and technical solutions for satellite data for a sound data flow need to be set up. To better understand the requirements for making satellite data part of an operational ecosystem monitoring program, NIVA arranged an international workshop in Oslo, which gathered European remote sensing experts to share their experiences. From this workshop, a roadmap for an operational service and suggestions for future research were developed and presented. With this report we have taken a large step closer to implementing an operational system for remote sensing data in combination with in situ data for lake water quality monitoring. Still, in this study we have investigated a limited number of lakes with limited optical measurements. For the future it would be necessary to use more time on the different optical conditions within the various lakes to determine the best remote sensing water quality products.

Oppsummering

Tittel: Ytelser og anvendelser ved bruk av fjernmålingsdata i overvåking av vannkvalitet for norske innsjøer. Evaluering av MERIS, Sentinel-2 og Sentinel-3 produkter
År: 2019
Forfattere: Anna Birgitta Ledang, Therese Harvey og Sabine Marty
Kilde: Norwegian Institute for Water Research, ISBN 978-82-577-7178-2

Formålet med dette prosjektet har vært å teste bruk av fjernmålingsdata i innsjøovervåkingsprogram drevet av Miljødirektoratet. Miljøovervåking av norske innsjøer er utfordrende ettersom det er et stort antall innsjøer samt at flere av disse har en fjerntliggende beliggenheten. Bruk av kostnadseffektive metoder som fjernmåling kan gi et supplement til in situ overvåkingen som brukes i dag. Innsjøene blir i hovedsak vurdert enten ved stedlig overvåking; gruppering og ekstrapolering til lignende innsjøer eller basert på ekspertvurdering. Med EU-kommisjonen sitt Copernicus-program med flere satellittsensorer inkludert i programmet tilpasset for bruk til miljøovervåking av vannkvalitet, kan benyttelse av optiske satellitt data utvikles til en operasjonell tjeneste. For at et operativt system skal kunne være på plass er det flere trinn som må utvikles, og noen trinn er tatt gjennom dette arbeidet. Studier fra fem forskjellige innsjøer er gjennomført; Mjøsa, Tyrifjorden, Steinsfjorden, Vansjø og Hemnessjøen. For det første er ytelsen til noen satellittalgoritmer testet for MERIS, Sentinel-2 (S-2) og Sentinel-3 (S-3), og resultatene er generelt gode for Klorofyll a (Klf-a), totalt suspendert materiale (TSM) og siktdyp. Reflektansspektra fra henholdsvis MERIS og S-2 og S-3 viser forventet spektral signatur for resultatene fra atmosfære korreksjon algoritmen FUB (Free University Berlin) og C2RCC (Case2RegionalCoastColour). Spektrene ser imidlertid annerledes ut mellom de ulike innsjøene og noen ganger også mellom ulike stasjoner innenfor samme innsjø. Dette kan forklares med naturlig variasjon i de ulike vannkvalitetsparameterne som Klf-a, TSM og farget oppløst organisk materialet (cDOM). Likevel vil ytterligere in situ reflektansmålinger være helt nødvendig for å kunne bekrefte disse antagelsene. Tidsserien med MERIS-data viser en god overenstemmelse med overvåkingsdatasettet samt at kvaliteten på parameterne fra S-2 for årene 2016-2018 virker lovende. Den tidsmessige variasjonen i S-2 dataene følger Klf-a fra in situ data i de fleste tilfeller, selv om det er avvik mellom tidspunktene for observasjonene. I Mjøsa fanger S-2 data opp vårsmeltingen med høyt partikkelinnholdet ved elveutløpet av Gudbrandalslågen, mens det ikke er tilfellet for in situ datasettet. De månedlige analysene viser god sammenheng mellom in situ og fjernmålte data, selv om det er noen forskjeller mellom individuelle stasjoner og måneder. S-3 data fungerer bra for Klf-a og TSM. En stor fordel med fjernmålte data er den romlige dekningen. Denne kan utnyttes til å studere de romlige variasjonene innen en innsjø samt vannkvaliteten og klassifiseringsnivåene for hele vannforekomsten. Resultatene fra Klf-a klassifiseringen for de ulike innsjøene er basert på data fra hele vannforekomsten i stedet for ett enkelt datapunkt in situ, og disse viste tydelig romlig mønstre for Klf-a for de tre siste årene i de fleste av innsjøene. Datamengden i form av observasjonsdager er også høyere for fjernmålte data spesielt hvis man bruker både S-2 og S-3 data. Disse dataene sammen med in situ data vil kunne gi en mye bredere og mer detaljert informasjon av vannkvaliteten i innsjøen over forskjellige årstider og år. For å kunne utnytte fjernmålte data på en best mulig operativ måte innen overvåking, må det settes opp metode for nedlastning, prosessering og tekniske løsninger for best mulig dataflyt. NIVA arrangerte et internasjonalt seminar i Oslo hvor europeiske eksperter innen fjernmåling deltok med sine erfaringer. Fra dette seminaret er det presentert et veikart nettopp for en slik operativ tjeneste samt forslag til fremtidig forskning. Med denne rapporten har vi tatt et stort skritt nærmere et operativt system for bruk av fjernmålingsdata i kombinasjon med in situ data for miljøovervåking av innsjøer. Likevel er det i dette studiet jobbet med et begrenset antall innsjøer og med begrensede optiske målinger. For fremtiden vil det være helt nødvendig å bruke mer tid på å studere de forskjellige optiske forholdene i ulike innsjøer for å bestemme de beste fjernmålte vannkvalitetsproduktene.

1 Introduction and background

Regular monitoring and assessment of the water quality in Norwegian lakes is a challenge due to their large numbers, and some in remote locations. Norway is obligated through the European Water Framework Directive (WFD) to assess and report the ecological and chemical status of all Norwegian lake water bodies (required for lakes with a surface area > 0,5 km^2) every 6^{th} year, based on a monitoring, grouping or expert judgment. Only a very small fraction of Norwegian lakes is currently monitored, and the rest are assessed using grouping (by extrapolating from monitored lakes of the same water type assuming the same level of environmental pressures) or expert judgement (using catchment information to estimate pressures). The general requirements for assessing ecological status in Norwegian lakes that are monitored are that these are based on minimum 3-years of monitoring data (Vannforskriften 2018). The need for more frequent and reliable data to be used with the assessment are obvious, particularly for the lakes that are not monitored. Here state-of-the-art satellites can provide several water variables, such as Chl-a, colour, Secchi disc depth and turbidity.

With the Copernicus program run by the European Commission, the possibilities to include new techniques have increased and water quality monitoring using remote sensing data are now developed and can be used more operational. This is due to a stable and long-term commitment of the satellite program with a shift from research satellites to operational satellites in orbit that will be operational until at least 2030 (European Commission 2019). Norwegian conditions with steep fjords, high altitude lakes and steep mountains can be a challenge for remote sensing, and thus motivates for developments of remote sensing products targeted to Norwegian conditions that can provide high temporal monitoring data. This is further supported by the strategic investment in earth observation (EO) data from both the European Space Agency (ESA) and the national Norwegian Space Agency (NRS). The Norwegian Environmental Agency (NEA) is therefore interested in the possibilities for incorporating the use of satellite remote sensing data within operational monitoring activities in lakes. This report is the final product of the NEA financed R&D project assessing the use of the historical observations from MERIS and the two Copernicus twin-satellites Sentinel-2 (S-2) and Sentinel-3 (S-3) for the use of water quality assessment.

In Norway, the use of remote sensing observations is mainly focused on marine applications, although limited testing of the technology for lakes were initiated in the 1980s under the State Program for Pollution Monitoring. Here, the land resource satellite Landsat-5 was used (Aas et al. 1993; Magnusson and Sørensen 1993). NIVA lead several projects for the Norwegian State Pollution Control Authority (SFT) under this program as well as the Outer Oslofjord monitoring (K. Sørensen and Lindell 1990). Other R&D projects financed by The Research Council of Norway (NFR) and SFT were also carried out in the Glomma, Hvaler and Ytre Oslofjord area (K. Sørensen et al. 1990). With the launch of the ESA satellite ENVISAT in 2002, at that time new promising tests were carried out with the sensor MERIS (Medium Resolution Imaging Spectrophotometer) (Sørensen, unpub.). Although the MERIS sensor was dedicated to marine environments and applications the studies showed promising results for some water quality parameters in Norwegian fresh water. NIVA participated in the project "Development of MERIS lake water algorithms" funded by ESA (European Space Agency) together with several Nordic and European partners. The focus was on eutrophic and brown lakes and two algorithms for water quality were developed and tested (Koponen et al. 2008). NIVA participated with experiences from Lake Victoria together with University of Bergen and Makerere University in Kampala, Uganda (Okullo et al. 2007; Sørensen et al. 2008).

The EU GLASS project "GloBal Lakes Sentinel Services" carried out initial evaluations of S-2 data for a selection of European lakes. The project, which was completed in 2016, focused on Landsat-8 (L-8) and MERIS data and used a simulation of S-2 reflectance and data from ESA as the work was carried out before the actual launch of S-2. Various algorithms for Chl-a concentration and total biomass (GLaSS 2014[1]) estimation were tested for a large variety of lakes with different optical properties (e.g. clear waters, eutrophicated waters, low transparency due to resuspension), in different countries (e.g. Germany, Italy, Tanzania, Sweden, Finland, USA) where remote sensing observations were used together with in situ data for calculation and analysis of the the ecological status class (Alikas et al. 2015).

In Reinart et al. (2003) and Uudeberg et al. (2019), satellite derived optical spectra were used together with traditional measurements to create an optical classification of different water types in Estonia. A cluster analysis was applied to the optical spectral data which resulted in five classes; clear, moderate, turbid, very turbid and brown. Many of the lakes in Estonia were found to be brown, meaning that they had a high content of coloured dissolved organic matter (humus, cDOM). This is an optical property that will affect and modify the reflected signal by absorbing the blue light strongly and the water will look brownish red (see details in chapter 1.2). This is therefore also relevant for many Norwegian lakes, which are rich in humic substances. A requirement for using remote sensing data for water quality parameters and status classification is to test which algorithms are best suited for the lake conditions studied and which variables that can be retrieved for the different lakes. The most common approach is to collect optical in situ data simultaneously with a satellite over-pass, so-called match-up sampling (IOCCG 2000), or alternatively compare to available in situ data in time series for a rough estimate of the performance. With the Copernicus program and the two twin-satellite sets of S-2 and S-3, the possibilities for remote sensing monitoring has never been better, and there are several ongoing efforts for research and application development within Europe to continuously improve the data quality. To be able to incorporate remote sensing data into the Norwegian ecosystem monitoring program, the new satellite sensors and their algorithms, need to be tested and tailored to the regional or local conditions. For those reasons, the goals of this project were:

- Study in situ optical properties of selected Norwegian lakes
- Provide water quality parameters using satellite data in selected Norwegian lakes
    - Study the performance of MERIS
    - Study the performance of Sentinel-2
    - Study the performance of Sentinel-3
- Use remote sensing for water quality assessment according to the WFD
- Arrange a workshop on best practices for operational use of optical remote sensing data
- Present a roadmap for an operational remote sensing system
- Suggest future research and development

Parts of this report describe the theory and concepts of ocean color satellite remote sensing and the most detailed theory sections are found in Appendix A and B.

1.1 Remote sensing

Remote sensing includes both active and passive sensors on e.g. satellites. An example of active sensors on satellites are the synthetic-aperture radar (SAR), which sends out pulses of radio waves and the echo of each pulse is received and recorded. Passive sensors, such as optical sensors measure the electromagnetic radiation from the sun reflected from the atmosphere, land, lakes and the ocean. The

[1] http://www.glass-project.eu/downloads/

satellite, which is located around 700 km above the sea surface, capture this signal/radiation with a variety of spectral bands ranging from the visible wavelengths (VIS, 300-750nm) and into the near infrared (NIR, 750-1100nm) part of the electromagnetic spectrum. The signal received by the sensors has travelled from the sun through the atmosphere and the water and this path affects the light before reaching the satellite sensor (IOCCG 2000). The sensors used within this project are all passive, using the reflected sun light.

1.2 Bio optics and remote sensing data

An optical sensor is measuring the reflectance signal which carries information of how the light has interacted with water and its components as well as with the air molecules and aerosols. This interaction between the light in natural waters, the living organisms, and the dissolved and suspended material are the essence of bio-optics and important for the use of optical remote sensing data. The information needed for bio-optical models and algorithm developments are both the concentrations of the parameters, but also their physical characteristics regarding absorption and scattering. It is therefore necessary to study the optical parameters related to a water body, such as algae and particles, both in coastal and inland waters. To have the full picture, data on other important variables are also needed such as; incoming and water leaving reflectance (i.e. light), light conditions within the water and the reflectance data itself. The different variables are divided into three groups depending on their characteristics and are described in detail below; Bio-optical components (Chp. 1.2.1); Apparent Optical Properties (AOPs) (Appendix A) and Inherent Optical Properties (IOPs) (Appendix B).

Considering that about 10% of the signal which reach the sensor at the top of the atmosphere (TOA) in very clear oceanic waters carries the information about the water and less than 1% of the signal is related to the water in cDOM dominated waters (like many lakes), it is very important that assumptions are based on sound empirical derived relationships from in situ data. Therefore, a comprehensive in situ data set is preferable and makes it possible to adjust and develop local or regional adaptations of the remote sensing algorithms.

Validation of remote sensing data means that one compares the observations from in situ data with the satellite products data. A so-called matchup measurement should be conducted by measuring in situ the same optical parameters at the same time as a satellite overpass. Depending on the water type, one hour is recommended as the time difference, but should be less in dynamic waters or can be increased in stable areas up to 3 hours to increase the number of match-up points (EUMETSAT 2019). The data needs to be collected according to a common strict protocol developed by an expert group, in which NIVA is a part of for the OLCI sensor (S-3) matchup protocols (EUMETSAT 2019) and for MERIS (Doerffer 2002). Note that the same principles are relevant also for S-2 validation. As of today, there is very little optical data collected for Norwegian lakes that can be used for actual match-up validation, which is why this project collected a small data set focusing on validation.

1.2.1 Bio-optical components

The bio-optical components are the variables affecting the absorption and scattering within the water. There are three absorbing and scattering components; phytoplankton (assessed by Chl-a as a proxy), total suspended matter (TSM), and coloured dissolved organic matter (cDOM). Pure water also absorbs and scatters light and need to be accounted for, as it has a background effect on the remote sensing signal. The characteristics (absorption and scattering) of the optical components are all wavelength dependent. The typical blue appearance of the ocean is due to light absorption and scatters at different

wavelengths in water. For example, the absorption is low in the blue and green part of the spectrum, while increasing towards the yellow part of the spectrum, to high absorption in the red and near infrared (NIR), to very high absorption in the infrared. The two optical processes, absorption and scattering, will strongly affects the reflectance signal. Chl-a is one of several photosynthetic pigments in micro algae that captures the sun light and contributes to the reflectance through its absorption. TSM mostly scatters light and are different organic and inorganic material that remain suspended within the water, e.g. clay, sand or silt particles, minerals (e.g. chalk in Norwegian alpine lakes colouring the water turquoise). TSM can also be composed by phytoplankton and zooplankton and other organic material. Humic matter that decomposes stays dissolved within the water and make up the cDOM pool, which basically is a mix of humic and fulvic acids. cDOM is measured as absorption and is typically measured as the absorption coefficient of cDOM (λ), usually measured approximately around the mid-point of the maximum photosynthetic peak by the Chl-a pigment in the blue, i.e. between 440-443 nm (Kirk 2011). In Norwegian lake monitoring the humic part is not measured as the quantity cDOM but as the old laboratory parameter FARGE, which is in principle the same as cDOM (see Chapter 4.1 and Eq. 1 for details).

The reflectance and the light interactions with water are not only dependent on its constituents but also on both the incoming and outgoing light path. The variables describing the light conditions within the water are called apparent optical properties (AOP´s) and depend both on the medium (e.g. water and the constituents) as well as the light field within, i.e. the angular distribution and the ambient light field (Kirk 2011). Those are e.g. irradiance, radiance and reflectance and are described in detail in Appendix A.1. The scattering and absorption characteristics of the water constituents are referred to as Inherent Optical Properties and are described in detail in Appendix A.2.

2 Satellites used for water quality purposes

There are several satellite sensors adapted or partially adapted to quantifying water quality. This project has focused on the most recent ones from ESA, however each satellite sensors is described below. For the lake case studies the focus was requested to be on the current operational Copernicus satellites, the S-2 and the S-3, although the previous data from MERIS, as well as for operational NASA´s satellites (e.g. MODIS Aqua, MODIS Terra and Landsat 8) and are still available and important for the use of e.g. time-series analyses and to increase the available data for e.g. coastal and lake waters.

2.1 MERIS

The European Space Agency (ESA) launched the satellite ENVISAT in March 2002. This satellite was an advanced polar-orbiting Earth observation satellite and provided measurements of the atmosphere, ocean, land and ice. The optical sensor onboard, the MEdium Resolution Imaging Spectrophotometer (MERIS), was developed as a research instrument with the main aim of providing R&D data. NIVA was part of the development of MERIS as a member of the Scientific Advisory Group and contributed with experiences from ocean colour remote sensing and good contact with the end users. The ENVISAT had an orbit of about 800 km altitude with a complete orbit every 100 minutes. The repeat cycle of the reference orbit was 35 days, resulting in a revisiting time of 2-3 days for Norway. The MERIS instrument operated in the solar reflective spectral range between 390 nm to 1040 nm. This sensor was primarily dedicated to ocean colour observations, with a high spectral and radiometric resolution and two spatial resolutions (1200 m and 300 m). MERIS scanned the Earth's surface using the "push broom" method over a field of view (FOV) of 68,5 ° equivalent to 1150 m in 15 programmable bands (Table 1,

Figure 1). Five identical cameras shared the FOV in a fan shape configuration (Bourg and Delwart[2]). In April 2012, ESA lost contact with the satellite and the ENVISAT era (2002-2012) finished.

Table 1. Channels and spectral bands for ENVISAT MERIS.

Channel	Band centre (nm)	Band width (nm)	Description Band used for calculations of;
1	412.5	10	Yellow substance and detrital pigments
2	442.5	10	Chlorophyll absorption maximum
3	490	10	Chlorophyll and other pigments
4	510	10	Suspended sediment. red tides
5	560	10	Chlorophyll absorption minimum
6	620	10	Suspended sediment
7	665	10	Chlorophyll absorption and fluorescence reference
8	681.25	7.5	Chlorophyll fluorescence peak
9	708.75	10	Fluorescence reference. atmosphere corrections
10	753.75	7.5	Vegetation. cloud. O2 absorption band reference
11	760.625	3.75	O2R-branch absorption band
12	778.75	15	Atmosphere corrections
13	865	20	Atmosphere corrections
14	885	10	Vegetation. water vapor reference
15	900	10	H_2O absorption region. water vapour retrieval

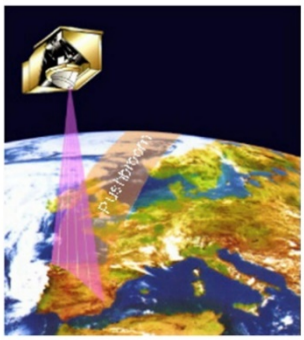

Figure 1. The MERIS observation concept. Picture collected from Bourg and Delwart[1].

2.2 Sentinel-2

The S-2 mission consists of a twin pair of polar-orbiting satellites (S-2A and S-2B), which have the same orbit but phased 180° to each other. Their main mission is to monitor the variability in land surface conditions. The high revisit time of five days at the equator with two satellites (2-3 days at mid-latitudes, like Norway) will support monitoring vegetation within the growing season. The meridional coverage range of the earth is from 56° south to 84° north. The S-2 carries an optical instrument, the Multi-Spectral Instrument (MSI), that samples at 13 spectral bands (Figure 2, Table 2) and the FOV is at 290 km. The mean orbital altitude is 786 km and these measurements are also conducted by the same method as MERIS, i.e. the "push broom" method. The spatial resolution of S-2 is between 10-60 m, depending on the bands used. For water products, the 60 m resolution is used, due to the broader band with at 10 m, creating a noisier signal from water.

[2] https://earth.esa.int/c/document_library/get_file?uuid=ccaeeb98-d7f0-4117-b1ea-c30a25a9821d&groupId=10174

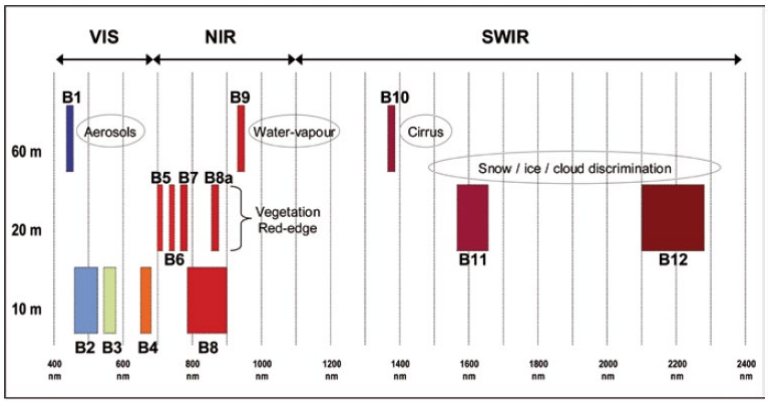

Figure 2. Spectral bands versus spatial resolution on S-2 MSI. Image collected from ESA Special Publication 1322/2.

Table 2. Channels, resolution and spectral bands for S-2 MSI.

Channel	Spatial resolution (m)	Band (nm)	Band width (nm)	Description Band used for calculations of;
1	60	433-453	20	Aerosol concentration in the atmosphere. Atmospheric correction.
2	10	458-522	65	Absorption of chlorophyll in green vegetation.
3	10	543-577	35	Reflection peak from green vegetation.
4	10	650-680	30	Absorption in chlorophyll in green vegetation.
5	20	697-712	15	"Red edge". Where reflection for green vegetation decreases rapidly from high levels in NIR to bottom in red.
6	20	732-747	15	Same as for Channel 5.
7	20	773-793	20	Same as for Channel 5.
8	10	784-899	20	Strong reflection from green vegetation. strong absorption in water.
8b	20	855-875	30	Same as for channel 5.
9	60	935-955	20	Water vapour in the atmosphere. Atmospheric correction.
10	60	1365-1395	30	Detection of cirrus clouds. Correction of other channels.
11	20	1565-1655	90	Separation between snow. ice and clouds. Sensitive for moist detection in vegetation and soil.
12	20	2100-2280	180	Same as for Channel 11.

2.3 **Sentinel-3**

The S-3 mission consists of a twin pair of polar-orbiting satellites (S-3A and S-3B), which have the same orbit but phased 180° to each other. The mission main objectives are to measure sea surface topography, sea and land surface temperature, and ocean and land surface colour. The mission is driven by the need for a continuation in the provision ENVISAT and SPOT vegetation data as well as for ocean colour (MERIS). The mission is jointly operated by ESA and EUMETSAT (which is an independent global operational satellite agency). S-3 carries four main instruments: Ocean and Land Colour Instrument (OLCI), Sea & Land Surface Temperature Radiometer (SLSTR) Altimetry and MWR Microwave Radiometer, where OLCI is based on the imaging design of ENVISAT MERIS. NIVA is involved in the development and validation of OLCI via the validation team S3VT (Validation team), providing input and in situ data. OLCI is also a push broom imaging spectrometer with five tilting cameras in

westerly direction for mitigation of sun-glint contamination. The sensor samples at 21 bands (Table 3) with a swath width of 1270 km and a spatial resolution of 300 m. The mean orbital altitude is 814.5 km with a near-polar and sun-synchronous orbit with a repeat cycle of 27 days (the time taken for the satellite to pass over the same geographical point on the ground) and with 27 orbits per day.

Table 3. Channels, resolution and spectral bands for S-3 OLCI.

Channel	Spatial resolution (m)	Band centre (nm)	Band width (nm)	Description Band used for calculations of;
Oa1	300	400	15	Aerosol correction. improved water constituent retrieval.
Oa2	300	412.5	10	MERIS heritage; yellow substance and detrital pigments (turbidity).
Oa3	300	442.5	10	MERIS heritage; Chl absorption maximum. biogeochemistry. vegetation.
Oa4	300	490	10	MERIS heritage; High chl. other pigments.
Oa5	300	510	10	MERIS heritage; Chl. sediment. turbidity. red tide.
Oa6	300	560	10	MERIS heritage; Chlorophyll reference (Chl minimum)
Oa7	300	620	10	MERIS heritage; Sediment loading.
Oa8	300	665	10	MERIS heritage; Chl (2^{nd} Chl abs max.). sediment. yellow substance/vegetation.
Oa9	300	673.75	10	Improved chlorophyll fluorescence measurement and to better account for smile together with band 665 and 680nm.
Oa10	300	681.25	7.5	MERIS heritage; Chl fluorescence peak. red edge.
Oa11	300	708.75	7.5	MERIS heritage; Chl fluorescence baseline. red edge transition.
Oa12	300	753.75	7.5	MERIS heritage; O2 absorption/clouds. vegetation.
Oa13	300	761.25	2.5	MERIS heritage; O2 absorption band/aerosol corr.
Oa14	300	764.375	3.75	Improved cloud top pressure (height). atmospheric correction.
Oa15	300	767.5	2.5	O2A used for cloud top pressure. fluorescence over land.
Oa16	300	778.75	15	MERIS heritage; Atmospheric correction/aerosol correction.
Oa17	300	865	20	MERIS heritage; Atmospheric correction/aerosol correction. clouds. pixel co-registration.
Oa18	300	885	10	MERIS heritage; Water vapour absorption reference band. Common reference band with SLSTR instrument. Vegetation monitoring.
Oa19	300	900	10	MERIS heritage; Water vapour absorption/vegetation monitoring (max. reflectance).
Oa20	300	940	20	Improved water vapour retrieval. Water vapour absorption. atmospheric/aerosol correction.
Oa21	300	1020	40	Atmospheric /aerosol correction.

3 Atmospheric correction and RS data retrieval

The effects from the atmosphere and the ocean surface needs to be removed from the signals measured by the satellite sensor at various spectral bands (IOCCG 2010). Therefore, atmospheric correction (AC) is performed when quantifying ocean properties by satellite remote sensing. There are many factors influencing the signal to the sensor and those are illustrated in the conceptual Figure 3, and detail described in Appendix A.

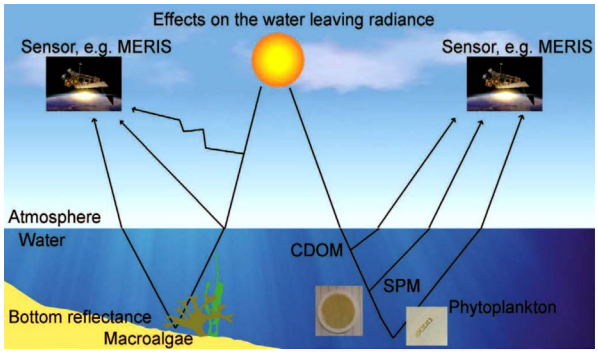

Figure 3. Schematic illustration of factors influencing the water-leaving radiance detected by the remote sensing sensor and the atmospheric correction. Hence, what effects the remote sensing reflectance and the following retrieval of the water quality parameters. The surface roughness, both atmospheric and in water absorption and scattering in the atmosphere all affects and change the water leaving radiance. TSM (here named SPM), phytoplankton and water itself as well as the cDOM absorption is contributing to the absorption and scattering. Also, the absorption and reflectance from macro algae may influence the radiance together with possible bottom reflectance. Figure from Harvey (2015).

3.1 **Remote sensing data**

In remote sensing, remote sensing reflectance (R_{rs}) is the signal used to interpret the water signal reaching the satellite sensor, which is closely related to the water leaving reflectance (IOCCG 2000). There are in principle two ways of modelling in water remote sensing and bio-optics; 1) Forward modelling and 2) Inverse modelling (Figure 4). In forward modelling the IPOs and concentration of the optical parameters are used to model the reflectance data and the inverse model is the other way around having the spectral as input to retrieve the IOPs and optical parameters. These models are used when training a neural network, that will be used within the remote sensing processors and the difference between the forward and the inverse models can be used to tune these models.

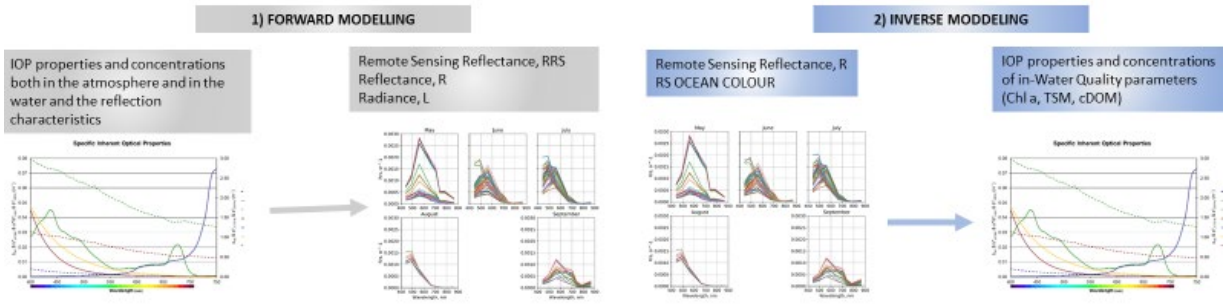

Figure 4. Illustration of the concepts for forward and inverse bio-optical and remote sensing models.

A typical reflectance signature depends on the content within the water which depends on the lake and its constituent. In Figure 5 different spectra shapes are presented from different water type. As seen from the differences in the R_{rs} they are associated to different combinations of Chl-a, cDOM and TSM. The spectral shape can be used to divide lakes into different water types as developed by Hieronymi et al. (2017) and further applied in lakes by Uudeberg et al. (2019).

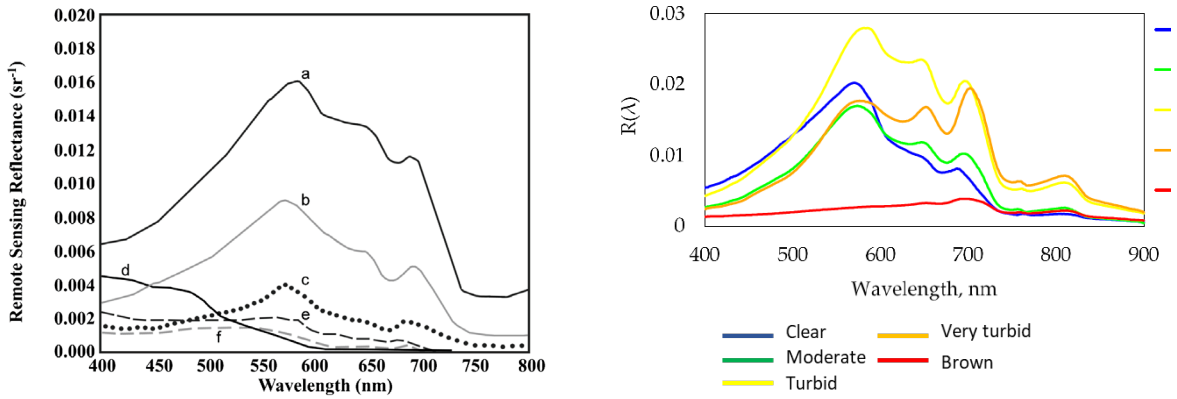

Figure 5. The spectra shape of different water types. a) Waters with very high suspended particle concentration and cDOM absorption (organic material), b) high sediment and cDOM absorption. c) moderate sediment and cDOM absorption with some phytoplankton, d) clear water, e) waters with moderate chlorophyll and sediment concentrations, f) waters with moderate chlorophyll concentrations. On the right optical water types defined for Estonian lakes using S-2 and S-3 data. Reprinted from IOCCG (2000) to the left and from Uudeberg (2019) to the right.

3.2 Case 1 and Case 2 waters

Different waters types can be divided into two categories; Case 1 water, where the optical properties (absorption and scattering) is only dependent on water itself and phytoplankton (Chl-a) and associated pigments. This is typically open sea waters or clear oligotrophic lakes; Case 2 waters contain in addition to phytoplankton the optically active parameter i.e. humic substances (cDOM) and particles (TSM). The bottom reflectance can also influence the R_{rs} in shallow Case 2 waters (IOCCG 2000). This influences the R_{rs} and the AC and many coastal areas and lakes are Case 2. Atmospheric correction schemes for Case 1 waters have been developed since the launch of the Coastal Zone Colour Scanner (CZCS) in 1978 and the TOA radiance is easier to split in an AC and water part, based on the assumptions described in Appendix B.1. and followed below (Gjertsen et al. 2014 and Bouvet et al. 2008 and ref. therein):

- The $L_{path}(\lambda)$ can be split in a Rayleigh and an aerosol scattering component
- The water-leaving radiance in the near- infrared (NIR) spectral bands is neglectable, due to high water absorption. Therefore, will the TOA radiance, after subtracting the Rayleigh scattering, only be influenced by aerosols.
- The spectral extinction of aerosols can be described by an exponential function, which is extrapolation from the NIR to the blue-green range.

With the emergence of new generation satellite ocean colour sensors with more and narrower spectral bands, other procedures to retrieve water substances have been developed. The radiative transfer equation describes the radiant field within the ocean-atmospheric system (Mobley 1989). For a passive medium such as optical sensors (i.e. with no internal source of radiation), the radiative transfer equation accounts for the loss of radiance due to scattering and absorption in the direction of propagation, and for the gain of radiance due to scattering from other directions. Monte Carlo simulation is used to generate the TOA total radiances for Rayleigh or compound (molecules plus

aerosols) atmospheres. Algorithms based on the assumptions for Case 1 waters tend to fail in Case 2 waters and more complex models are needed to resolve the inverse model (Antoine and Morel 2011).

3.3 Remote sensing algorithms

The absorption peaks of Chl-a (*in vivo*) are found in the visible part at 443 and 675 nm and by using this knowledge it is possible to estimate Chl-a using remote sensing applications (Ansper and Alikas 2019). The approach used is either model-based or empirical. In the model-based approach bio-optical models are used to estimate the water leaving reflectance or the R_{rs} or the TOA radiance spectra with specified water constituents. The empirical approach is widely used and is based on band-ratio algorithms (IOCCG 2000; Matthews 2011; Ansper and Alikas 2019). Band-ratios might have smaller sensitivity and might not always hold true for very optically complex waters with high cDOM absorption or other Case 2 waters, but they are easier to develop and apply.

Some of the different atmospheric correction and water methods have been tested within this project. For the MERIS data we have run the FUB processor and for the S-2 data we have run the C2RCC (Brockmann et al., 2016) and Acolite (Vanhellemont 2019 and ref. therein). For the S-3 data we have run C2RCC and Polymer (through the Copernicus Global Land Service) atmospheric processors (Steinmetzet al., 2011). In this project we focused on S-2 data as there is a high application potential, particularly for lakes, due to the higher spatial resolution compared to S-3. Furthermore, we have previously worked with MERIS in lakes and it has shown to work well, and as S-3 is the continued development of MERIS, many of the same algorithms for MERIS can be applied to S-3. Therefore, the remote sense results presented are dominated by S-2 data. No results for the Acolite processor are presented as they showed to be failing for our case studies by overestimating in the red part of the spectra. Several of the band ratio algorithms have coefficients that can be tuned to a region by running an optical radiative transfer model, like Hydrolight. This has not been done in this project and already defined coefficients are used. This concerns the band ratio algorithms OC2_443, OC2_490 and OC3_443 (Pereira-Sandoval et al. 2019) and the three-band algorithm (Moses et al. 2009; Zhang et al. 2014; Ansper and Alikas 2019) shown in Appendix B. There are several more algorithms to test, which would need more focus in later studies. In Figure 6 the schematic model of the bio-optical model in C2RCC processor and the processing steps is presented as an example. The figure shows how the five IOP output (pigment absorption apig, absorption detritus ad, absorption colored dissolved organic matter ag, sediment scatter bp and white sediment scatter bw (representing calcareous sediments)) from neural-networks (NN) determines the Chl-a, adg (absorption of detritus and cDOM) and the TSM products (Brockmann et al. (2016). Comparisons between the in situ determined apig and remote estimated apig from NN can be used to check whether a regional tuning of the conversion factors are needed. Details about the AC algorithms used are found in Appendix B1-B.5.

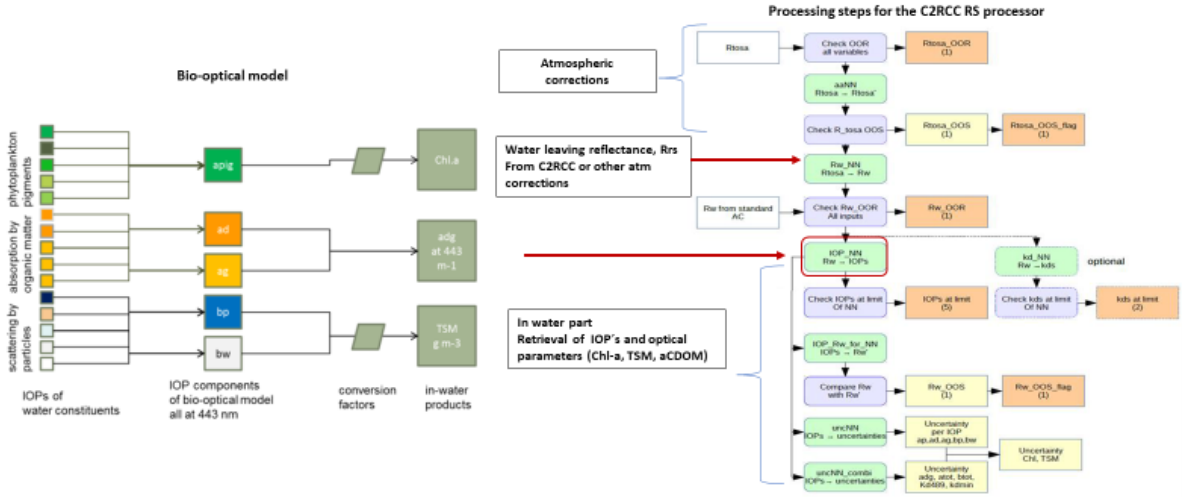

Figure 6. Bio-optical model used in the C2RCC processor and processing steps, where the R_{rs}, IOP´s and optical parameters (e.g. Chl-a, TSM) are the main output. Apig can be used to adjust the conversion factors within the bio-optical model for the retrieval of optical parameters for Norwegian or local conditions. Imaged adjusted from Brockmann et al. (2016).

4 Case studies

4.1 The Lakes

The case studies were selected based on having a wide range of natural variability, and to ensure that different water types were covered ranging from humic lakes as Lake Vansjø to clearer waters as Lake Mjøsa. During the summer of 2017 a one-day campaign was spend on collecting some extra samples from Mjøsa and from Storsjøen. In 2019 dedicated in situ data campaigns were conducted in Lake Tyrifjorden and Lake Vansjø. Table 4 shows the differences in the water type definitions based on the monitoring categories within the WFD and an image for each of the lakes is presented in Figure 7. The water quality parameters from the lakes monitoring program between 2016-2018 are summed up in Table 5. Lake Vansjø stands out with the lowest Secchi disc depth, high cDOM and FARGE values. The clearest lake was Mjøsa with the highest Secchi disc depth and lowest FARGE values. This was also confirmed in the 2019 sampling with Vansjø having the highest values of TSM, Turbidity, cDOM and FARGE (Table 8). The different water colour of Lake Vansjø compared with other lakes is clearly seen by the remote sensing RGB image in Figure 7.

Tyrifjorden is the fifth largest lake in Norway with an area of 137,38 km^2 and a maximum depth of 288 m (average 93 m). Four rivers have their inflow into Tyrifjorden; Henåa, Skjærdalselva, Sogna and Storelva. The lake is divided into three basins of which Nordfjorden is the northwest arm of Tyrifjorden and Storfjorden covers the widest area and stretches to the south in Vikersund. Holsfjorden is the south basin and stretches southeast and includes the deepest part of the lake. Steinsfjorden is situated in the northeast part with a maximum depth of 24 m and shallow average depth of 10.2 m. The water exchange is very low in this part of the lake and equal to 4.6 years for a total renewal of the water and Steinsfjorden is considered a separate water body. Tyrifjorden flows into the rivers Sogna, Storelva and Storfjord.

Lake Mjøsa is the largest lake in Norway, and the 35th biggest lake in Europe, with an area of 365 km^2 and maximum depth is 453 m. Several big cities are located along the lake, including Lillehammer, Gjøvik, Hamar, Moelv and Brumunddal. Mjøsa is the main source for drinking water for 50 000 to 100 000 people. There are plenty of rivers with outflows to the lake; Gudbrandalslågen, Mesna, Vismunda, Moelva, Stokkeelva, Hunnselva, Brumunddal, Flagstadelva, Svartelva, Lenaelva and Vikselva. Lake Mjøsa inflow to Vorma which connects to Lake Glomma further south.

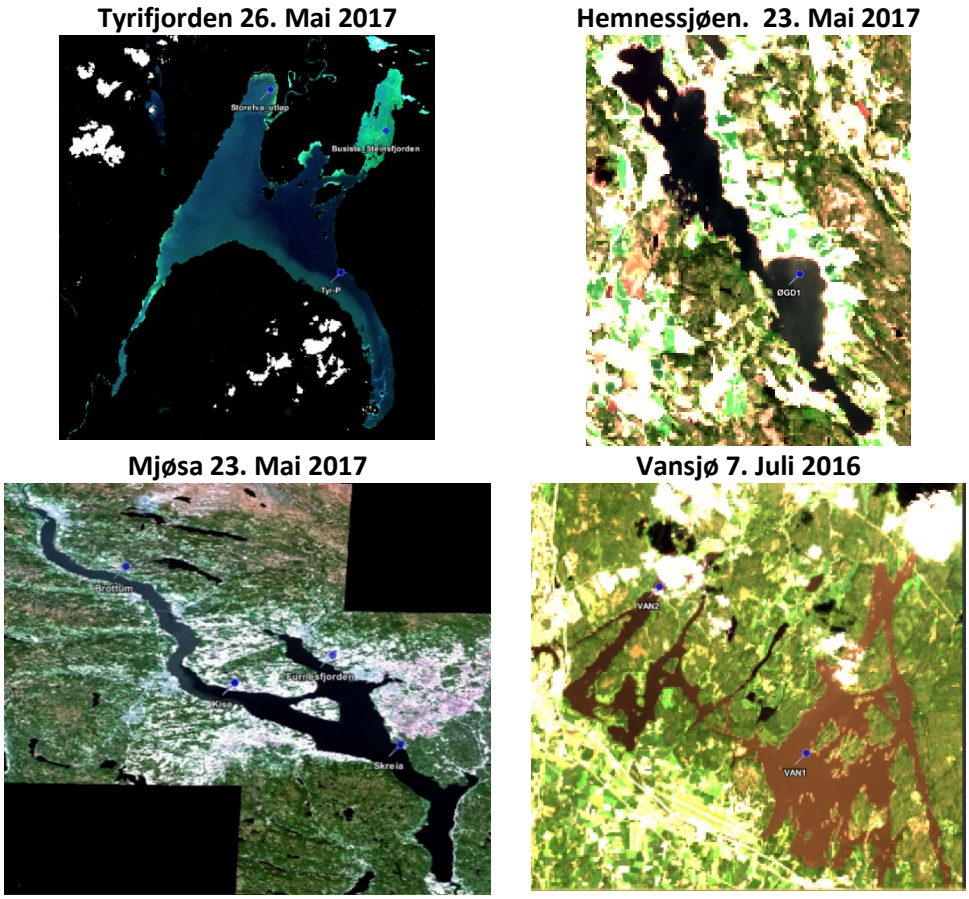

Figure 7. S-2 RGB images of the four study lakes with the in situ stations marked with blue pins.

Hemnessjøen (also called Øgderen) is a smaller lake compared with Mjøsa and Tyrifjorden with an area of 12,66 km^2 and maximum depth is 35 m. The nature reserves Kragtorpvika and Kollerudvika are situated along the lake with agriculture landscape in the eastern part. The lake is a part of Haldenvassdraget and the rivers Dalselva, Stomperudbekken and Kopperudbekken have their outflow into Hemnessjøen, and the lake inflow to Hemneselva.

Lake Vansjø is a bigger lake than Hemnessjøen with an area of 35,6 km^2 with a maximum depth of 37 m (average 7,4 m). Vansjø has its inflow to Mosseelva, which has its outflow to Oslofjorden in Moss. Several other smaller lakes have their inflow to Vansjø: Hobølelva, Svinna, Mørkelva and Veidalselva. The nature reserves Vestre Vansjø and Moskjæra is within the lake area. The drinking water for approximately 60 000 people comes from the lake.

Table 4. Characteristics based on water type definitions (Vann-nett. 2019[3]). The total Nitrogen and total Phosphorus values are averages derived from the lake monitoring program between 2016-2018.

Lake	**Tyrifjorden**		**Mjøsa**	**Hemnes-sjøen**	**Vansjø**	
Subarea	***Steins-fjorden***	**Tyri-fjorden**			**Store-fjorden**	**Vanem-fjorden**
Water body id	012-522-1-L	012-522-2-L	002-118-1-L	001-327-L	003-291-2-L	003-291-1-L
Size	Large	Very large	Very large	Large	Large	Large
Nat. water type	L109/L-N1	L107/L-N1	L206/L-N6	L108/L-N8	L108/L-N8	L108/L-N8
Climate zone	**Low** <200 MASL	**Low** <200 MASL	**Middle** 200-800 MASL	**Low** <200 MASL	**Low** <200 MASL	**Low** <200 MASL
Calcium, Ca mg/L	**Rich** > 20	**Moderate** 4 - 20	**Low** 1 - 4	**Moderate** 4 - 20	**Moderate** 4 - 20	**Moderate** 4 - 20
Alkalinity, A_T meq/l		0.2-1	0.05-0.2	0.2-1	0.2-1	0.2-1
Humic	**Clear**	**Clear**	**Humic**	**Humic**	**Humic**	**Humic**
FARGE, mg Pt/l	< 20	< 30	30-90	30-90	30-90	30-90
TOC, mg/l		2 - 5	5-15	5-15	5-15	5-15
Nutrients, µg/l	**Average**	**Average**	**Average**	**Average**	**Average**	**Average**
Tot Nitrogen	269	437	374	472	*1004*	*705*
Tot Phosphorus	24.4	5	5.7	25.7	28	*25*.1
Turbidity	**Clear** STS < 10 mg/L, inorganic part min 80%					

There is a large historical data set from the lakes of the water colour measured as FARGE (mg Pt/L). FARGE is the traditional parameter used to express the true colour of lakes and is based on an absorbance measurement at 410 nm of a filtered water sample. The FARGE is measured spectrophotometrically just as cDOM and they are therefore correlated. Hence, cDOM absorption at 443 nm can be derived from FARGE (Eq. 1) taking into account the Platina calibration standard (factor 387 for 5 cm cuvette at NIVA-laboratory), cuvette length (5 cm), the conversion from absorbance to absorption (LN[10] = 2,303), spectral slope (average for the lakes investigated = 0.462) and a conversion factor to absorption unit m^{-1} (20). The following conversion are used:

$$a_{cDOM,\,443} = (FARGE/387) *20*2.303*0.462 \qquad \text{Eq. 1}$$

[3] https://vann-nett.no/portal/

Table 5. In situ data from the monitoring programme between 2016 to 2018 from the different lakes. The data from Hemnessjøen are from 2016 and 2017. The data is presented as min-max, mean and standard deviation. Absorption of cDOM (a_{cDOM}) was calculated from FARGE according to Eq. 1.

Lake/ Station	Chl-a, µg/l	Secchi depth, m	Turbidity FNU	FARGE, mg Pt/L	a_{cDOM} 443 nm, m^{-1}
Tyrifjorden					
Steinsfjorden	**2.4-7.7**	**4.5-5**	**-**	**-**	**-**
	4.6	***4.8***			
	2.07	**0.4**			
Tyr-P	**0.9-2.1**	**4.5-8.5**	**-**	**18-22**	
	1.2	***5.4***		***19.4***	***1.1***
	0.5	**1.5**		**1.5**	
Mjøsa					
Brøttum	**0.8-3.2**	**4.2-8.3**	**0.46-2.4**	**7-16**	
	1.6	***6.6***	***1.06***	***10***	***0.6***
	0.8	**1.3**	**0.67**	**3**	
Kise	**1-4**	**5.8-8.8**	**-**	**8-16**	***0.6***
	2.3	***7.5***		***10.9***	
	0.9	**1.1**		**2.2**	
Skreia	**0.7-4**	**7.8-9.7**	**0.18-0.85**	**9-14**	***0.6***
	2.0	***8.5***	***0.43***	***11***	
	0.8	**0.9**	**0.16**	**1.8**	
Furnesfjorden	**x-x**	**6.1-6.5**	**-**	**-**	**-**
	2.5	***6.3***			
	x	**0.2**			
Hemnessjøen					
Øgd1	**9.6-11**	**1.5-2.1**	**-**	**27-31**	***1.6***
	10.2	***1.9***		***28.3***	
	0.7	**0.2**		**2.3**	
Vansjø					
Van1	**1.7-16**	**0.6-1.7**	**-**	**55-69**	***3.4***
	6.3	***1.3***		***62.5***	
	3.2	**0.4**		**5**	
Van2	**3.9-21**	**0.7-1.7**	**-**	**47-71**	***3.0***
	11	***1.3***		***55.2***	
	4.3	**0.3**		**9**	

The values in Table 6 are included to illustrate the average cDOM absorption at 443 nm in some marine water from the river mouth (salinity < 5) to open waters. The reason for this is that cDOM are one of the main factors that influence the retrieval of Chl-a from the remote sensing algorithms. We know from the Oslofjord area that cDOM absorption, more that 1-2, can cause problems of the satellite retrieved Chl-a.

Table 6. Statistics historical data of a_{cDOM} (m^{-1}) at 443 nm from marine waters (Sørensen unpubl.)

Salinity	Average	Stdev	Min	Max	n
0-5	3.50	0.93	1.72	5.33	21
5.1-15	1.98	1.42	0.15	5.04	109
15.1-25	0.71	0.37	0.12	1.60	74
25.1-34	0.25	0.12	0.07	0.75	137

4.2 Optical in situ measurements

Optical in situ data serves several purposes as they 1) provide a more comprehensive picture of all the parameters affecting the light (Chl-a, TSM and cDOM) and thus the signal received by the satellite sensors, 2) provides data for possible matchups with the satellite overpasses and algorithm testing, 3) inherent optical data, such as absorption and attenuation, are used for algorithm development and for bio-optical water models. The results from the in situ campaign are presented in Table 8. In Lake Tyrifjorden and Vansjø surface particulate backscattering (bbp) had been measured at 6 different wavelengths using an Hydroscat-6 and absorption (a) and attenuation (c) were measured at 9 different wavelengths using an AC9 instrument. The data were corrected from pure water contribution as well as temperature and salinity effects (Sullivan et al. 2006; Röttgers et al. 2013) and from residual scattering (Röttgers et al. 2013). The particle backscattering (bp) has been calculated from the AC9 measurements. The results for Tyrifjorden showed that the absorption values (a m^{-1}) were lowest in Steinsfjorden and highest near the outflow from Storelva closely followed by station Tyr-P whereas the absorption slopes (S m^{-1}) were similar (Figure 8, Table 8). The attenuation (c m^{-1}) followed the same pattern in light attenuation with the steepest slope close to the river outflow (Utløp Storelva) (Figure 8). For Vansjø both the absorption, scattering and attenuation were more than twice higher than in Tyrifjorden, indicating more turbid and darker waters. The absorption was very similar between the two stations whereas the attenuation was slightly higher at station Van2. By looking at the ranges of the optical values in Table 5 and the results of the IOP´s one can also confirm the patterns seen within the lakes in the RBG images. The different water basins in Tyrifjorden are also seen in the results with higher particle backscatter coefficients, m^{-1} (Figure 8) as well as turbidity and Chl-a values in Steinsfjorden, whereas the cDOM absorption is higher at station Tyr-P, but highest close the river outlet at station Storelva. The total absorption in the blue wavelengths are used to derive the sum of phytoplankton, cDOM and non-algal particle absorption, according to Eq. 6 in Appendix A.2. MERIS and S-3 has a band at 442.5 (blue) nm to capture the chlorophyll maximum and one at 412.5 (violet) to distinguish the contribution from cDOM and non-algal particles.

The pigment absorption is related to the phytoplankton Chl-a concentration and is the basis for the conversion factor used in the bio-optical model of e.g. the C2RCC processor (Figure 6). The relation in the processor is based on a CHL factor of 21, which is developed for marine waters (Sørensen et al (2007), Sørensen et al. (2008)). This relation can be different for lakes and the assumed conversion factor affects the performance of the retrieval of Chl-a from the R_{rs}. Therefore, some preliminary studies of this relationship have been done in 2019, and the absorption by algae (apig m^{-1}) was derived (Table 8) and compared to the measured Chl-a concentrations (Figure 9). A test to illustrate how this can affect the results of Chl-a is shown in Table 7. The resulting Chl-a concentrations are quite different depending on both the apig value and the of the equation used, with larger differences between the equations for higher apig values. Although, the best relationship can be derived, and the different models can be statistically tested when more lake in situ data has been gathered. When the best model has been derived this can be used to tune or adapt the remote sensing algorithms and it would improve the accuracy of the Chl-a data retrieved. This should also be tested as a second step, see e.g.(Sørensen et al. 2007; Sørensen et al. 2008) for a local derived Chl-a conversion factor in the Skagerrak.

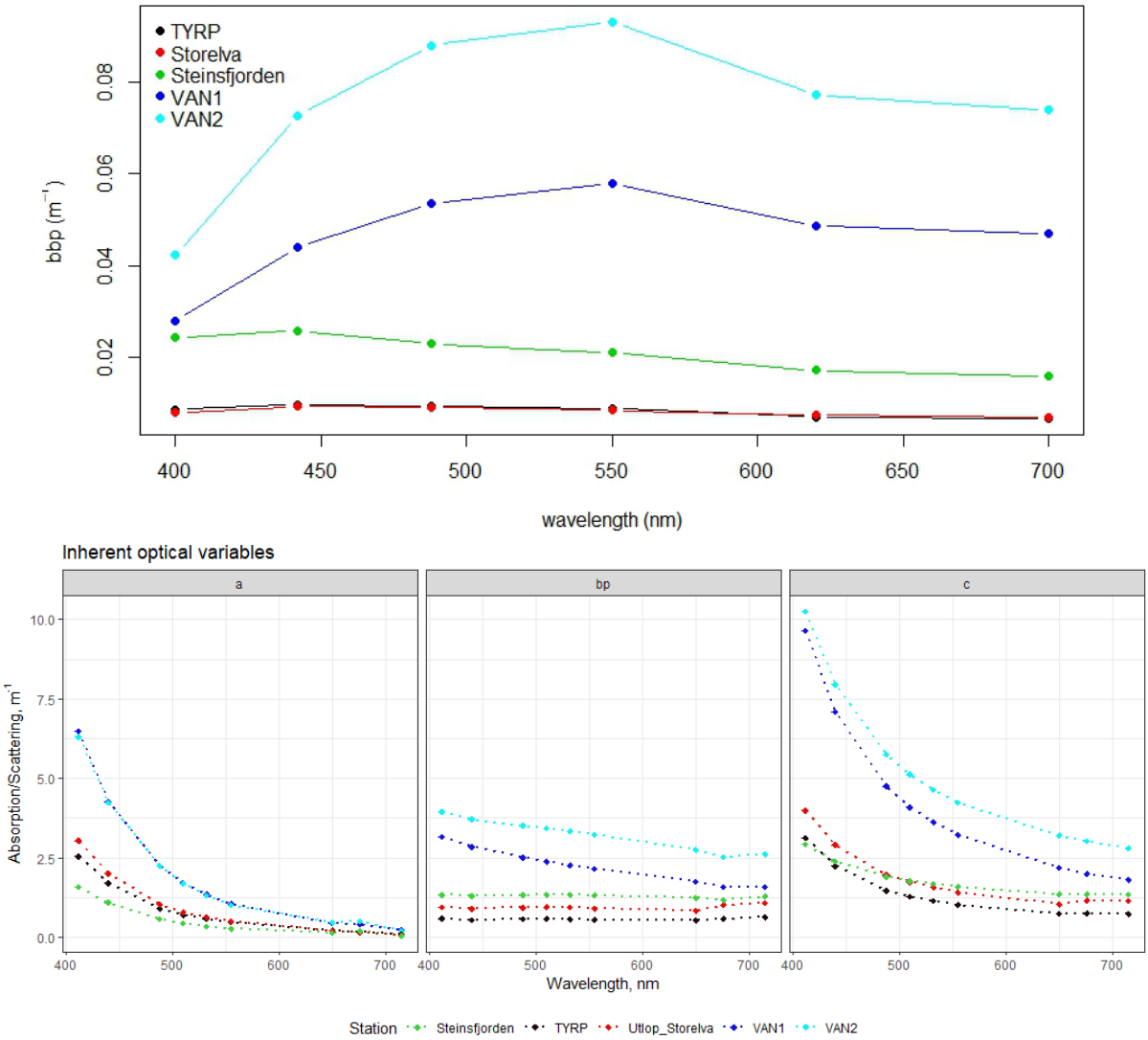

Figure 8. Upper panel: The particle backscattering coefficient, bbp (m^{-1}) on the y axis and wavelength (nm) on the x-axis from in situ sampling on 25.6.2019 in Tyrifjorden and on 28.6.2019 in Vansjø. Lower: The absorption (a. m^{-1}) on the left, the particle scattering (bp, m^{-1}) in the middle and on right the attenuation coefficient (c, m^{-1}) for the same stations.

Based on the very few data from Table 8, one can derive the conversion factor between the bp443 (lower middle of Figure 8) and the TSM values (TSM = 1.68 x bp443). This are close to the C2RCC conversion factor 1,72 indicating that conversion factor for TSM maybe are close to the marine derived factor. No conclusion can be drawn on these few datapoints, still this illustrate what needs to be done in the future research on the IOP.

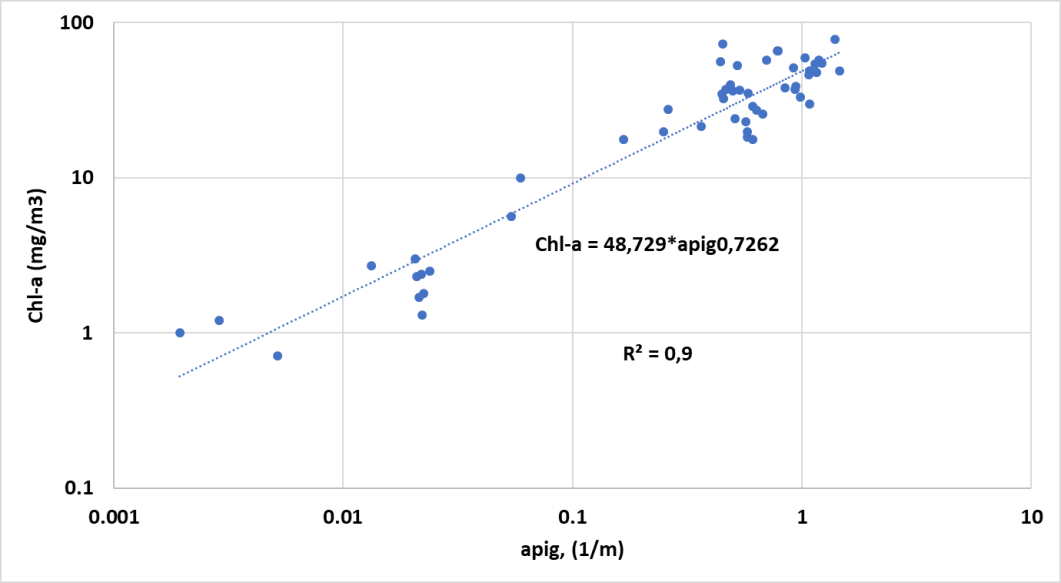

Figure 9. Relation between pigment absorption (Apig m^{-1}) and Chl-a concentration mg m^3 from the present study compared together with historical lake data from different Estonian lakes used with permission from Uudeberg, Equation #3 in Table 7), .

Table 7. Empirical relationships between apig (443 nm) and Chl-a concentrations. Chl-a is theoretically calculated based on different apig values from 0.01-2 m^{-1}. Data are from Sørensen, unpubl; Uudeberg unpubl.; Okullo et al. (2007); Kangro et al (2018).

		Chl-a µg/l for different Apig (443nm) value					
		Apig (443nm) value					
Source	**Equation**	*0.01*	*0.05*	*0.1*	*0.5*	*1*	*2*
1 Original (MERIS, S2, S3) Used in e.g. C2RCC	Chl-a=21 *apig^1.044	0.17	0.92	1.90	10.19	21	43.30
2 This study only 2019 data	Chl-a=21.3 * apig^0.55	1.70	4.11	6.01	14.53	21.26	31.11
3 This study 2019 + Estonian lake data (Uudeberg, unpupl.)	Chl-a=48.7 * apig^0.73	1.72	5.54	9.16	29.46	48.73	80.60
4 Okullo et al (2007)	Chl-a=46.5 *apig^1.06	0.75	3.07	5.65	23.30	42.88	78.92
5 Kersti Kangro et al. (2018)	Chl-a=28.3 *apig + 2.39	2.67	3.81	5.22	16.56	30.72	59.05

Table 8. The in situ data collected in 2019.

Lake	Stations	Date	Depth m	Secchi depth m	Secchi color	TSM mg/l	Turbidity FNU	bp at 440 nm m^{-1}	TOC mg C/l	FARGE mg Pt/l	a_{cDOM} at 443 nm m^{-1}	Chl a µg/l	a_{pig} at 443 nm m^{-1}	$S_{400-550\ nm}$ m^{-1}
Mjøsa	Brøttum	9.7.2019	0.5	4.6	green yellow	0.95	1.45	-			0.38	1.7	0.021	0.0170
	Brøttum	5.8.2019	0.5	4.6	yellow green cloudy			-			0.49	1.9		0.0148
	Kise	9.7.2019	0.5	4.7	yellow green	0.84	1.07	-			0.77	2.3	0.021	0.0168
	Kise	5.8.2019	0.5	5.6	yellow green			-			0.55	3.1		0.0162
	Furnesfjorden	9.7.2019	0.5	6.5	green yellow	0.66	0.78	-			-	3.0	0.021	-
	Skreia	9.7.2019	0.5	6	Yellow green	0.72	1.18	-		18	0.68	2.4	0.022	0.0178
	Skreia	5.8.2019	0.5	6.5	yellow green			-			0.64	3.2		0.0173
Tyrifjorden	Outflow Storelva	25.6.2019	0.5	4.5		0.8	1.34	0.9	3.8	28	1.65	1.8	0.022	0.0176
	Tyr-p	25.6.2019	0.5	4.8		0.66	1.34	0.53	3.4		1.21	2.5	0.023	0.0178
	Tyr-P	9.7.2019	0.5			0.39	0.77	-		20	1.37	1.3	0.022	0.0166
	Tyr-P	14.8.2019	0.5			0.79	1.63	-			0.81	2.7	0.013	0.0188
	Steins-fjorden	25.6.2019	0.5	4.0		1.8	1.95	1.3	4.5	16	0.66	10.0	0.059	0.0175
Vansjø	Van1	28.6.2019	0.5	1.2	Brown	6.47	5.27	2.85	8.9	60	4.16	5.6	0.054	0.0172
	Van2	28.6.2019	0.5	1.2	Brown	5.31	4.89	3.71	8.8		3.52	14.0	NA	0.0174

5 Remote sensed observations and monitoring in situ measurements

The estimated concentrations of the parameters. e.g. Chl-a is based on the reflectance data provided as the input, it is therefore important to validate the atmospheric correction to make sure this is working properly. This validation exercise should ideally be done with in situ reflectance data, but since this is not available from these lakes the shape and the range and magnitude of the spectra is considered. Once this quality check is been done the satellite output from the different dates are extracted. All scenes had clear sky with no clouds nor cirrus clouds (high thin clouds). In addition, various quality flags have been included to exclude non-valid data and all data have passed the criteria set by Rrs_1 < Rrs_2. This means that there are potential more data (more dates) that can be included, but this also means more manual investigations which time demanding and out of the scope for this work.

The most common way to compare or validate the remote sensing products against the in situ data is to do a 1:1-plot to inspect the correlation between the data. Still, this rely on having match-up data that overlaps in space and time. The overpass of the satellite should be within a limited time difference of the in situ sampling (1-3 hours) and requires clear sky since the optical satellite sensors cannot see through clouds. The monitoring programme within the lakes is not designed to take this into account. Therefore, there is no available data for direct comparisons between remote sensing and in situ data, which is why we performed a time series comparison instead. This will not show the correlation, but instead a possible coherence between the two time-series regarding the ranges and the variability. Weather and hydrographic changes between the dates will affect the result, and it can therefore be greater differences compared with stable conditions or dedicated match-up data.

5.1 Spectral signature with MERIS

In Figure 10 the R_{rs} from MERIS from the four stations Skreia, Brøttum, Furnesfjorden and Kise in Mjøsa are presented. For each station, a pixel extraction is done 1x1 around the station point resulting in one spectrum for each date. They are all processed with the FUB processor. These data have been quality controlled in advance through various quality flags, and data from before April and after October have been excluded as there is great danger of ice during this period in addition to low sun elevation which in turn gives poor light conditions and a weak reflectance signal to the sensor (i.e. a high signal to noise ratio).

For station Brøttum in lake Mjøsa in Figure 10, the intensity is clearly stronger compared to the other stations. High particle content will give a higher reflectance intensity compared to a water mass with low particle concentration due to a higher scattering. At the same time there is a clear maximum reflectance for the wavelength 560 nm (in the green part of the spectrum) which corresponds to the wavelength with minimum Chl-a absorption. The reflectance is lower in the blue part of the spectrum (412-490 nm), and it is in this part of the spectrum that cDOM and Chl-a have high absorption. This indicates that for the station Brøttum there are both algae and particles present as well as humic substances. Gudbrandalslågen has a river outflow a little further north of Brøttum. The river can contain a lot of particles due to snow melting in the mountains, discharge from flooding, and probably some inorganic material from glaciers. The R_{rs} from the other stations in Mjøsa indicate moderate amounts of particles, humic and some algae. The shape on the spectra shows the same maximum reflectance at 560 nm but with lower magnitude. For some periods, the reflectance spectrum indicates

clear water or moderate amounts of particles and algae and in other periods a situation with more algae and particles.

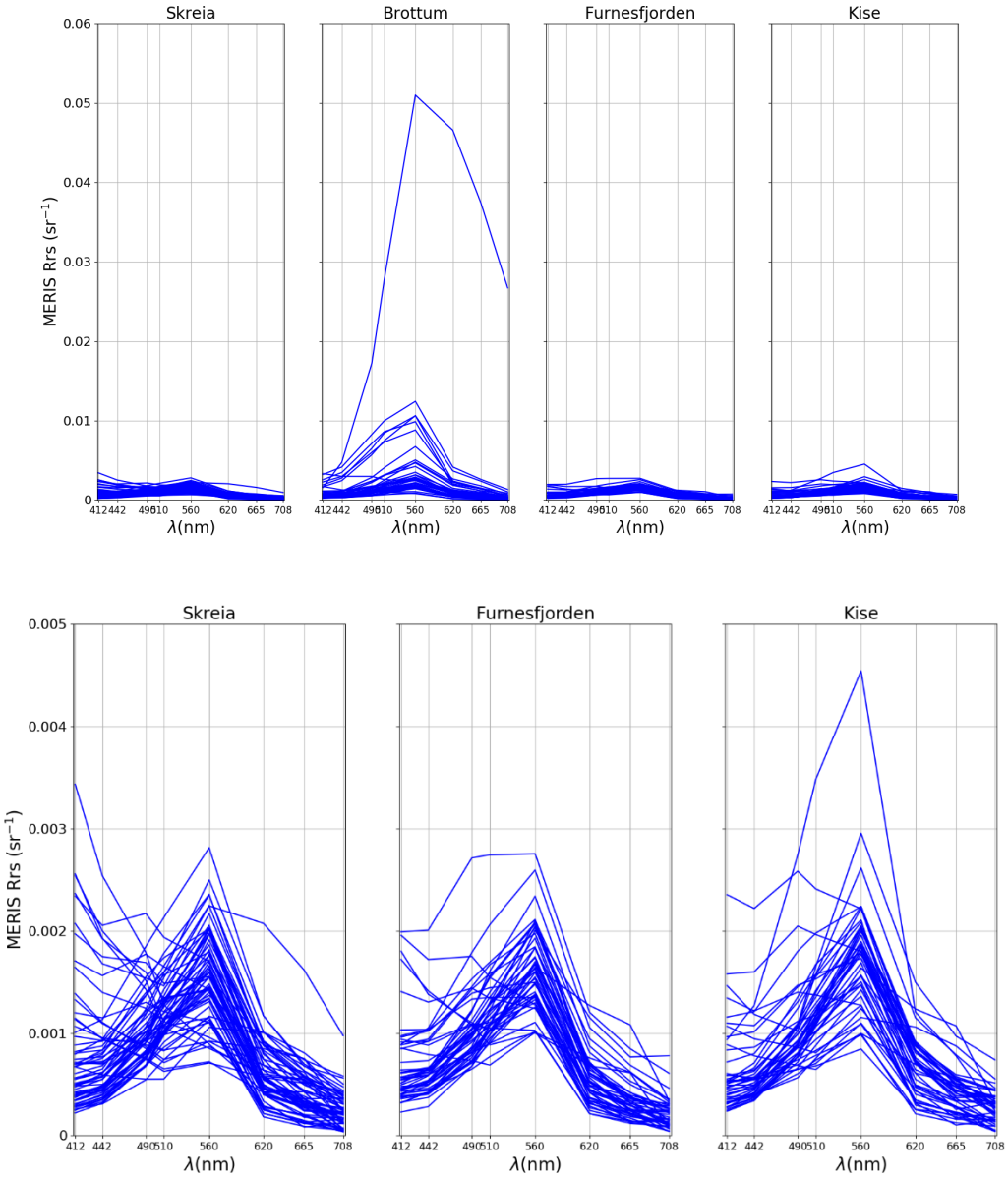

Figure 10. The R_{rs} from MERIS from the four stations in Mjøsa. The remote sensing observations are from 2002 to 2012. Data are processed with FUB. The two panels differ in the scale of the y-axes, showing the differences between Brøttum and the other stations in Mjøsa.

5.2 Time series of Chl-a and TSM with MERIS data from Mjøsa

For the stations in Mjøsa, Chl-a and TSM data were extracted from the remote sensing observations from MERIS for the period 2002 to 2012. These are compared with the in situ measurements from the same stations.

The time series for the station Brøttum is presented in Figure 11. Brøttum is located in a considerably narrower part of the lake (Figure 7) which may present greater challenges regarding land-affected signals. With pixels close to land, water pixels can be influenced by reflected signal from land. These effects are called the adjacency effect and can give incorrect values. When applying quality flags and including only data between April and October, there are few remote sensing observations left. Maybe the quality flags have been too strict and there are dates where the remote sensing observations are of good quality, but these would then need to be assessed manually for each station. The comparisons show that for some periods there is good agreement between the remote sensing observations and the in situ. The remote sensing observations and the in situ measurements differ in time, and in periods where there seem to be great difference this can also be due to changes in the water conditions and not necessarily "bad" remote sensing observations. For 2007, 2010 and 2011 it seems like MERIS has captured Chl-a concentration, but the absolute values are higher for MERIS. Low Secchi disc depth were measured during the same period. The same time series is presented for Skreia. The comparison shows that remote sensing observations are within the same order of magnitude as the in situ data and the remote sensing observations often follow the same pattern.

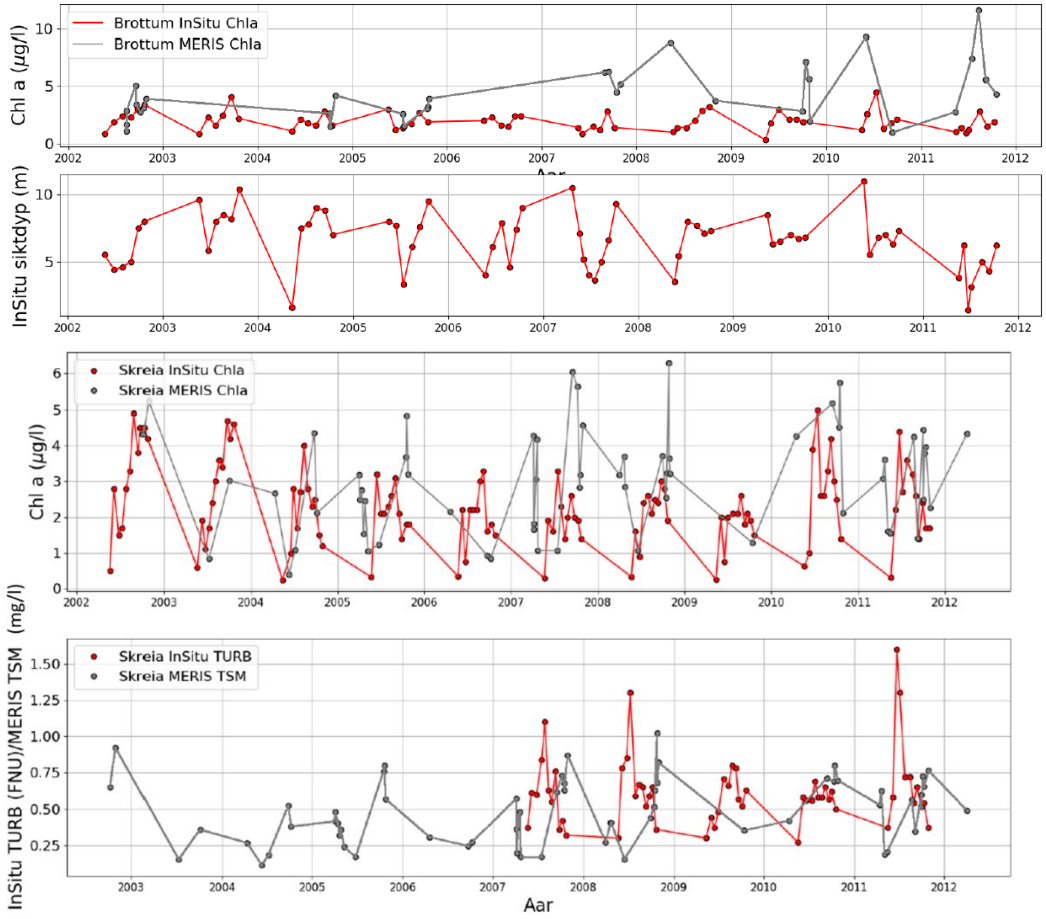

Figure 11. Time series of remote sensing observations from MERIS and in situ data from Mjøsa, Chl-a and Secchi disc depth in the two top panels for station Brøttum and Chl-a and Turbidity/TSM for station Skreia in the two lower panels.

5.2.1 Conclusions

- There is an overall good performance of the spectral retrieval from FUB for MERIS
- There is a spatial variability between the stations within the lake

5.3 Spectral signature with S-2

The reflectance from the water is used to derive water quality products. The spectral signature of each of the lakes and the various stations is presented below. For each station, a pixel extraction is done 3x3 around the station point resulting in 9 spectral shapes for each date. Each spectra consists of Remote sensing reflectance (R_{rs}) values from 8 bands (described in Appendix B2).

5.3.1 Steinsfjorden in Tyrifjorden

The S-2 R_{rs} spectra from Steinsfjorden from 2016 to 2018 is presented from C2RCC in Figure 12, and looks reasonable. In waters with high sediment and organic matter concentrations (Figure 5) the R_{rs} will have higher values in the wavelengths greater than 750 nm (NIR) than for the spectra with lower sediment/particles.

The spectra show maximum R_{rs} in the 560-band, which is the absorption minimum for phytoplankton. The R_{rs} also show low R_{rs} values in the blue (443nm) and a small dip in the 665-band. The 443-band is the wavelength with maximum absorption for chlorophyll and the 665 band are associated with the red absorption peak (675 nm) This shape is the most frequent shape in the spectra's from Steinsfjorden. The spectra shape resembles the shape of 'c' and the 'moderate' and 'clear' in Figure 5. In September the spectra have the same feature at wavelengths greater than 750 nm as in 'a' with increasing R_{rs}. This could be due higher particle concentrations this month compared to the other months.

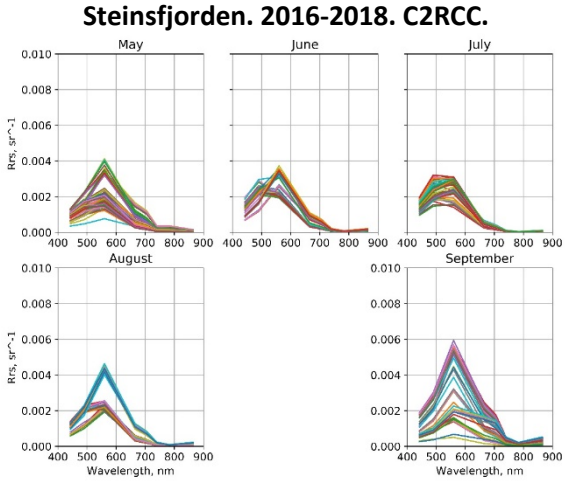

Figure 12. Remote sensing reflectance (R_{rs}) from C2RCC processed S-2-data extracted from the monitoring station in Steinsfjorden. All data are from 2016 to 2018 and from clear sky scenes.

5.3.2 Tyrifjorden

The spectra shape are more heterogenous at Tyr-P than in Steinsfjorden (Figure 13). There are several spectra with a maximum at the 560-band (phytoplankton absorption minimum) with higher R_{rs} values in May and in August, due most likely to high absorption in the Chlorophyll absorption band 443. The spectra with maximum in wavelength 560 are typical for the shapes a, b and c and the Optical Water Types (OWT) in Figure 5. These are characteristics for water with concentrations of particles, organic matter and phytoplankton for different magnitudes, and for the OWT Clear, Moderate and Turbid. There are also episodes with maximum R_{rs} in the 490. This shape resembles most d) in Figure 5 which is the signature for clear waters. Still, the 490 nm band is the maximum and therefor higher than 443-band which is the maximum in d). The spectra from the river runoff close to Storelva has more of the

shapes with maximum at 560 nm. As for the other stations in the previous lakes, the R_{rs} falls often to a minimum around 740 and 783 and then increasing again in the NIR. The increase of reflection in NIR is most likely due to scattering from particles in the lake.

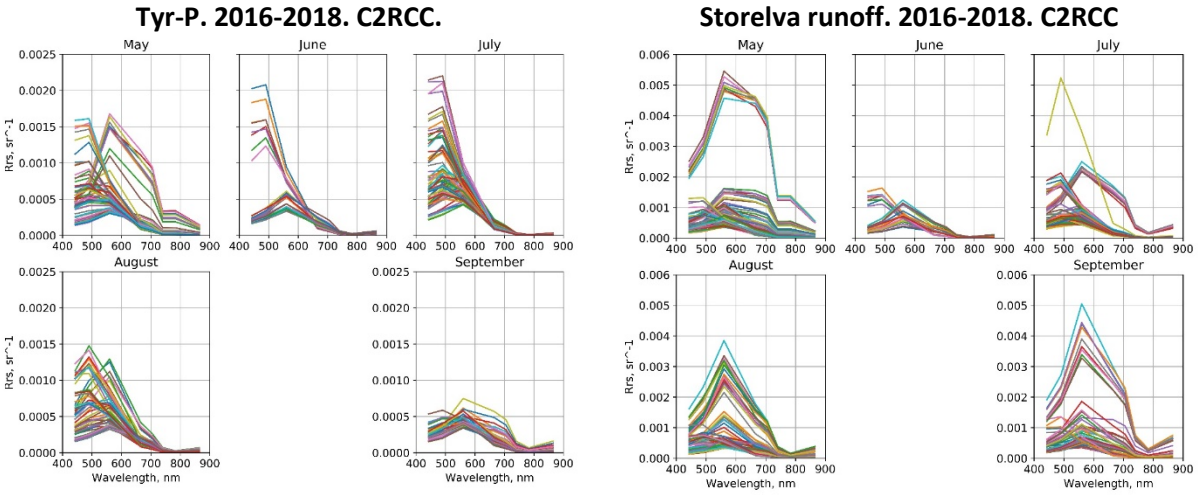

Figure 13. Remote sensing reflectance (R_{rs}) from C2RCC processed S-2-data extracted from the monitoring station Tyr-P and Storelva runoff in Tyrifjorden (bottom), presented in Figure 7. All data are from 2016 to 2018 and from clear sky scenes.

5.3.3 Mjøsa

In Brøttum some of the spectra in May have a good resemblance with high sediment and cDOM absorption spectra shape (b) in Figure 5 and spectra shape for moderate in Figure 5, with no R_{rs} increase from 783 nm to 865 nm. This indicates less phytoplankton present and moderate particle and humic concentrations. A similar pattern can be seen also for station Skreia in May, but not with equally high values. Other months have the maximum in the 560-band, but there are also other patterns as seen in Tyr-P. The R_{rs} from Kise and Furnesfjorden are included in Appendix C.

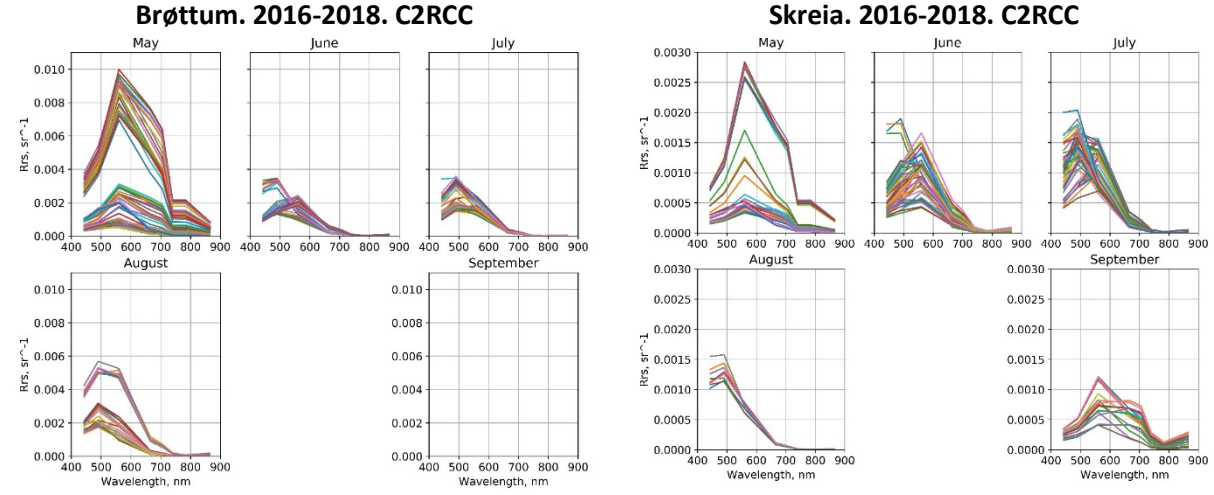

Figure 14. Remote sensing reflectance (R_{rs}) from C2RCC processed S-2-data extracted from Brøttum and Skreia in Mjøsa. All data are from 2016 to 2018 and from clear sky scenes.

5.3.4 Vansjø

The spectra of Vansjø differs from the other lakes with a clear second maximum around the 705 nm band. The shape resembles the spectra of turbid and very turbid OWT shown in Figure 5. This is consistent for all months and for both Van1 and Van2. For both stations in May there are no increase of reflectance in the NIR in neither of the spectra. Since the spectral shape looks like the turbid and very turbid OWT case, but there is no indication on scattering, it seems likely that May data have either high amount of phytoplankton and/or humic substances. The height of the spectra is not that high for the other months with a clear increase from red to NIR. The increase from red to NIR is due to increased particles and therefore scatter, while the smaller magnitude of the R_{rs} in the band of minimum absorption by Chl-a (at wavelength 560 nm), the amount of phytoplankton could be less for instance in June compared with May but increasing in July and then decreasing again. It seems to be minor variation in the red to NIR slope, likely due to small variation within the particle concentration in the lake.

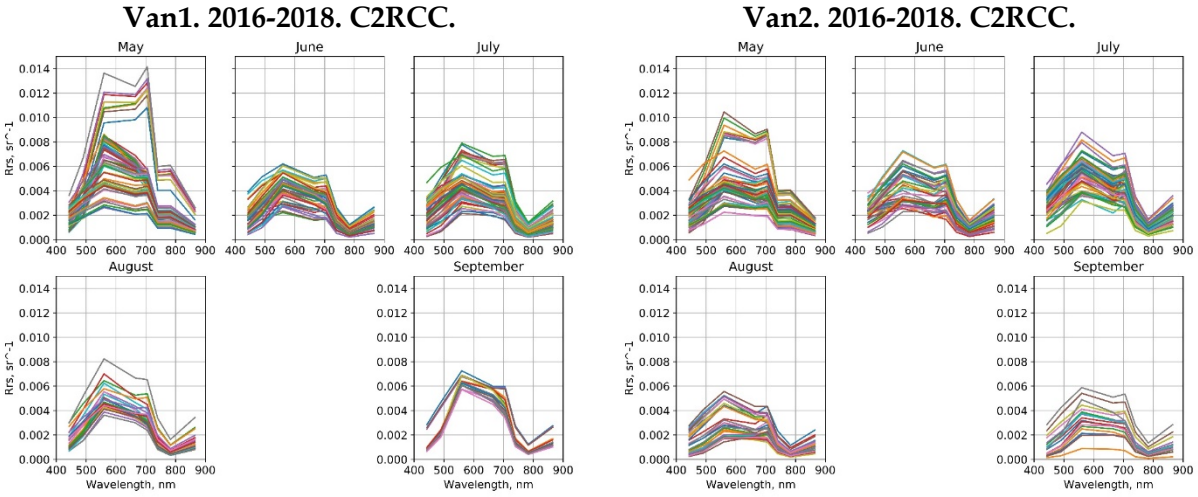

Figure 15. Remote sensing reflectance (R_{rs}) from C2RCC processed S-2-data extracted from the monitoring station Van1 and Van2 in Vansjø. All data are from 2016 to 2018 and from clear sky scenes.

5.3.5 Conclusions

- There is an overall good performance of the spectral retrieval from FUB for MERIS and C2RCC for S-2 and S-3, while tests with the Acolite processor seem to fail in those waters.
- More satellite data can be derived if partial cloudy days are included to the dataset.
- The spectral signals may be affected by adjacency effects or sun glint which can be mathematically corrected for.
- The spectral data and the shape of the spectral signature indicates there are optical information that we still don't have fully used and understand and should be studied better
- In situ spectral data should be collected for comparisons.

5.4 Time series of Chl-a, Secchi disc depth, turbidity and TSM with S-2

The time series presented below show the mean concentration and the corresponding standard deviation for each date extracted from satellite dataset. Comparisons between several other algorithms and the in situ Chl-a are presented in Appendix D.

One Secchi disc depth (SDD) algorithm have been applied on two AOP-products (only one presented here), which is from the C2RCC data (kdz90max). The equation used for the SDD algorithm is empirical derived, based on data from the Baltic Sea, 14 Estonian and 7 Finnish lakes (Alikas and Kratzer, 2017);

$$SDD_{kdz90max} = 2.62 * (kd_{z90max}{}^{(-0.79)}). \quad \text{Eq. 2}$$

5.4.1 Tyrifjorden

In Figure 16 the time series of Chl-a concentration and Secchi disc depth from Steinsfjorden is presented from both in situ data and derived from satellite data. Since only Steinsfjorden have three years of data, this is the only station presented as time series from Tyrifjorden. The time series show that C2RCC in most cases have values which fit the ranges of the in situ data. There are also some low and high values, but since the in situ Chl-a sampling is only once a month, the high values could be due to increased phytoplankton not detected by in situ sampling. Changes in weather conditions may also have an impact in the lake between the in situ sampling and remote sensing observation dates. The right panel in Figure 16 show that the AOP-product from C2RCC resembles the in situ SDD value.

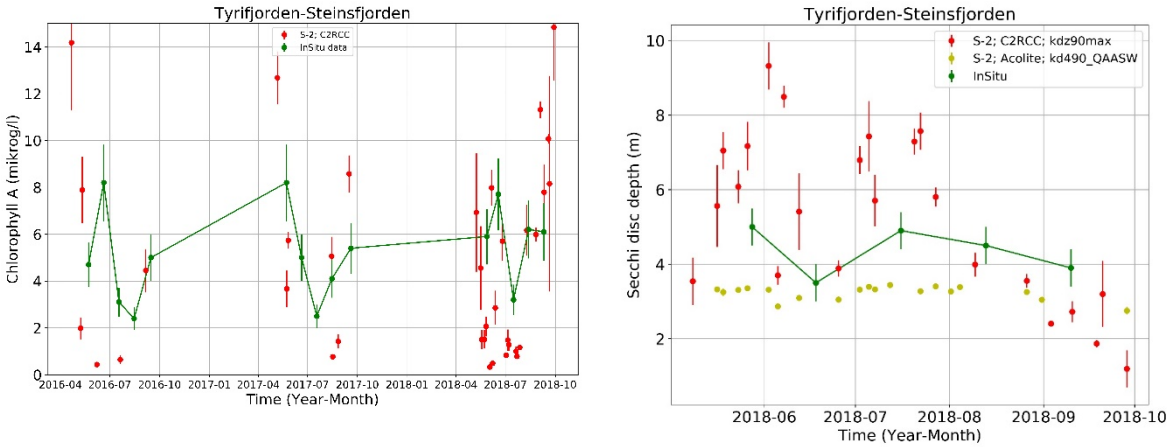

Figure 16. A time series of Chl-a (left panel) from 2016 to 2018 and Secchi disc depth (right panel) from 2018 from Steinsfjorden in Tyrifjorden.

5.4.2 Mjøsa

In Figure 17 the time series from Brøttum show low Chl-a concentrations measured in situ. For most of the data from S-2, the C2RCC also calculates these ranges of concentrations. In end of 2018 C2RCC underestimates the Chl-a. Both the Secchi disc depth and the turbidity data, calculated with S-2, seem to be in line with the in situ measurements. However, both the Chl-a concentration and the turbidity for the S-2 were a bit higher in May 2018, a pattern not seen in the in situ data. The Secchi disc depth was measured 22nd of May 2018, but remote sensing observations showed a large particle plume from the outflow of Gudbrandalslågen, on May 16th 2018 (Figure 18), most likely with inorganic particles passing the Brøttum station. This explain the high TSM concentrations in the S-2 observations from this period.

The in situ measurements of the Chl-a concentration from Skreia (Figure 19) show low concentrations through the whole period. The C2RCC calculations from the remote sensing observations are within the range in 2016 and 2018 but are also overestimating for some dates. As seen in Tyrifjorden, with very low Chl-a concentrations and low particles, this could result in higher noise levels influencing the results. Although, when investing the scene from 31st of May 2018 (Figure 20), wind is affected the surface, which could have affected the R_{rs} signal back to the sensor (glint). The sun glint can be corrected for in the processing but was not done for this study.

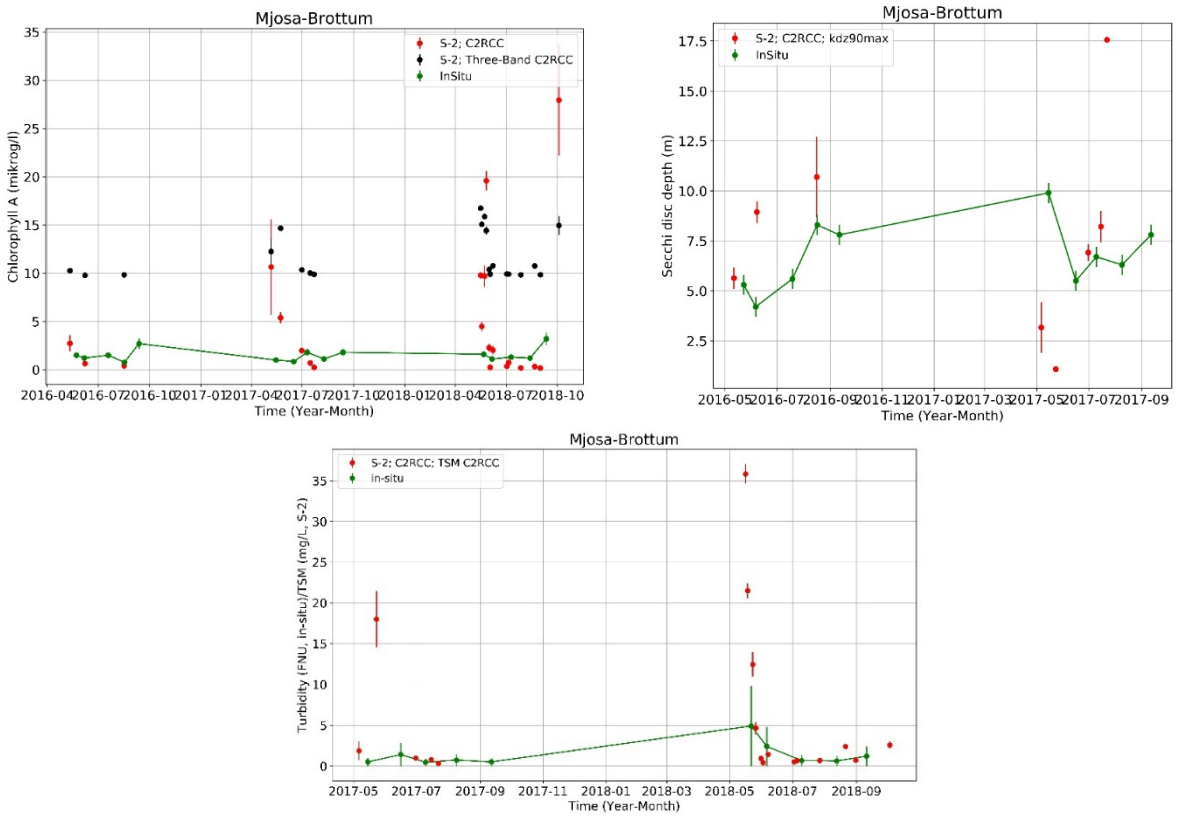

Figure 17. A time series of Chl-a (top left panel) from 2016 to 2018, Secchi disc depth (top right panel) from 2017 and 2018 and turbidity (water samples) and TSM (S-2) from 2017 and 2018 (bottom panel). All three from Brøttum in lake Mjøsa.

Figure 18. An RGB image from S-2 on the 16th of May 2018 showing the result of melting in the mountains with a particle plume coming from the outflow of Gudbrandalslågen further north of this station.

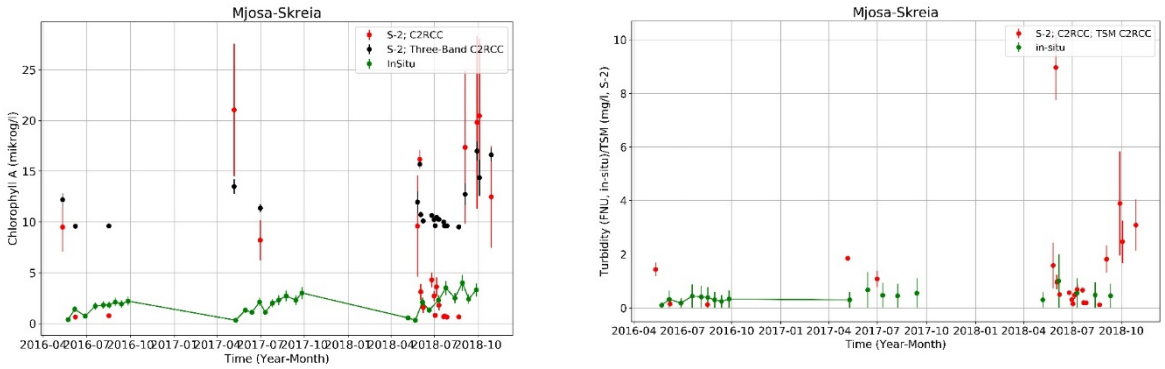

Figure 19. Time series of Chl-a from 2016 to 2018 (left panel) and turbidity (water samples) from 2016 to 2017 (right panel) from station Skreia in lake Mjøsa.

Figure 20. An RGB image from Skreia 31st of May 2018 where calculations from remote sensing observations give very high Chl-a and TSM concentrations compared to the in situ data.

5.4.3 Vansjø

In Figure 21 the time series of Chl-a from C2RCC data is compared with the in situ Chl-a from the stations Van1 and Van2 in Vansjø. The sampling frequency in Vansjø is twice a month. which gives a much higher in situ data frequency than the other lakes investigated. For both Van1 and Van2, the C2RCC seems to be in the correct size order than the in situ data. For some short periods, the C2RCC seem to underestimate the Chl-a concentrations as seen for the other lakes. The Three-Band algorithm gave higher values but follow the same pattern as C2RCC and by adjusting the coefficients the algorithm might fit better. The Chl-a concentration is lower in May for both stations.

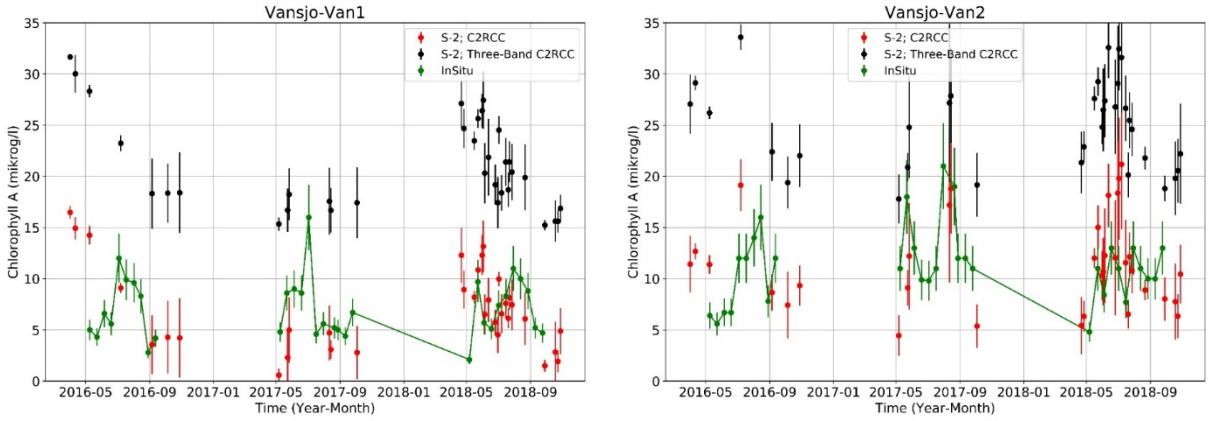

Figure 21. Time series of in situ Chl-a from 2016 to 2018 from Van1(left panel) and Van2 (right panel) in Vansjø.

5.4.4 Conclusions

- The increased retrieval of data from Remote sensing is complementary as it can detect events that the monthly in situ monitoring sampling misses to identify.
- For all lakes, October data seems to be too challenging for S-2 to derive the Chl-a concentrations. This is likely due a too low sun-angle and therefore a longer path for the photons, and less signals reaching the MSI sensor and therefore increasing the noise within the scene.
- Dedicated match-up data should be collected.

5.5 Seasonal analysis of Chl-a and TSM with S-2 in three lakes

In the following a monthly analysis of clear sky satellite data from 2016-2018 has been analysed.
For all stations both Chl-a and TSM have been analysed. Kise and Furnesfjorden from Mjøsa are presented in the Appendix E.

5.5.1 Tyrifjorden

For Tyrifjorden all three stations are presented in Figure 22. The variation within one month between the three stations differ. The largest variation is for the station in the outflow of Storelva for Chl-a, and this big variation is within all months presented. There are defined outliers for four of five months at this station. The biggest variation in TSM is in Steinsfjorden. From the sampling in June 2019, Steinsfjorden was the station with highest Chl-a and TSM, and the lowest cDOM (Table 8). Even though Tyr-P is the lake with the most outliers, it is the station also with smallest variation. The outliers in Tyr-P for the Chl-a are most likely due to a failed atmospheric correction even though all scenes investigated are cloud free. The seasonal analysis from Steinsfjorden indicate that the Chl-a concentration have more variation within a season (from May to September) than in Tyrifjorden where the median value does not differ that much between the months. The exception is within July which show general low values for all three stations.

In Figure 23 a comparison between the monthly averaged Chl-a data from remote sensing and in situ data are shown including the standard deviation bar. Since Steinsfjorden is the only station with three years of data from 2016 until 2018, the comparison is only presented for this station. In general, for all months there are more remote sensing data for these months than in situ data. The in situ data are sampled once a month. Due to the cloud cover, there can be more remote sensing data in one month from one year to another. Even though there are differences between the remote sensing data and

the in situ data, the remote sensing -data are within the same order. The time series from Steinsfjorden indicates large variability within the in situ data from May to October, and it show denser data points from remote sensing data in July 2018 due to long periods with clear sky this year. Here the C2RCC mostly underestimates compared with the in situ Chl-a.

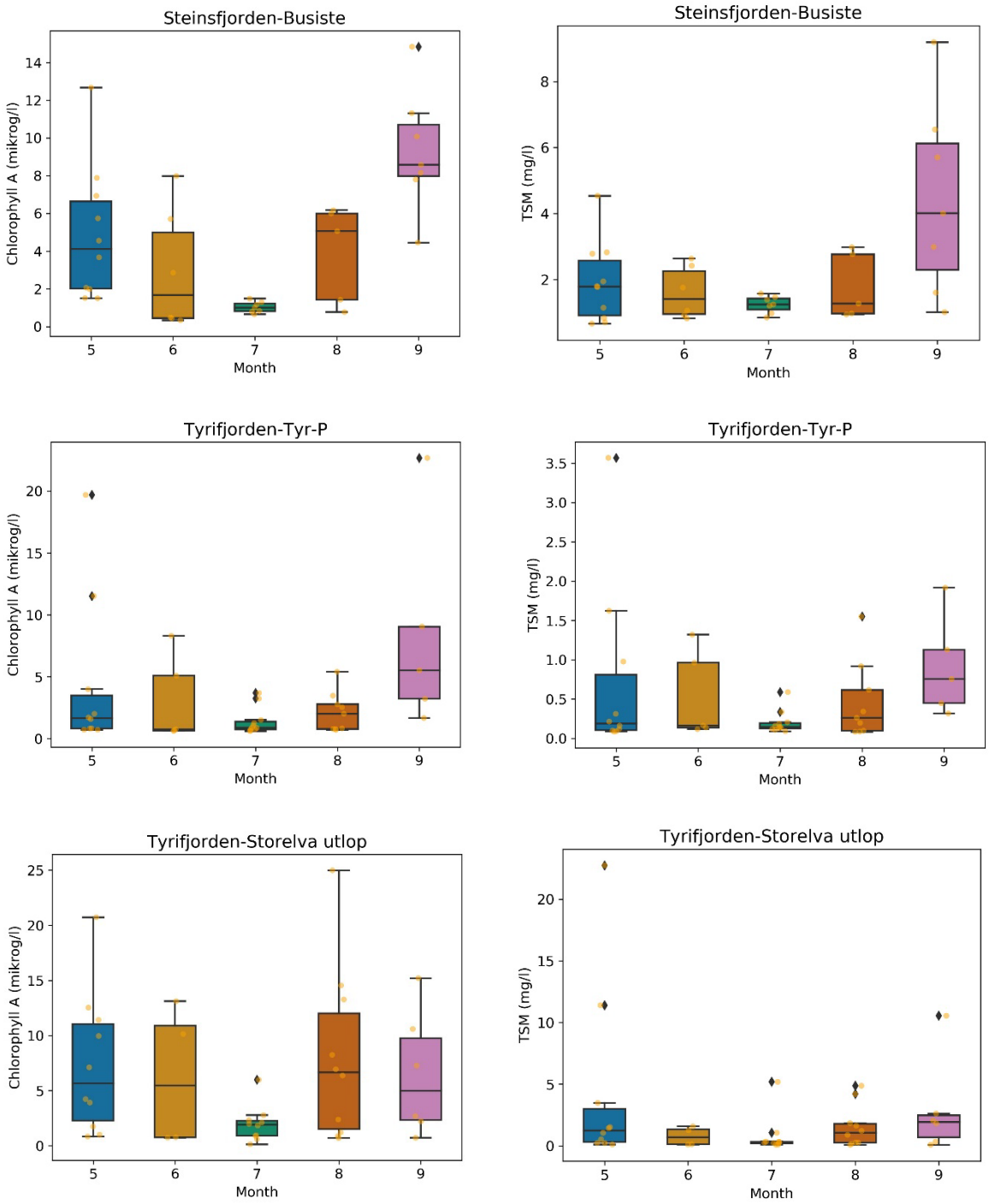

Figure 22. Monthly Chl-a and TSM shown as boxplots. The boxes present the 25th percentile (Q1), 50th percentile (median. Q2) and the 75th percentile (Q3) of the dataset. The outermost bar represents the "minimum" (Q1-1.5*interquartile range (IQR), lower bar) and the maximum (Q3+1.5*IQR, upper bar). The orange dots represent the remote sensing observations. The black diamond is defined as an outlier.

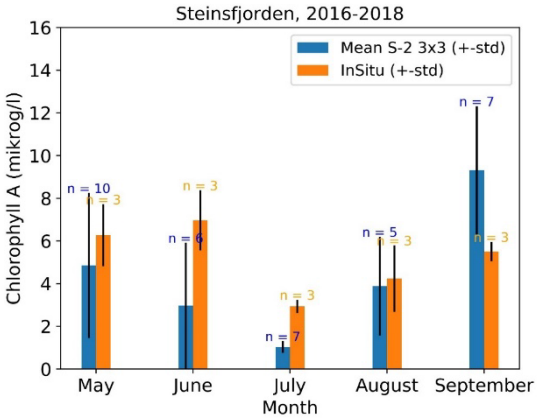

Figure 23. Monthly averages with standard deviation bars for remote sensing Chl-a data and in situ Chl-a data. The remote sensing data are CR2CC processed S-2 data.

5.5.2 Mjøsa

As Brøttum is located south of the outflow from Gudbrandalslågen, and Skreia is in the main basin south of Hamar, there will be different impact from the rivers in these stations as seen in Figure 24 and Figure 25.

The top panel show the variation in the remote sensing observations within each month. Since Brøttum is affected by Gudbrandalslågen, there is large variation both in Chl-a and TSM in May, as expected. The variation though is larger within the remote sensing observations than compared to the in situ measurements. As seen in the time series in Figure 17 and the RGB-image in Figure 18, the remote sensing observations captured the particle plume from the Gudbrandalslågen outflow in May 2018. The defined outlier for the Chl-a and the maximum TSM are from this episode. The variation within the other months are much less, both in remote sensing observations and in situ.

At Skreia the biggest variation is within May in both Chl-a and TSM in the remote sensing observations (Figure 20), and the variability seems related to the strong winds affecting the surface water. In September, the Chl-a and TSM concentrations are from two dates with clear sky and no evident wind effects. It seems that also for these dates, the signal from the water is too low resulting in too much noise in the calculated products. The variation within the other months are small, and comparable with the in situ measurements.

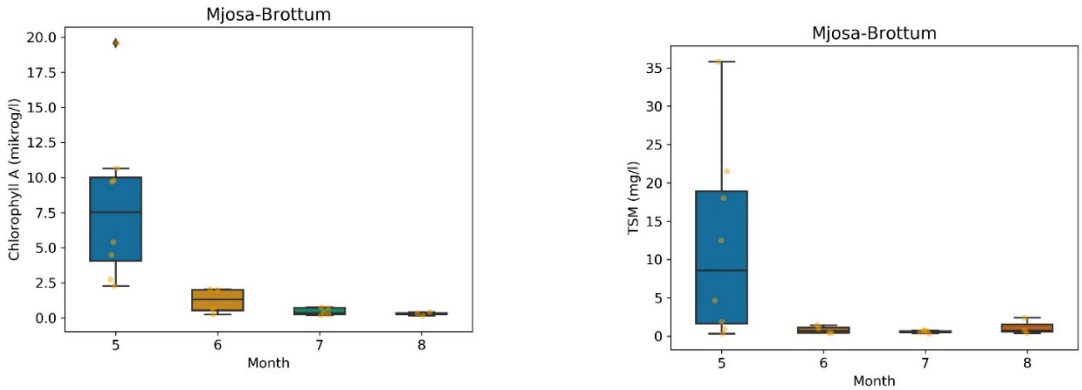

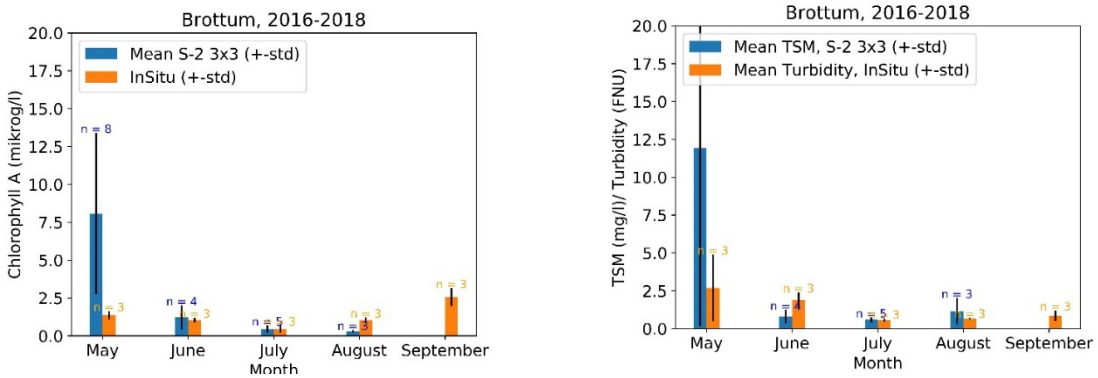

Figure 24. Top panel: Satellite monthly Chl-a and TSM shown as boxplots. The boxes represent the 25th percentile (Q1), 50th percentile (median, Q2) and the 75th percentile (Q3) of the dataset. The outermost bar represents the "minimum" (Q1-1,5*interquartile range (IQR), lower bar) and the maximum (Q3+1,5*IQR. upper bar). The orange dots represent the remote sensing observations. The black diamond is defined as an outlier. Bottom panel: Monthly averages with standard deviation bars for remote sensing Chl-a and TSM data and in situ Chl-a and turbidity data. The remote sensing data are CR2CC processed S-2 data.

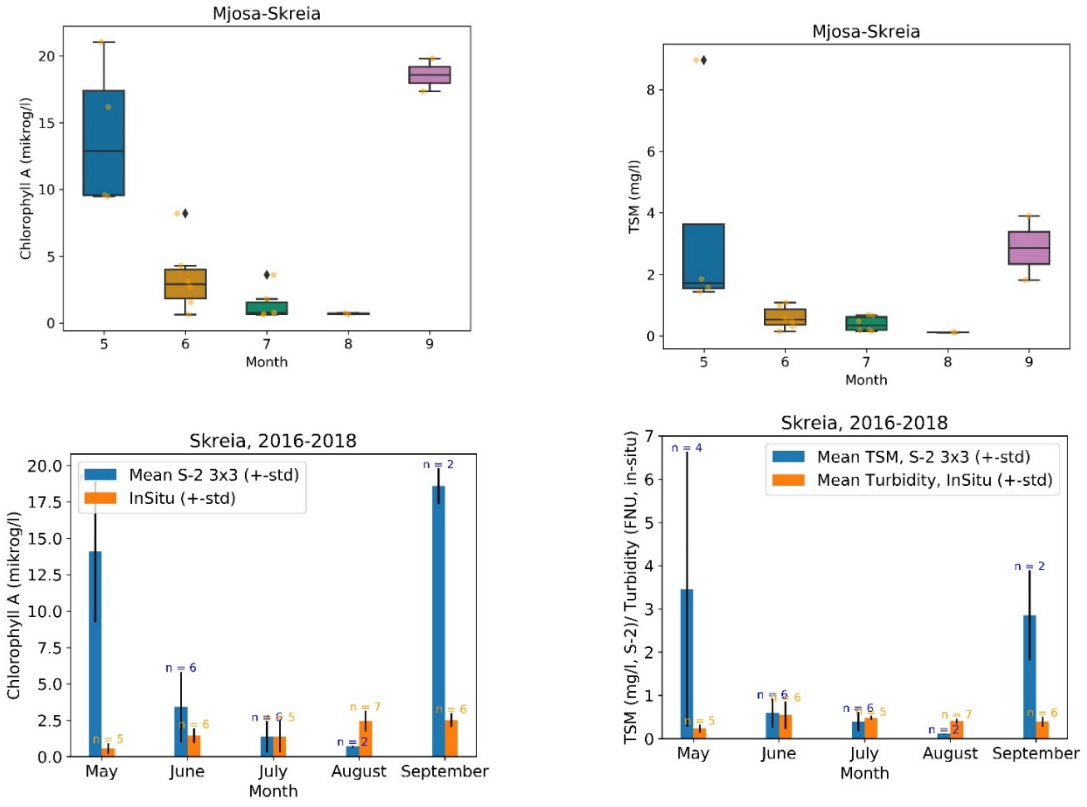

Figure 25. Top panel: Satellite monthly Chl-a and TSM shown as boxplots. The boxes represent the 25th percentile (Q1), 50th percentile (median, Q2) and the 75th percentile (Q3) of the dataset. The outermost bar represents the "minimum" (Q1-1,5*interquartile range (IQR), lower bar) and the maximum (Q3+1,5*IQR, upper bar). The orange dots represent the remote sensing observations. The black diamond is defined as an outlier. Bottom panel: Monthly averages with standard deviation bars for remote sensing Chl-a and TSM data and in situ Chl-a and turbidity data. The remote sensing data are CR2CC processed S-2 data.

5.5.3 Vansjø

In Van2 (Figure 26), a clear pattern is seen with increasing median Chl-a concentrations towards July and decreasing towards September. In Van1 the pattern is similar except from May, which have the highest median value and variation compared with the other months. In Van2, the highest variation is in July. The same pattern is seen for TSM in Van2. The remote sensing observations are comparable with the in situ measurements.

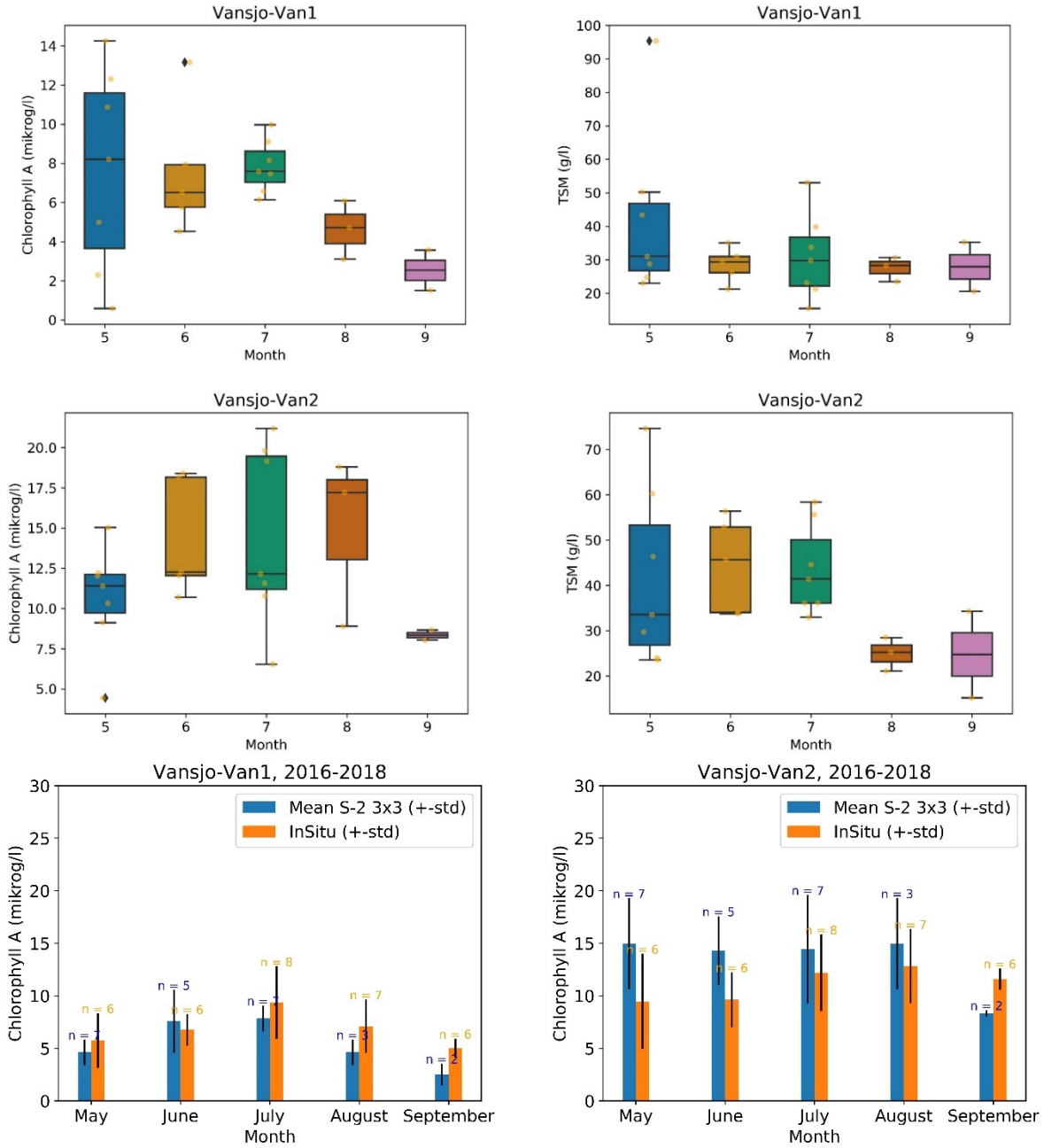

Figure 26. Top and central panel: Remote sensing monthly Chl-a and TSM shown as boxplots. The boxes represent the 25th percentile (Q1), 50th percentile (median, Q2) and the 75th percentile (Q3) of the dataset. The outermost bar represents the "minimum" (Q1-1,5*interquartile range (IQR), lower bar) and the maximum (Q3+1,5*IQR, upper bar). The orange dots represent the remote sensing observations. Black diamond are defined outliers. Bottom panel: Monthly averages with standard deviation bars for remote sensing Chl-a and TSM data and in situ Chl-a and turbidity data. The remote sensing data are CR2CC processed S-2 data.

5.5.4 Conclusions

- Monthly comparisons show that remote sensing observations are comparable with in situ data.
- The outliers found in the remote sensing data can either be from events captured by the remote sensing observations or it can be from failed atmospheric corrections.
- Including also partial cloudy scenes will increase the number of remote sensing observations.

5.6 Spectral signature with S-3

The Copernicus Global Land Service[4] and its Lake Water Quality (LWQ) products use Polymer for the AC. The LWQ-product is a 10 days average. Here we only look at the spectra from Polymer since the turbidity product from Brøttum gave poor results and these are therefore not presented. Since the phytoplankton product is given as a trophic state and not as Chl-a concentrations these are not considered and cannot be evaluated.

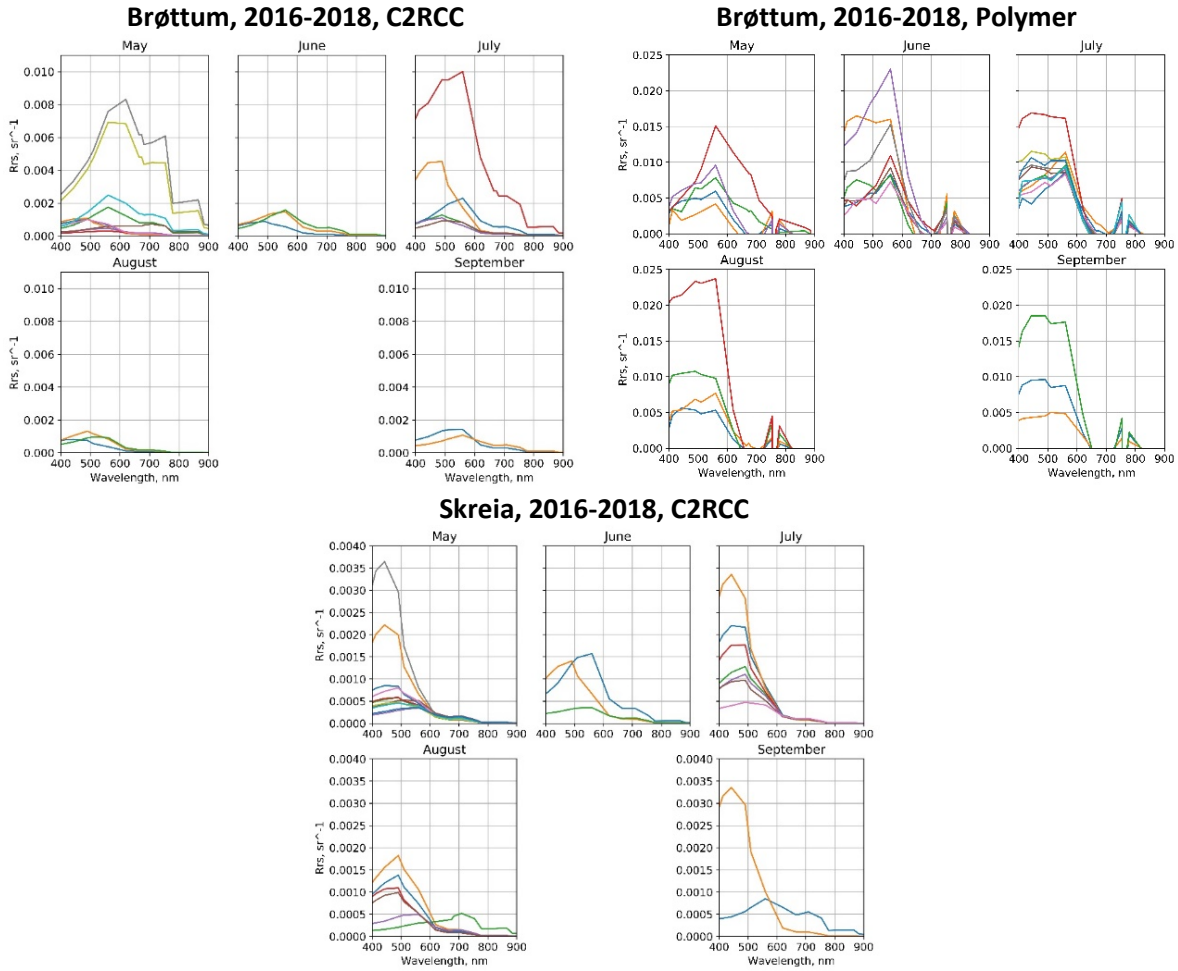

Figure 27. Remote sensing reflectance (R_{rs}) from C2RCC and polymer processed S-3-data extracted from Brøttum and Skreia in Mjøsa. All data are from 2016 to 2018 and from clear sky scenes.

The shape of the R_{rs} spectra from S-3 using C2RCC and Polymer AC in Mjøsa are shown in Figure 27 for station Brøttum (C2RR and Polymer) and Skreia (C2RCC only). The C2RCC spectra in Brøttum and Skreia

[4] https://land.copernicus.eu/global/products/lwq

differ, and the spectra differ in-between the months. At Brøttum, the high intensity of the spectra in May was also seen in the S-2 data, whereas July in the S-3 data have the highest R_{rs} peak in 560 nm for all the months. The shape between May and July in Brøttum differ, where two days in May has its maximum in the 620-band (channel for particle loading, Table 3) with an increase from red to NIR. As seen in Figure 18, the result of melting in the mountains gave a particle plume from the runoff from Gudbrandalslågen in May. The R_{rs} from one date in July have a clear peak in the 560-band, while the peak for the other shapes in July vary.

The spectra from the Polymer AC for the 10 days product have different magnitude and shapes than the C2RCC and it is also giving negative R_{rs} for some dates. It is difficult to compare the shapes between these two AC processors directly since the Copernicus product is not giving the daily results, but rather an average or composite, and the seasonal product is not directly relevant for the Norwegian WFD purpose. Within the product itself, there are no information on which days that are included in the 10-days average.

5.6.1 Time series of Chl-a and TSM with S-3 from Mjøsa

In Figure 28 the time series of Chl-a and turbidity from S-3 C2RCC in Brøttum and Skreia show that the low values are well captured. Still for some dates the Chl-a seem to be underestimated, particular in 2016 and in end 2018. This is seen also for the other time series from the S-2 observations. The high values in May was seen also in the S-2 data and are as explained due to the particle plume from Gudbrandalslågen, also shown in the S-3 RGB image in Figure 29.

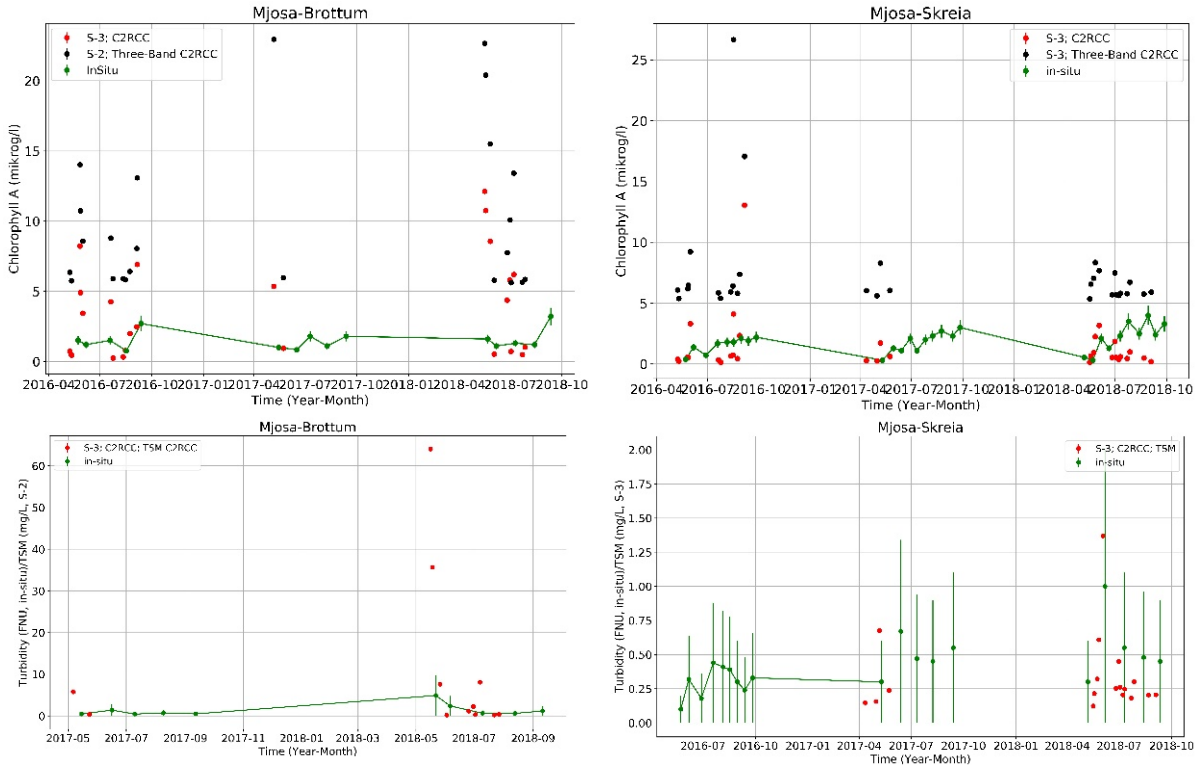

Figure 28. Time series of Chl-a and turbidity from S-3 from Brøttum and Skreia in Mjøsa.

Figure 29. An RGB image from S-3 on the 16th of May 2018 showing the result of melting in the mountains with a particle plume coming from the outflow of Gudbrandalslågen further north of this station.

5.6.2 Seasonal analysis of Chl-a and TSM with S-3 from Mjøsa

In Brøttum in Figure 30 (a and b) the variation is largest within May for both Chl-a and TSM, as seen also with S-2. For TSM there are defined outliers, but these are likely from the shown plume even though the TSM concentrations is very high. The biggest difference between S-3 data and in situ data is within the Chl-a and in May and June. There were no remote sensing observations from S-2 in September, but the other months have the same pattern as for S-3 with decreasing Chl-a until August. In Skreia in Figure 31 the pattern is different with larger variations within August and September. The measuring frequency of in situ data was higher in Skreia than in Brøttum, resulting in generally more available in situ data than remote sensing observations. The large variation in September is based on observations from only two dates resulting in the largest difference we found between the RS observations and the in situ data.

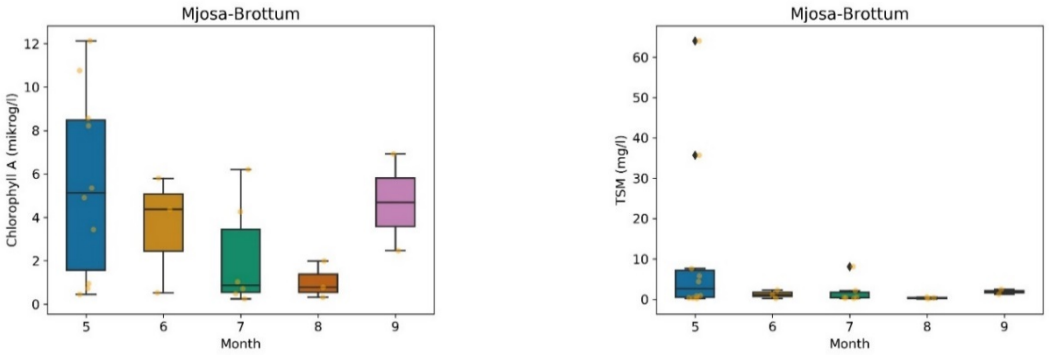

Figure 30a. Top panel: RS monthly Chl-a and TSM shown as boxplots. The boxes present the 25th percentile (Q1). 50th percentile (median. Q2) and the 75th percentile (Q3) of the dataset. The outermost bar represents the "minimum" (Q1-1.5*interquartile range (IQR). lower bar) and the maximum (Q3+1.5*IQR. upper bar). The orange dots represent the RS observations. The black diamond is defined as an outlier.

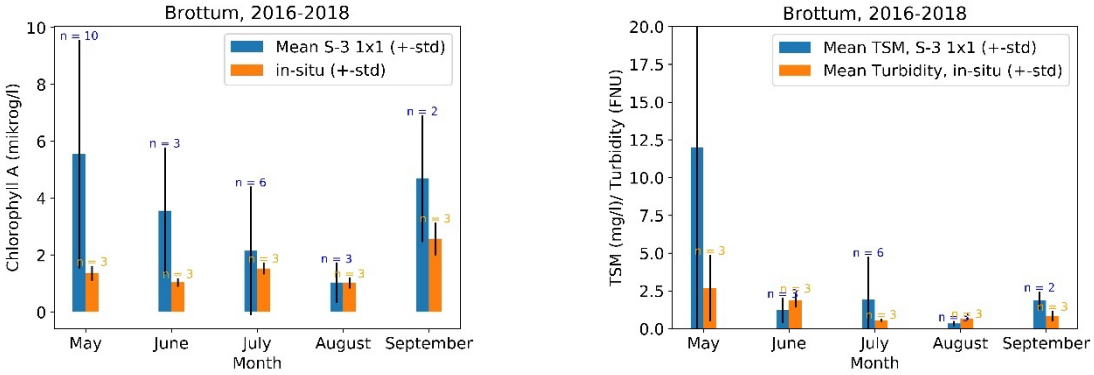

Figure 30b. Bottom panel: Monthly means of Chl-a and TSM from S-3 and comparison to in situ data for station Brøttum in lake Mjøsa.

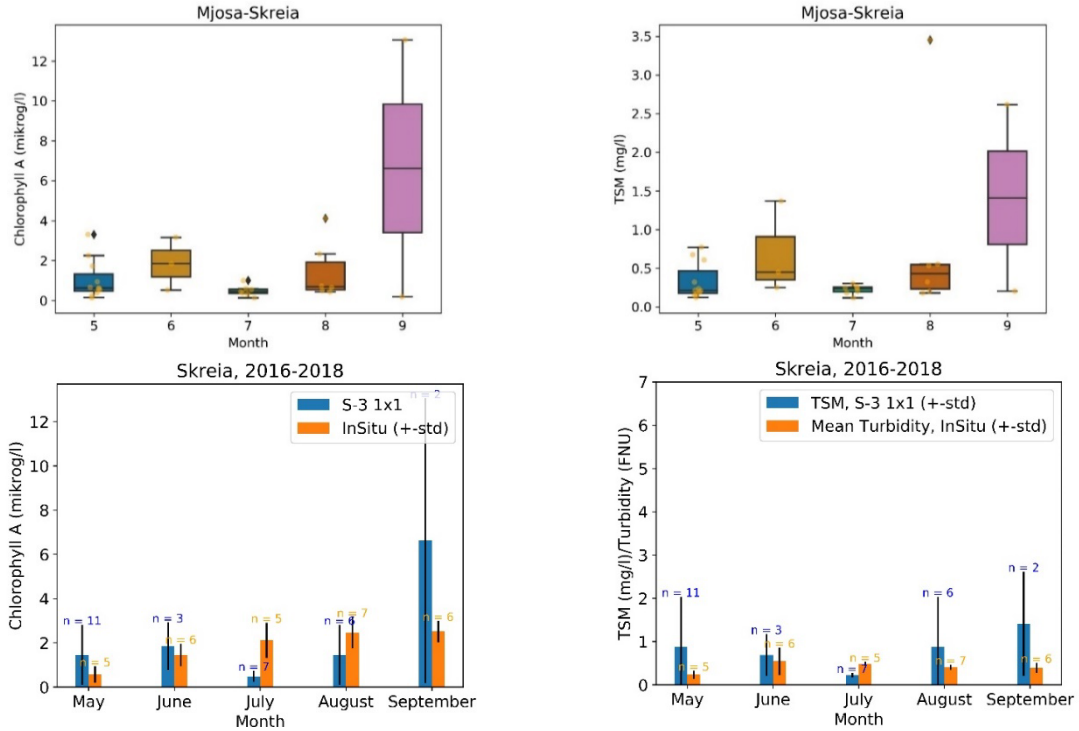

Figure 31. Top panel: RS monthly Chl-a and TSM shown as boxplots. The boxes present the 25th percentile (Q1), 50th percentile (median, Q2) and the 75th percentile (Q3) of the dataset. The outermost bar represents the "minimum" (Q1-1,5*interquartile range (IQR), lower bar) and the maximum (Q3+1,5*IQR. upper bar). The orange dots represent the remote sensing observations. The black diamond is defined as an outlier. Bottom panel: Monthly means of Chl-a and TSM from S-3 and comparison to in situ data for station Skreia in lake Mjøsa.

5.6.3 Conclusions from S-3

- The shapes of the spectra look overall reasonable for S-3, but in situ reflectance data is needed to validate these properly.
- The Copernicus Global Land Service and the Lake Water Quality product was difficult to evaluate for since the products is predefined 10-days composite and the days are not specified.
- Including remote sensing data will increase the data retrieval and events is captured with these data not identified with in situ data.
- More scenes can be derived if partial cloudy days are included to the dataset after thorough quality control.

6 Chl-a WFD status classification

6.1 Method

With the use of remote sensing data in WFD classification Chl-a, Secchi disc depth, TSM and other products such as cyanobacteria products can be used. In this report, the Chl-a classification is presented. The Chl-a classification from each of the lakes have been produced using the L3 binning module in Snap. Snap is the processing tool for earth observations (EO) data developed for ESA by several companies. It includes toolboxes for MERIS, S-2 and S-3 among other satellite sensors. Newly developed processors, such as the OC-Smart (Marty, 2018, 2019), can be included into Snap as plug-ins. The clear sky scenes from 2016 to 2018 have been averaged pixel by pixel giving each pixel an average Chl-a value for these three years with a spatial resolution of 100 m. The binning period used is May to September. Remote sensing data from October don't provide any realistic values and is therefore not included in the binning. Each lake is defined as a certain water type dependent on its typology, and the correct status class-range is used for the corresponding lake type. Each pixel is then given a colour corresponding to the water quality class. In this work nEQR values are not calculated.

The calculated statistics for each of the lakes are based on a defined lake polygon (Region of Interest, ROI) where each pixel within the polygon is considered. With these statistics, the average concentration of Chl-a at the station point can be compared with the average concentration for the whole lake. The Hemnessjøen classification is placed in Appendix F.

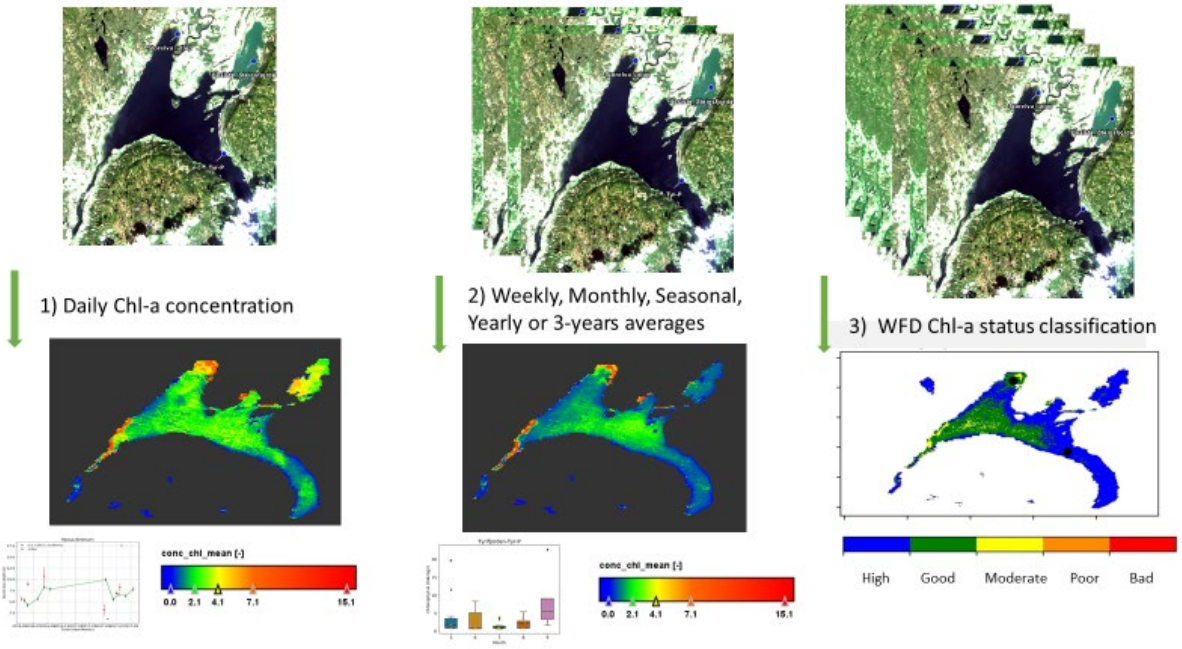

Figure 32. Remote sensing data for operational monitoring, WFD reporting and WDF status classification.

6.2 Steinsfjorden

In water quality monitoring, Steinsfjorden is considered as another water body than the rest of Tyrifjorden, and therefore the L3-data in Figure 33 is produced only for Steinsfjorden. The classification shows no large spatial variations within the lake and the status based on remote sensing observations is "High status". The statistics from Steinsfjorden (Table 9) show a mean value of Chl-a concentration

for the whole lake of 4,04 µg/l and 90% of the pixels in the lake have concentrations below 4,8 µg/l which clearly indicate small spatial variations.

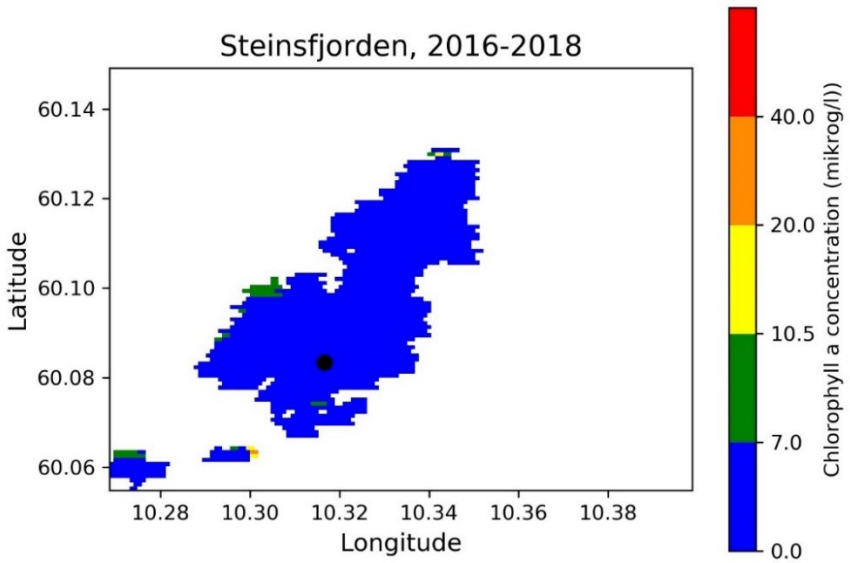

Figure 33. Classification per pixel (100 m resolution) for Steinsfjorden based on scenes from 2016 to 2018 for water type L109/L-N1. The station point used as monitoring station is marked as black circle point.

In Figure 34, the pixel distribution of the mean Chl-a concentration (left) and the calculated percentile distribution (right) are shown graphically. Up to 99% of the pixels in the lake have mean Chl-a concentrations below 6 µg/l. In Figure 35 different scales of classification are presented showing the mean Chl-a concentration for the whole lake (blue), remote sensing data from the monitoring station point (orange) and from in situ data (grey). The differences between these scales are very small. The figure illustrates the low spatial variation within the lake, and the remote sensing observations give comparable values with the in situ data.

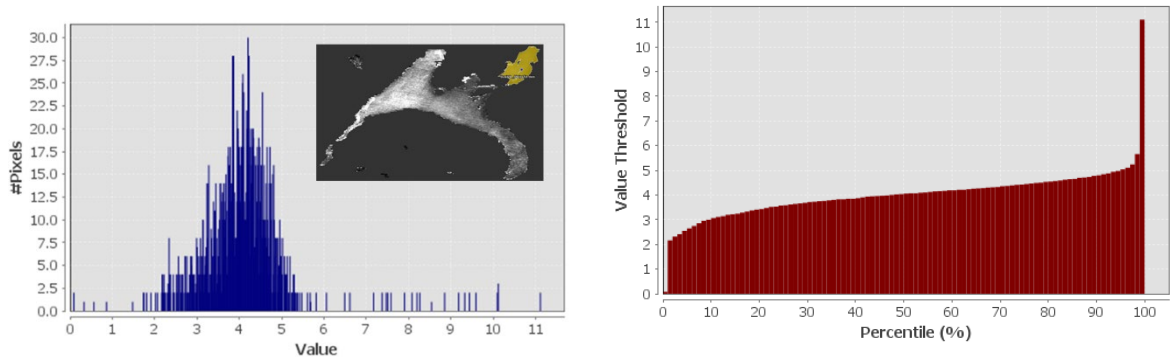

Figure 34. The mean Chl-a concentration distribution over the pixels and the percentile distribution of the pixels with value threshold of the mean Chl-a concentration in Steinsfjorden (shown as yellow polygon).

Table 9. The mean Chl-a concentration distribution over the pixels and the percentile distribution of the pixels with value threshold of the mean Chl-a concentration in Steinsfjorden.

Number of considered pixels:	2265
Minimum:	0.08
Maximum:	11.11
Mean:	4.04
Standard deviation:	0.92
P10 threshold:	3.07
P25 threshold:	3.59
P50 threshold:	4.06
P75 threshold:	4.45
P90 threshold:	4.80

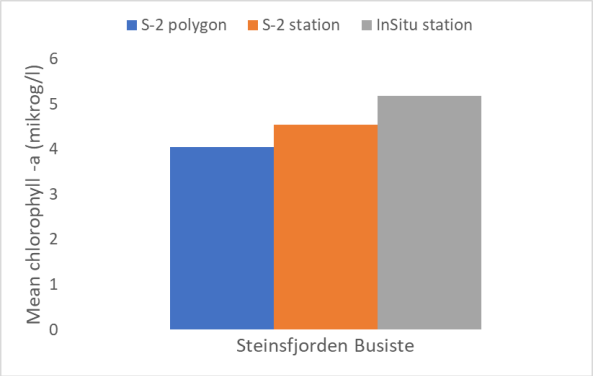

Figure 35. Average of different scales for Steinsfjorden with blue bar showing the mean Chl-a value for the whole lake (all pixels included, npixels = 2265), orange the remote sensing data for the monitoring station (npixels = 136) and grey the in situ data (nobs = 15). Data from May to September 2016 to 2018.

6.3 Tyrifjorden

At the main Tyrifjord station, Tyr-P, there is larger spatial variation than in Steinsfjorden. There were unfortunately no in situ measurements from the outflow of Storelva other than the ones taken in 2019. Hence, it is hard to determine whether the higher mean Chl-a concentrations in this area (black point northwest in Figure 36) are generally this high or if it is an area high of particles (TSM was higher at Storelva outflow, 0,8 mg/l, than at Tyr-P with an average on 0,61 mg/l) or high on cDOM. Both the cDOM values and FARGE was higher at the river outlet than at Tyr-p (Table 8) while Chl-a was lower. In addition, there are different spectra shapes between station Tyr-P and the outflow of Storelva (Figure 13).

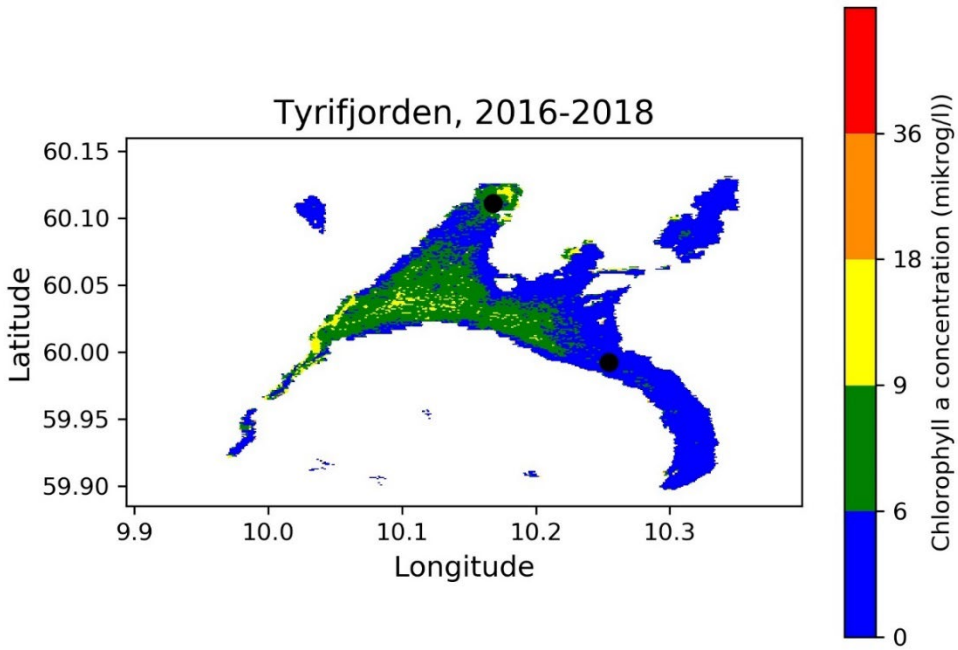

Figure 36. Classification per pixel for Tyrifjorden based on scenes from 2016 to 2018 for water type L107/L-N1. The station point used as monitoring station is marked as black circle points.

The pixel distribution of the mean Chl-a concentration from Tyrifjorden in Figure 37 show a bigger spread of pixels over the mean Chl-a concentrations than what was seen for Steinsfjorden. 90% of the pixels have concentrations between 2,5 µg/l (status "High") and 8,31 µg/l (status "Good") (Table 10).

There are in situ data only from 2016 for Tyr-P, and no in situ data from the outflow area of Storelva. Therefore, no comparisons between remote sensing observations and in situ data are shown. Still, when comparing each of the station points with mean Chl-a concentrations from the entire polygon, Storelva have higher mean concentrations while Tyr-P have comparable concentrations with the mean of the polygon. When classifying using the remote sensing -observations the mean Chl-a concentration correspond to "High status", the same for station Tyr-P while at Outflow Storelva it would be "Good status". The in situ mean Chl-a (May to September in 2016) from Tyr-P is clearly lower than the remote sensing observations. At Tyr-P during 2016 to 2018 there are some scenes with too high concentrations, and as discussed this is likely due to noise.

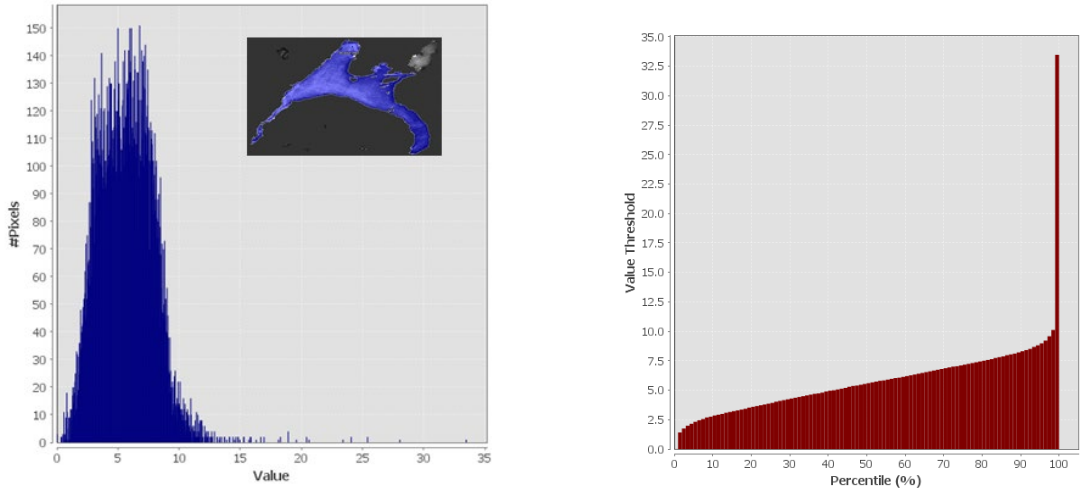

Figure 37. The mean Chl-a concentration distribution over the pixels and the percentile distribution of the pixels with value threshold of the mean Chl-a concentration in Tyrifjorden (shown as blue polygon).

Table 10. The mean Chl-a concentration distribution over the pixels and the percentile distribution of the pixels with value threshold of the mean Chl-a concentration in Tyrifjorden.

Number of considered pixels:	**22822**
Minimum:	0.01
Maximum:	33.47
Mean:	5.64
Sigma:	2.20
P10 treshold:	2.85
P25 treshold:	3.92
P50 treshold:	5.60
P75 threshold:	7.17
P90 threshold:	8.31

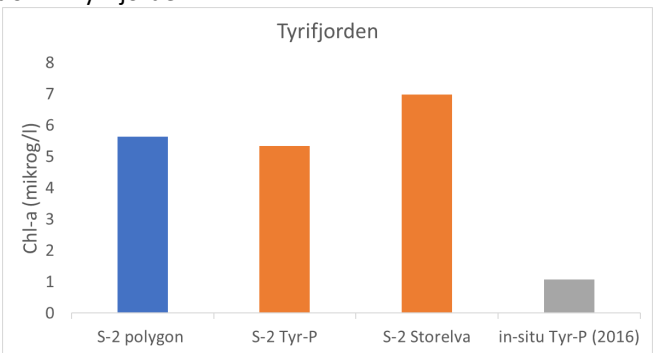

Figure 38. Average of different scales for Tyrifjorden where blue bar indicates the mean Chl-a value for the whole lake (all pixels included) (npixels = 22822), orange remote sensing data for the monitoring station (npixles = 54) and grey from the outflow Storelva station (npixels = 19). Data from May to September 2016 to 2018.

6.4 Mjøsa

As in Tyrifjorden there were spatial variations within Mjøsa. For the area around Skreia (the southernmost station point) the higher concentrations were likely affected by the situation seen 31st

of May 2018 (shown in Figure 20). High winds have seemed to affect the water surface resulting in specular reflection of the signal to the detector, called “glint”. This results in very high, but false, calculated Chl-a concentrations. Such episodes need extra consideration, either to decide if they should be included in the final product or if additional processing is needed (e.g. glint handling).

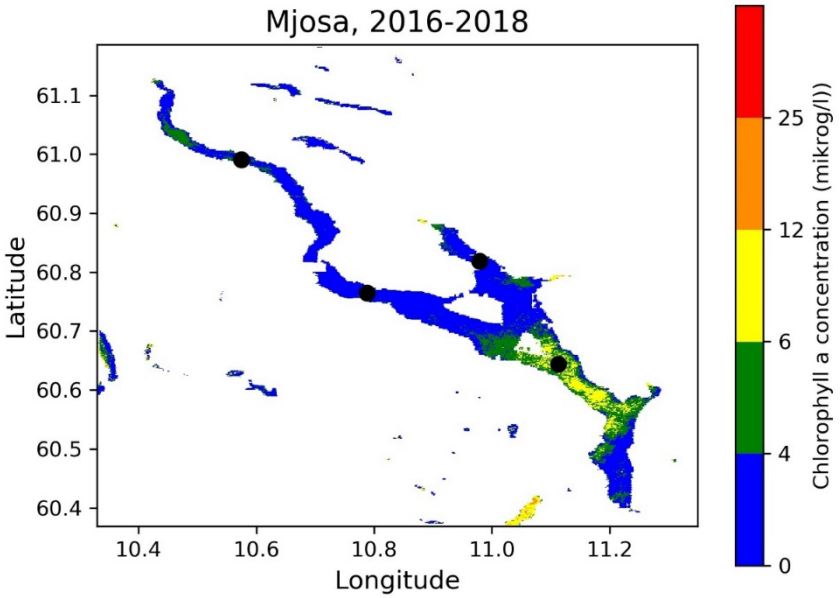

Figure 39. Classification per pixel for Mjøsa based on scenes from 2016 to 2018 for water type L206/L-N6. The station point used in as monitoring station is marked as black circle point.

The pixel distribution of the mean Chl-a concentration from Mjøsa (Figure 40) show as distribution around 3,29 Chl-a µg/l (status “High”). In Mjøsa 90% of the pixels have mean Chl-a concentrations below 5,79 µg/l and 75% below 4,35 µg/l. The mean Chl-a concentration of the whole lake is 3,65 µg/l equivalents with status “high”. The classification of the remote sensing observations from Brøttum is similar as the mean of the whole lake, but when compared with the same classification based on in situ measurements the remote sensing mean value is higher, but within same status class. This difference is due to outflow plume observed in the remote sensing data in May 2018, but not captured by the in situ data (shown in Figure 18). From both Kise and Furnesfjorden, the remote sensing and in situ classification are comparable. Skreia is the station that differ the most from the mean of the whole lake and based on the remote sensing classification the stations would status “good”. As for Brøttum there are clear differences between the remote sensing and the in situ data. Clear sky scenes from Mjøsa showed two situations in September 2018 resulted in unrealistic high Chl-a concentrations. One date seemed to have a large wind effect on the lake and one date seemed to have a lot of noise. For those cases, even with clear sky a more thorough processing is needed.

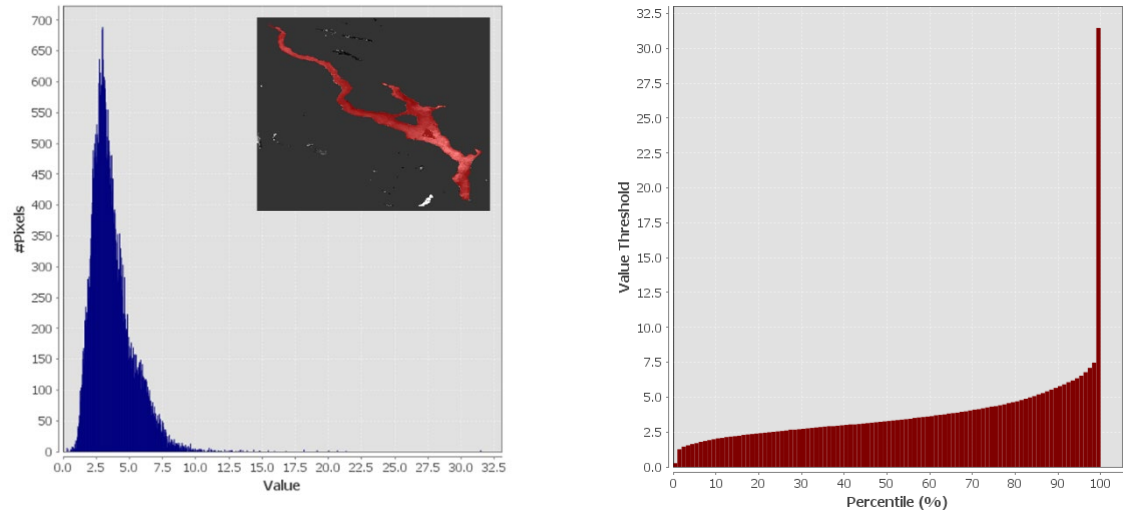

Figure 40. The mean Chl-a concentration distribution over the pixels and the percentile distribution of the pixels with value threshold of the mean Chl-a concentration in Mjøsa (shown as red polygon).

Table 11. The mean Chl-a concentration distribution over the pixels and the percentile distribution of the pixels with value threshold of the mean Chl-a concentration in Mjøsa.

Number of considered pixels:	**53040**
Minimum:	0.27
Maximum:	31.47
Mean:	3.65
Standard deviation:	1.53
P10 threshold:	2.05
P25 threshold:	2.58
P50 threshold:	3.29
P75 threshold:	4.35
P90 threshold:	5.79

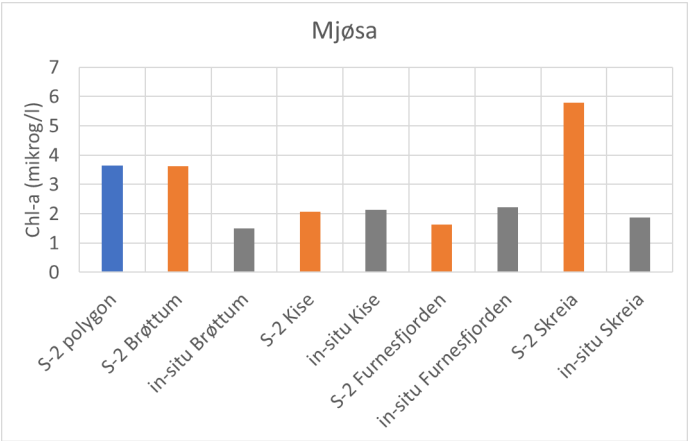

Figure 41. Average of different scales for Mjøsa where the blue bar indicates the mean Chl-a value for the whole lake (all pixels included) (npixels = 53040), orange remote sensing observations from the monitoring stations (npixels_Brøttum = 18, npixels_Kise = 69, npixels_Furnesfjorden = 68,5, npixels_Skreia = 45) and the grey from the in situ measurements from the monitoring stations (nobs_Brøttum = 15, nobs_Kise = 21, nobs_Furnesfjorden = 15, nobs_Skreia = 29). Calculations based on May to September from 2016 to 2018.

6.5 Vansjø

The classification for Vansjø in Figure 42 showed differences between Vanemfjorden (the basin to the left) and Storfjorden (to the right). With the WFD classification, most of the pixels in Vanemfjorden have Chl-a concentrations equivalent to status “moderate”. In Storfjorden several pixels have concentrations equivalent with status “moderate”, but several of these are very close to land and could be influenced by signal from land. With pixels close to land, water pixels can be influenced by reflected signal from land. These effects are called the adjacency effect and can give incorrect values. Most of the pixels in Vansjø have status “good”, but there are several with status “high” located close to station Van1.

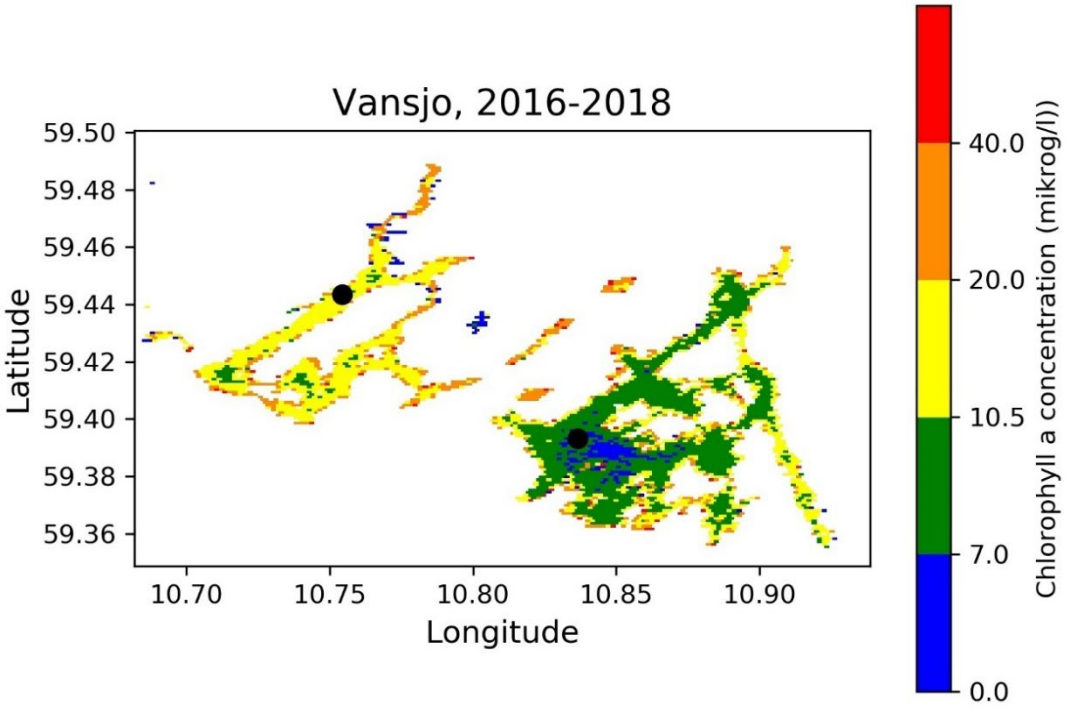

Figure 42. Classification per pixel for Vansjø based on scenes from 2016 to 2018 for water type L108/L-N8. The monitoring stations are shown as black points.

The pixel distribution in Vansjø (Figure 43) is quite distinct from the other lakes where 90% of the pixels have concentrations above 7,3 µg/l (in status "good" or worse), 75% is above 8,2 µg/l and 50% of the lake has concentrations above 10,9 µg/l (in status "moderate" or worse). These percentiles include also all pixels close to land.

Looking at the Chl-a from the station points from both remote sensing data and the in situ data, they are very comparable. Van2 is defined with status "moderate" for both remote sensing and in situ data. The mean in situ Chl-a from Van1 is 7,03 µg/l which is within status "good" while the mean remote sensing Chl-a is 6,6 µg/l which is within status "high". The remote sensing calculated mean of the whole lake is equivalent with status "moderate".

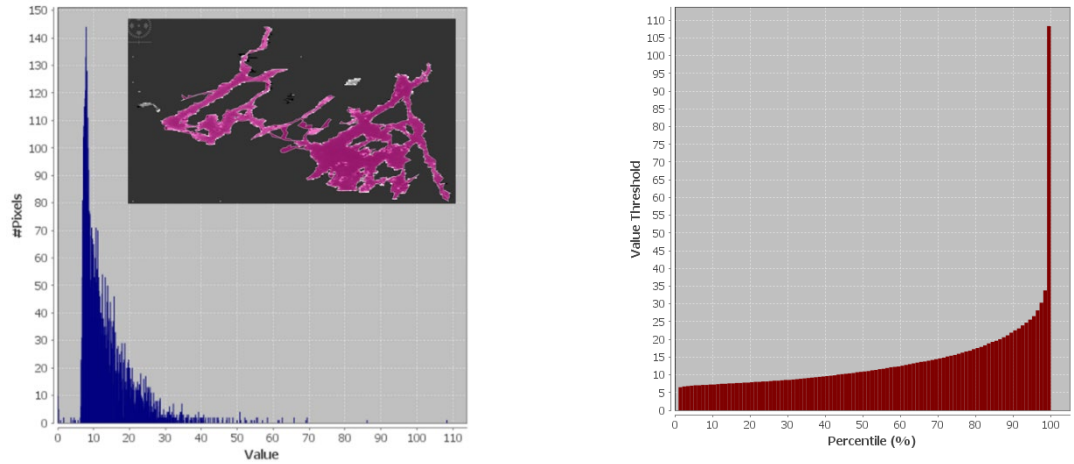

Figure 43. The mean Chl-a concentration distribution over the pixels and the percentile distribution of the pixels with value threshold of the mean Chl-a concentration in Vansjø (shown as red polygon).

Table 12. The mean Chl-a concentration distribution over the pixels and the percentile distribution of the pixels with value threshold of the mean Chl-a concentration in Vansjø.

Number of considered pixels:	**6468**
Minimum:	3.65E-04
Maximum:	108.4
Mean:	13.3
Standard deviation:	7.3
P10 threshold:	7.3
P25 threshold:	8.2
P50 threshold:	10.9
P75 threshold:	15.9
P90 threshold:	22.5

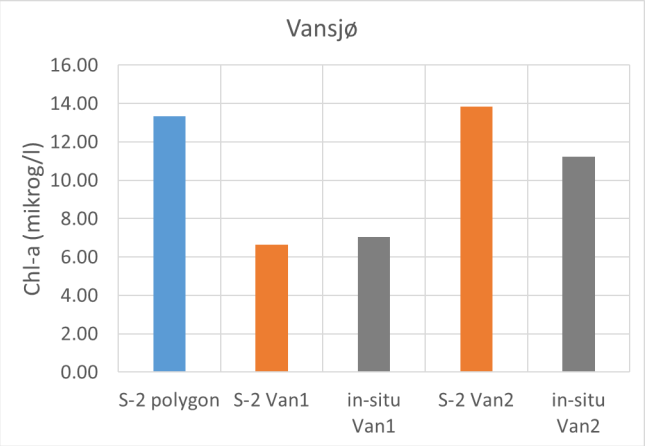

Figure 44. Average of different scales for Vansjø where the blue bar indicates the mean Chl-a value for the whole lake (all pixels included) (npixels = 6468), orange remote sensing observations from the monitoring stations (npixels_Van2 = 96, npixels_Van1 = 24) and the grey from the outflow Storelva station (npixels = 19). Calculations based on May to September from 2016 to 2018.

6.6 Conclusions

- Satellite data providing the mean concentration of each pixel within a lake shows large spatial variations and gives and important additional information of the status of the Lake
- In lakes with less spatial variations, the remote sensing classification for the lake as a whole and from the in situ station point reach similar classification
- The WFD status classification, based on the whole water body, in lakes with large Chl-a spatial variation will deviate more from the status assessment classification based on single points/ pixels, as seen in Tyrifjord.
- Events such as particle plumes from river outflow is captured by the remote sensing data and will be included in the classification product, which is not necessary the case for the in situ data.
- The spatial information gained from the satellites gives a better understanding for the representativeness of the in situ stations placements within the lakes.
- Scenes with failed atmospheric correction, either due to features such as “glint” or high noise, will affect the end-product due to false high Chl-a concentrations and need to be handled either by removing the scene from the binning or by additional processing.
- The Copernicus Global Land Service and the Lake Water Quality product was difficult to evaluate for the use WFD classification use since the products is a predefined 10-days composite.

7 Conclusions from the remote sensing Workshop in Oslo

A workshop on remote sensing in lakes and marine waters was arranged by NIVA in Oslo on the 5th and the 6th of September 2019. In the workshop 15 participants from eight different institutions attended including representatives from the NEA and the Norwegian Space Agency. Some of the participants (seven) were specifically invited to share their expertise on the use of applied remote sensing data

products for lakes and coastal waters. The participants of the workshop presented examples on remote sensing-based user applications for lake monitoring and cyanobacteria alert indicators. A part of the workshop was to receive the participants input to some specific discussion questions on how Norway can move forward to an operational use of remote sensing products for Norwegian lakes and coastal waters. The comments from the three discussion groups are presented below.

1) ***What products are mature to be used for monitoring of lakes and coastal areas and what are good enough accuracy for such a product?***
   - In general, does the Chl-a products work well. SYKE has developed and tested regional algorithms that takes the lake water types into consideration. They have also tested cDOM and turbidity products with good results. For high cDOM waters the CRCC2X algorithm has been used. The Flemish Environment Agency has started with a "proof of concept" for a smaller area that can be expanded.
   - Good enough accuracy depends on the area as well as the service provided. The expectations should be reasonable and in accordance with the purpose of the use.
   - The reflectance data from lakes can be very variable so it is a good practice to measure spectral data from different types of lakes. In Estonia they have built up a good dataset, but some lakes are still problematic for the use of remote sensing data.
   - It is preferable to connect the remote sensing products and data viewers to already existing information and data products websites, instead of developing completely new ones. Examples of this are the Finish TARKKA website and could be done for Norway as well as on a European level, in e.g. WISE[5].
   -
2) ***What steps next would you suggest for NEA to implement an operational remote sensing system (a service)? enough accuracy for such a product***
   - NEA should be precise in the needs for the service so the products can be targeted against the actual needs and be implemented.
   - Access to data and processing capacity is essential in addition to scientific support and tools to interpret data.
   - Can we predict a "bloom" forecast from Lake Mjøsa and can we use EO data for that?
   - Can be based on Calvalus or other Cloud services such the different DIAS's.

3) ***How can remote sensing fulfill/add important missing information to monitoring?***
   - More lakes can be monitored.
   - The spatial coverage is better.
   - More years with data - can fill the gap.
   - Maybe trend analysis can be performed when including historical remote sensing data.
   - Ice on lakes can be included, but maybe radar data are better. Still, RGB data can also be used.

4) ***How can we make the development continuous and not project dependent?***
   - SYKE development has been project based funding form H2020 and some from national funding.
   - A success that SYKE are both a "directorate and R&D institute"
   - NEA can easier use internal resources for development than external use of e.g. NIVA

[5] WISE Water Framework Directive Database (https://www.eea.europa.eu/data-and-maps/data/wise-wfd-3)

- R&D projects are still an important funding source
- As all monitoring is tender based it is important that remote sensing-based products are included in the tenders. Longer time of tenders can provide better services (e.g. 5 years from wetlands in Sweden).

5) What requirements do you see as essential for succeeding?

- SYKE work on the influence of the WRD to include new techniques.
- Need to use the most sensitive parameters (e.g. Chl-a).
- Always use the in situ data for continuous validation.
- Data used should always have a high quality.
- Choose the best algorithm that is already there and only develop your own when it is needed.
- Start simple. The Flemish started using data they got and with that they got experience. They started with time series and the Viewer. Changes can be added on when the users see the products and start working with them.
- Develop products and work with new algorithms in
- Continuous communication with the users
- Allocate both time and resources for a service to be developed. Acknowledge the development time and have along perspective
- Facilitate so that joint forces can be made, and parallel projects can benefit from each other.
- Include experienced experts in projects and cover the time they should spend on the project.
- Remote sensing is complementarity data- and there are different expectations on accuracy on the data. When is absolute or relative values needed?

6) What research activity are still needed

- Work more on OLCI (S-3) data
- Include rivers in the system
- Use spectral information to characterize the lakes
- SYKE used optical “classification” for algorithm testing and Estonia are working with it as well as different water types gives different reflectance data and may need a targeted choice of remote sensing algorithms.
- More hyperspectral data from lakes.
- Compare data between Nordic lakes. Finish, Swedish and Norwegian lakes are to some extent probable quite similar.
- Trend analyses on remote sensing data- supported for in situ data.
- Spatial changes of e.g. position of spring blooms or patterns over time- phenology-cyanobacteria.

7) Other suggestions or ideas?

- More functionality on the monitoring portals.
- Link to an existing service. Complementing on an already existing system. E.g. Aquamonitor-> Vannmiljø-> Wise[3] (end station). This concept was used for Cyanoalert, where an already website for bathing sites quality was in place and the input from real time remote sensing data was included to that service.
- Cyano-bacterial could e.g. come in as a new parameter/index.
- Include multi or hyper spectral measurements in the monitoring programs.
- Include more optical measurements in the monitoring programs.

- In Germany there is a current focus on remote sensing services for Lake temperatures. Lake ice. Phenology. Cyanobacteria and Grass roofs of federal buildings (as a climate change mitigation).

Some things were brought up several times and that was the identification from the users (e.g. NEA) for the purpose to start using the data- what applications should the focus be on. It is the applications that decides on the data requirements and the accuracy. What service is asked for - to whom and for what? The tenders should be precise on the requirements. Uncertainties should always be included. but at the right level for the use. e.g. may a warning for cyanobacteria at beaches have trigger values. but the accuracy may be lower. One other main point was to use current systems for water quality data and link it/ include remote sensing data in the databases. The need for longer strategic efforts was also stressed.

The workshop agenda and participant list are included in Appendix G.

8 Road map of an operational service

For an operational remote sensing system to be implemented for Norwegian marine waters and lakes we have identified several steps on the way. A conceptual model describing a general cycle of monitoring programs are illustrated in Figure 45, while Figure 46 is a road map for implementation of an operational system of remote satellite sensing data for lakes. However, it should be noted that this represent the general steps and that specifically defined end-products need a more detailed plan with additional implementation steps based on the defined product needs.

In Step 1 and 2 in Figure 46, these are the basis and is connected to the output of the conceptual model in Figure 45, where the products asked for are identified and developed (first box). Step 3 to 6 includes digital solutions such as cloud services for processing and storage as well as collaboration with the existing data dissemination platforms in Norway such as Satellittdata.no and colhub.met.no. This will take time to set up and require long-term development, but once it is running the system will be operational. A conceptual model for Step 3 to Step 6 is presented in Figure 47.

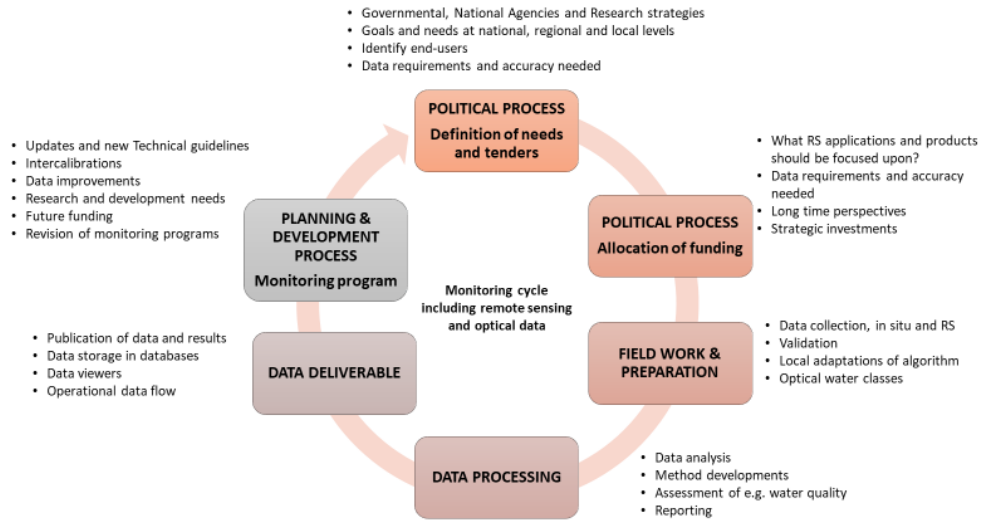

Figure 45. Conceptual model describing the cycle of monitoring programmes with inclusion and development of remote sensing and optical data. Adapted from Harvey et al. (2018).

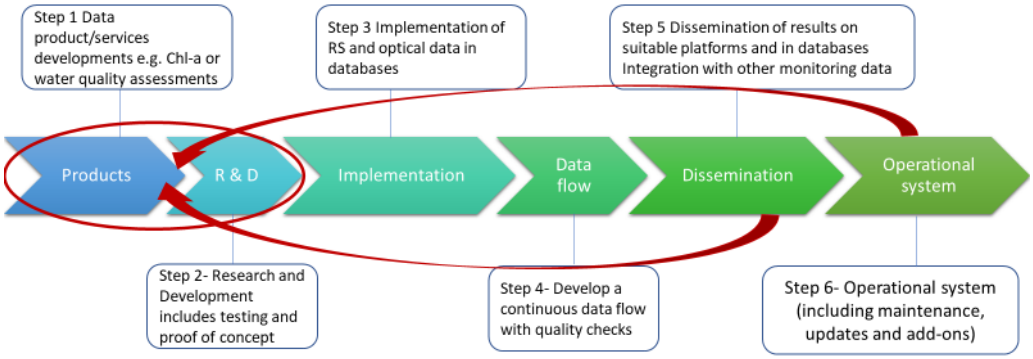

Figure 46. Road map for an operational system of remote sensing data in Norwegian lakes. The red ring marks the steps covered by this project and the two arrows represents feedback on the system for developments.

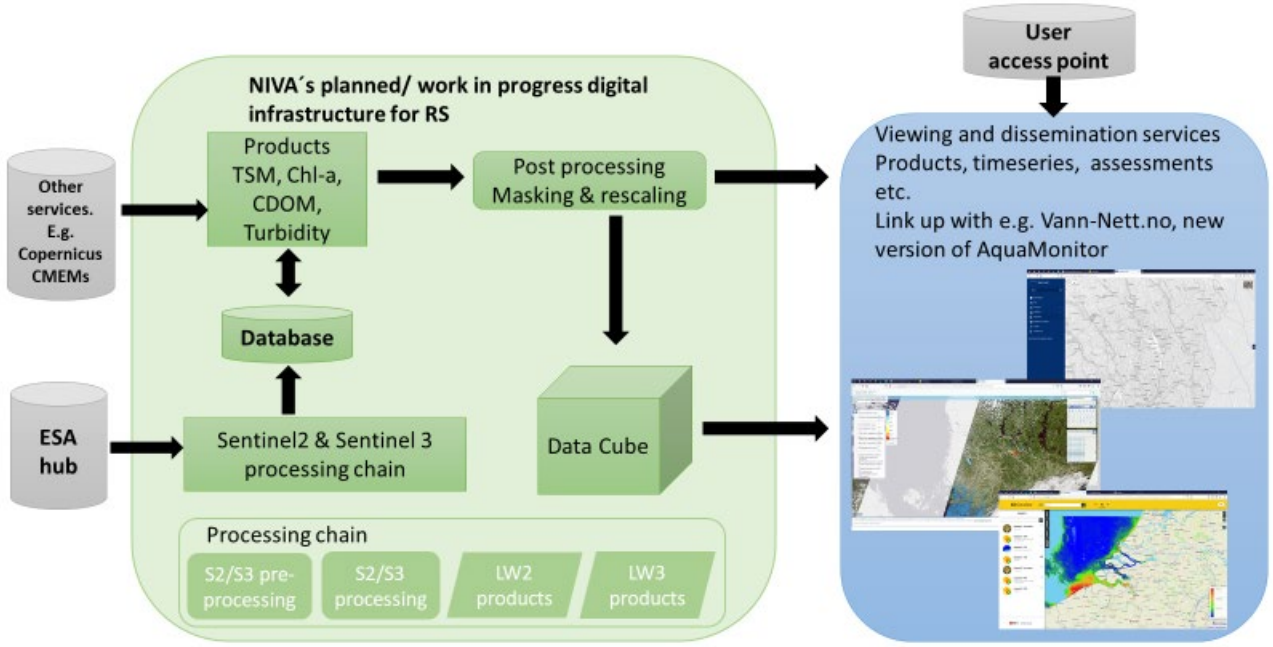

Figure 47. A schematic view of the data flow including download of data (dependent on data structure to handle data amount, either cloud or local storage) and processing data facilities (either local or on a cloud/Dias).

To move forward, different projects should be initiated. The results from this study with the production of remote sensing product, time-series and maps for Chl-a could be developed. These would for now be based on the C2RCC processor for a limited number of lakes. Still, in parallel a R&D project would be necessary for a proper validation of the R_{rs} data and an evaluation of the algorithm's conversion factors for these lakes. This requires additional sampling, both from the already defined monitoring program and extra sampling and measuring campaigns. For the evaluation of the conversion factors, analyses from water samples on Chlorophyll pigment absorption should be performed on samples from the monitoring program to establish the relation to Chl-a. In addition, UV and VIS absorption spectra should be analysed along with the parameter FARGE (for a conversion to cDOM). Since all remote sensing products are derived from the R_{rs} product, a dedicated match-up campaign is necessary for a sound validation of the derived R_{rs} from the atmospheric corrections. This should be done for several lakes with different optical properties. To make sure the dataset is solid, these projects should

be run for a certain time period. The lakes should be chosen from the ØKOSTOR Water Framework Directive monitoring program (e.g. Mjøsa, Gjende, Selbusjøen, Takvatnet, Vansjø, Femunden, Eikesdalsvatnet, Snåsavatnet, Salsvatnet, Limingen and Røsvatnet) starting already in 2020. For the parallel sampling we would collect in situ observations of:

- IOPs; UV and VIS absorption spectrum in addition to FARGE with min 5 cm cuvette to calculate spectral slopes of cDOM
- AOPs; radiance, irradiance and k_d measurements to validate the R_{rs}.
- IOPs; apig from water samples and possibly a and c from ac9 instruments and bbp from bb6 sensor.
- Secchi disc depth

In the reporting from the 2020 monitoring, products from remote sensing data can be included and below are examples of such products:

- Develop a merged product based on a combination of S-2 and S-3
- Daily Chl-a time series products based on S-2 and S-3 data per lake from location points in the lake
- Boxplots with monthly means
- Map of monthly means of Chl-a concentrations per lake (April to September)
- Map of monthly means of Secchi disc depth per lake (April to September)
- Map of monthly means of TSM per lake (April to September)
- Possibly map of monthly means of cDOM per lake (April to September)

The development of such maps will require IOP data (apig, bp, bbp, spectral slopes) for a proper dataset for deriving empirical relationships between apig and Chl-a concentrations, and between scattering and TSM products.

9 Future Research; priority for Norwegian lakes

More radiometric and IOP data is needed to validate the remote sensing reflectance and to gather a substantial in situ dataset that can be used to derive and evaluate if regional conversion factors for Chl-a and TSM would improve the satellite products for Norwegian lakes. This could be facilitated by collecting extra water samples, for Chlorophyll pigment absorption (apig), attenuation, total absorption and cDOM absorption analyses, as a part of the monitoring program for instance in lake Mjøsa, which is sampled yearly and therefore also in 2020. The absorption and scattering properties, light attenuation (kd (PAR)) and the water leaving reflectance needs to be collected in situ from boats. This could be solved by an expert joining the monitoring sampling and or training of the persons conducting the monitoring. By this way the resources would be used efficiently. Those data should ideally be gathered over several lakes, seasons and several years to be able to capture as much variability as possible and to build a robust dataset for building and testing of empirical algorithms. This should be set up as a parallel R&D work, running over 3-5 years and a focus should be on the improvement of the algorithms and to establish regional or lake type bio-optical models.

Ideally, there should be more match up programs with dedicated sampling campaigns when there are clear skies and overpasses of the satellite sensors within 1-3 h, but this is challenging. Fit for purpose match up data provides good comparisons and possibilities for correlation studies between the in situ parameters (Chl-a, TSM, Turbidity, cDOM and Secchi disc depth), reflectance and the remote sensing Atmospheric Corrections and products, such as R_{rs}. The match-up datasets will be used for testing regional empirical algorithms and conversion factors for Chl-a. Today we not fully understand what is

causing discrepancies between remote sensing data and the in situ data sometimes seen in the time-series; it can be caused by a failure in the AC, wrong conversion factors, high cDOM absorbance interfering with the Chl-a signal or simply differences in the timings, which is a known source of error. This type of sampling should initially be focused on a few lakes to make sure that the work is achievable and successful.

The downloading and processing of satellite data is a large part of the process and NIVA is currently building up the expertise and technical solutions for a smooth data flow and processing schemes. The current work is mainly focused on coastal areas (currently project based) but can as soon as it is established in full, also include lakes.

Specific warning systems for toxic algae blooms or other type of events can be developed. For example, warning systems are in place for potential toxic algae, flooding or cyanobacterial blooms in other countries, e.g. Sweden and Germany for lakes (CyanoAlert) or in the Baltic Sea (Cyanobacterial bloom prognoses for the Baltic Sea by SMHI). For this, a specific processor developed for MERIS and S-3 could be used; the MPH Processor calculates Chl-a concentrations by means of the **M**aximum **P**eak **H**eight and specific arithmetic expressions for different water types. Within the processor there are flags provided for floating material, eukaryote/cyanobacteria dominance and an adjacency effect indicator for each pixel.

Some more specific points of development have been identified during this work;

- Evaluation of OLCI (S3) data.
- Application of the MPH Processor in specific lakes.
- Expand the study areas to more lakes with more than one replicate of each lake type. Those lakes can be selected based on initial groupings into optical water types (OWT) based on the spectral information in the R_{rs}.
    SYKE used optical "classification" for algorithm testing, and this work is also done in Estonia as different water types gives different reflectance data and may need a targeted choice of remote sensing algorithms.
    Analyze the optical spectral signature of the different lakes to see if there are more "information" in the data
- Compare data between Nordic lakes. Finish, Swedish and Norwegian lakes are probably to some extent quite similar.
- More collection of optical in situ data to be used for;
    - Trend analyses on remote sensing data- supported for in situ data.
    - More hyperspectral data for algorithm development and identification of phytoplankton functional groups.
    - Examining spatial changes of e.g. position of spring blooms or patterns over time- phenology- cyanobacteria.
    - The inclusion of rivers in the system.
- Evaluate other AC's that have shown to be promising in other areas;
    - Polymer AC is applied with good results in Baltic regions/lakes.
    - C2RCCX AC (adapted to extreme waters and high cDOM absorption and TSM concentrations) for all lakes, since it is applied with good results in the Baltic regions/lakes, also in clear lakes.
- Develop operational quality checks of R_{rs} spectra (sometimes failing with an artificial peak at 490 nm, and "kicks" in the blue spectra).

10 Conclusion

The aim of this project was to test the use and applications of remote sensing data in selected lakes included in the lake monitoring programs run by the Norwegian Environment Agency (NEA). Monitoring of lake water quality for the Water Framework Directive (WFD) is challenging due to the large number of lakes, and the remote location on some of these, which results in that some lakes are not regularly monitored. With the European Commission Copernicus programme, several adapted satellite sensors for the retrieval of water quality data are in place. Today, this technique and the availability of data at high spatial resolution (60-300 m), enables an operational use of data collected by the satellite sensors, which in the near future can be merged and used as a complement to the regular monitoring programs.

Five different lakes have been studied in this work; Lake Mjøsa, Tyrifjorden, Steinsfjorden, Lake Vansjø and Hemnessjøen. The performance of different atmospheric correction processors and in-water algorithms for three different satellite sensors were studied. The remote sensing reflectance, R_{rs}, shows expected results for the FUB and C2RCC atmospheric corrections on MERIS (FUB), Sentinel-2 (C2RCC) and Sentinel-3 (C2RCC) data, indicating good performance of the atmospheric correction. However, the spectra look different between the lakes and sometimes also between the stations within the same lake, which can be explained by natural variation in the water quality parameters, i.e. Chl-a, total suspended matter (TSM) and coloured dissolved organic matter (cDOM). Nevertheless, in situ reflectance measurements from lakes are necessary to validate these results as all products are derived from the satellite sensors. Data from MERIS, Sentinel-2 and Sentinel-3 showed general good results for Chl-a, TSM, Secchi disc depth (SSD) and Turbidity. Still, some results show that in situations with very low signal from the water, likely due to small amount of phytoplankton and/or particles and/or high concentration of humic substances, the atmospheric correction is failing, resulting in too high concentrations of Chl-a. To correct for situation with low signals, one can either remove the scenes, use another atmospheric correction, or try if a sensor with higher spectral resolution (e.g. OLCI on S-3) will perform better. Fine tuning of local algorithms or conversion factors can also be tested. The temporal variability for remote sensing Chl-a is, in general, following the in situ data, although there is a discrepancy between the timing of the observations. The turbidity data from S-2 does sometimes catch river plumes with particles from the melting season in the spring, which is not detected by the in situ monitoring. The monthly means are overall very coherent between remote sensing and in situ observations, although there were some differences between individual stations and months. The S-3 data gave reasonable results for both Chl-a and TSM.

A significant advantage with remote sensing data is the spatial resolution and coverage, which can be utilized when studying spatial patterns within the lakes and when assessing the water quality and classification levels accordance to the WFD for whole waterbodies. We show the results of Chl-a classification for the case studies where the assessment was based on all pixels within the whole water body instead of a single in situ data point. The results showed spatial patterns for Chl-a over the last three years in most of the lakes. The amount of data, in terms of days of observations, was also much higher for remote sensing data, especially if one can use S-2 and S-3 data simultaneously. By using remote sensing data together with in situ data, a much broader and more detailed information of the water quality of the lake between seasons and years can be provided. The spatial dynamics can be used to identify the most suitable sampling points or help in redesigning of the sampling network of the lakes.

The Copernicus Global Land Service and Lake Water quality product was investigated for Lake Mjøsa. These data are 10 day composites of the remote sensing reflectance, turbidity and the trophic state based on Chl-a. The seasonal average made it difficult to compare with the derived C2RCC product, which were based on one day observations. The turbidity product was out of range and was therefore omitted from the presentation of the results and not further investigated. Hence, the current Copernicus trophic state classification data cannot be used for implementation in the assessment for Norwegian WFD Chl-a assessment or reporting. The trophic index is general for all waters and the thresholds are not comparable with the specific ones used for Norwegian conditions, which we used for the classification within the WFD examples. However, based on those results, the atmospheric correction algorithm, Polymer, will be given more attention in later studies. The Polymer atmospheric correction has also shown good results from similar waters in other countries.

To be able to make the best use of the remote sensing data in an operational manner for monitoring, practices for remote sensing processing and technical solutions for the data flow is crucial and should be developed and implemented systematically. In order to move forward NIVA arranged an international workshop on remote sensing in lakes and marine waters in Oslo in September 2019. The workshop gathered remote sensing experts from several European countries, which all presented and shared their experiences on the subject. Based on these results, a road map for an operational service and suggestions for future research are included in the report. With this report we have taken a large step closer to an operational system for remote sensing data in combination with in situ data for lake water quality monitoring. Still, the results represent a limited number of lakes with restricted optical measurements and more specific data needs to be collected. The example with the conversion factor between apig at 443 nm and Chl-a (Figure 9, Table 7) shows a good example of the differences in the retrieved Chl-a concentration that an incorrect relationship can give. For the future, it is therefore necessary to use more time on the different optical conditions within the various lakes to determine the best remote sensing water quality products. The advantages with an operational remote sensing system for implementation within the WFD was clearly seen in the results for the water basin classification. The use of remote sensing data can cover lakes that are not frequently or currently sampled by the monitoring program. By using remote sensing data, the yearly variations as well as the long-term trends can be observed in a reliable and consistent manner and status classification can be done for the whole lake. Hence, special events years or divisions from the trend can be identified and used initiate more detailed studies. Since there are a 4 years cycles in the national Lake monitoring the remote sensing data can supplement the interannual year when in situ data are missing, especially in lakes where robust algorithms are established.

11 References

Aas, E., J. Høkedal, and K. Sørensen. 2014. "Secchi Depth in the Oslofjord–Skagerrak Area: Theory, Experiments and Relationships to Other Quantities." *Ocean Sci.* 10 (2): 177–99. https://doi.org/10.5194/os-10-177-2014.

Aas, E., K. Sørensen, B. Faafeng, and T. Lindell. 1993. *Fjernmåling Av Vannkvalitet - Videreutvikling Av Optisk Satelittfjernmåling Som Metode for Overvåking Av Vannkvalitet*. Norsk institutt for vannforskning. https://niva.brage.unit.no/niva-xmlui/handle/11250/207179.

Alikas, Krista, Kersti Kangro, Reiko Randoja, Petra Philipson, Elar Asuküll, Jan Pisek, and Anu Reinart. 2015. "Satellite-Based Products for Monitoring Optically Complex Inland Waters in Support of EU Water Framework Directive." *International Journal of Remote Sensing* 36 (17): 4446–68. https://doi.org/10.1080/01431161.2015.1083630.

Alikas, Krista, and Susanne Kratzer. 2017. "Improved Retrieval of Secchi Depth for Optically-Complex Waters Using Remote Sensing Data." *Ecological Indicators* 77 (June): 218–27. https://doi.org/10.1016/j.ecolind.2017.02.007.

Ansper, Ave, and Krista Alikas. 2019. "Retrieval of Chlorophyll a from Sentinel-2 MSI Data for the European Union Water Framework Directive Reporting Purposes." *Remote Sensing* 11 (1): 64. https://doi.org/10.3390/rs11010064.

Bouvet, M., Fisher, J. and Brockmann, C., 2008. Atmosphere and glint correction Algorithm, AGC ATBD, GKSS-KOF-AGC-ATBD01, 45 p.

Brockmann, Carsten, Roland Doerffer, Marco Peters, Kerstin Stelzer, Sabine Embacher, and Ana Ruescas. 2016. "Evolution of the C2RCC Neural Network for Sentinel 2 and 3 for the Retrieval of Ocean Colour Products in Normal and Extreme Optically Complex Waters." In *Proceedings of the ESA Living Planet*, 6. Prague, Czech Republic: ESA.

Doerffer, R. 2002. "Protocols for the Validation of MERIS Water Products." PO-TN-MEL-GS-0043. European Space Agency.

EUMETSAT. 2019. "Recommendations for Sentinel-3 OLCI Ocean Colour Product Validations in Comparison with in Situ Measurements – Matchup Protocols."

European Commission. 2019. "Copernicus In Brief | Copernicus." 2019.

Gjertsen, A. K. Trollvik, J. A. Ledang, A. B., Danielsen, J. and Larsen, R. 2014. Preparations for acquisition and application of optical satellite data for Norway Digital - Part 2. Report ANB-11-05. Norwegian Mapping Authority. March 2014. 130 p.https://www.copernicus.eu/en/about-copernicus/copernicus-brief.

Harvey, E. Therese, Dorte Krause-Jensen, Peter A. Stæhr, Geoffrey Brian Groom, and Lars B. Hansen. 2018. "Literature Review of Remote Sensing Technologies for Coastal Chlorophyll-a Observations and Vegetation Coverage: Part of ReSTEK-Brug Af Remote Sensing Teknologier Til Opgørelse Af Klorofyl-Koncentrationer Og Vegetationsudbredelse i Danske Kystvande." No. 112. Technical Report from DCE - Danish Centre for Environment and Energy. Aarhus University, DCE – Danish Centre for Environment and Energy,. http://dce2.au.dk/pub/TR112.pdf.

Harvey, Therese. 2015. "Bio-Optics, Satellite Remote Sensing and Baltic Sea Ecosystems: Applications for Monitoring and Management." Stockholm: Department of Ecology, Environment and Plant Sciences, Stockholm University.

Hieronymi, Martin, Dagmar Müller, and Roland Doerffer. 2017. "The OLCI Neural Network Swarm (ONNS): A Bio-Geo-Optical Algorithm for Open Ocean and Coastal Waters." *Frontiers in Marine Science* 4 (May). https://doi.org/10.3389/fmars.2017.00140.

Hollstein, A., Bismarck, von J., Fishcer, J., and Preusker, R., 2010. Description of the vector radiative transfer model MOMO

IOCCG. 2000. "Remote Sensing of Ocean Colour in Coastal, and Other Optically-Complex, Waters." IOCCG Report 3. Reports of the International Ocean-Color Coordinating Group. Dartmouth, Canada.

———. 2006. "Remote Sensing of Inherent Optical Properties: Fundamentals, Tests of Algorithms and Applications." IOCCG Report 5. Reports of the International Ocean-Color Coodinating Group. Dartmouth, Canada.

———. 2010. "Atmospheric Correction for Remotely-Sensed Ocean-Colour Products." IOCCG Report 10. Reports of the International Ocean-Colour Coordinating Group. Dartmouth, Canada.

Kangro, Kersti , Alikas K., Jemai A., and Kangro E. 2018. The relationship between phytoplankton absorption coefficient and chlorophyll-a concentration for remote sensing applications in optically complex waters. Poster, Ocean Optics Conference 2018.

Kirk, John T. O. 2011. *Light and Photosynthesis in Aquatic Ecosystems*. 3rd ed. Cambridge, UK, New York: Cambridge University Press.

Koponen, S, R. Ruiz-Verdu, Thomas Heege, Jörg Heblinski, Kai Sørensen, Kari Kallio, Timo Pyhälahti, Roland Doerffer, Carsten Brockmann, and Marco Peters. 2008. "Development of MERIS Lake Water Algorithms." Validation Report.

Magnusson, J., and K. Sørensen. 1993. *Overvåking Av Hvaler, Singlefjorden Og Ringdalsfjorden 1990-91. Hydrografi, Hydrokjemi, Tungmetaller i Vann Og Fjernanalyse*. Norsk institutt for vannforskning. https://niva.brage.unit.no/niva-xmlui/handle/11250/207331.

Matthews, Mark William. 2011. "A Current Review of Empirical Procedures of Remote Sensing in Inland and Near-Coastal Transitional Waters." *International Journal of Remote Sensing* 32 (21): 6855–99. https://doi.org/10.1080/01431161.2010.512947.

Mobley, Curtis D. 1989. "A Numerical Model for the Computation of Radiance Distributions in Natural Waters with Wind-Roughened Surfaces." *Limnology and Oceanography* 34 (8): 1473–83. https://doi.org/10.4319/lo.1989.34.8.1473.

Moses, W. J., A. A. Gitelson, S. Berdnikov, and V. Povazhnyy. 2009. "Estimation of Chlorophyll-Aconcentration in Case II Waters Using MODIS and MERIS Data—Successes and Challenges." *Environmental Research Letters* 4 (4): 045005. https://doi.org/10.1088/1748-9326/4/4/045005.

Okullo, Willy, Taddeo Ssenyonga, Børge Hamre, Øyvind Frette, K. Sørensen, Jakob J. Stamnes, Andreas Steigen, and Knut Stamnes. 2007. "Parameterization of the Inherent Optical Properties of Murchison Bay, Lake Victoria." *Applied Optics* 46 (36): 8553–61. https://doi.org/10.1364/AO.46.008553.

Pereira-Sandoval, Marcela, Ana Ruescas, Patricia Urrego, Antonio Ruiz-Verdú, Jesús Delegido, Carolina Tenjo, Xavier Soria-Perpinyà, Eduardo Vicente, Juan Soria, and José Moreno. 2019. "Evaluation of Atmospheric Correction Algorithms over Spanish Inland Waters for Sentinel-2 Multi Spectral Imagery Data." *Remote Sensing* 11 (12): 1469. https://doi.org/10.3390/rs11121469.

Röttgers, Rüdiger, David McKee, and Sławomir B. Woźniak. 2013. "Evaluation of Scatter Corrections for Ac-9 Absorption Measurements in Coastal Waters." *Methods in Oceanography*, Special Issue: Advances in Ocean Optical Observing, 7 (September): 21–39. https://doi.org/10.1016/j.mio.2013.11.001.

Ruddick, Kevin G., Kenneth Voss, Emmanuel Boss, Alexandre Castagna, Robert Frouin, Alex Gilerson, Martin Hieronymi, et al. 2019. "A Review of Protocols for Fiducial Reference Measurements of Water-Leaving Radiance for Validation of Satellite Remote-Sensing Data over Water." *Remote Sensing* 11 (19): 2198. https://doi.org/10.3390/rs11192198.

Sørensen, K., E. Aas, and J. Høkedal. 2007. "Validation of MERIS Water Products and Bio-optical Relationships in the Skagerrak." *International Journal of Remote Sensing* 28 (3–4): 555–68. https://doi.org/10.1080/01431160600815566.

Sørensen, K., and T. Lindell. 1990a. *Eutrofisituasjonen i Ytre Oslofjord. Delprosjekt 3.7a: Optiske Observasjoner - Overflatevannets Kvalitet Sett Ut Fra Observasjoner i Overflatelaget Og Fjernmåling*. Norsk institutt for vannforskning. https://niva.brage.unit.no/niva-xmlui/handle/11250/205783.

Sørensen, K., J. Nilsen, H. V. Sæbø, and E. Holbæk-Hansen. 1990b. *Satelittfjernmåling Av Vannkvalitet. Testing Av Landsat-5 Thematic Mapper for Kartlegging Av Glomma- Og Iddefjordvannets Spredning i Hvaler Og Ytre Oslofjord*. Norsk institutt for vannforskning. https://niva.brage.unit.no/niva-xmlui/handle/11250/205978.

Sørensen, Kai, Are Folkestad, Kerstin Stelzer, Carsten Brockmann, and Roland Doerffer. 2008. "Validation of MERIS Products in the Skagerrak." In *Proc. of the 2nd MERIS/(A) ATSR User Workshop*. http://earth.esa.int/ers/pub/ESA_DOC/meris_workshop_2008/papers%20/o15_sore.pdf.

Sørensen, Kai, Are Folkestad, Kerstin Stelzer, Carsten Brockmann, Roland Doerffer, Willy Okullo, and Leon Schouten. 2008. "Performance of MERIS Products in Lake Victoria." In , 6.

Steinmetz, François, Pierre-Yves Deschamps, and Didier Ramon. 2011. "Atmospheric Correction in Presence of Sun Glint: Application to MERIS." *Optics Express* 19 (10): 9783–9800. https://doi.org/10.1364/OE.19.009783.

Sullivan, James M., Michael S. Twardowski, J. Ronald V. Zaneveld, Casey M. Moore, Andrew H. Barnard, Percy L. Donaghay, and Bruce Rhoades. 2006. "Hyperspectral Temperature and Salt Dependencies of Absorption by Water and Heavy Water in the 400-750 Nm Spectral Range." *Applied Optics* 45 (21): 5294–5309.

Uudeberg, Kristi, Ilmar Ansko, Getter Põru, Ave Ansper, and Anu Reinart. 2019. “Using Optical Water Types to Monitor Changes in Optically Complex Inland and Coastal Waters.” *Remote Sensing* 11 (19): 2297. https://doi.org/10.3390/rs11192297.

Vanhellemont, Q., Ruddick, K. 2018. Atmospheric correction of metre-scale optical satellite data for inland and coastal water applications. Remote Sens. Environ. (https://doi.org/10.1016/j.rse.2018.07.015)

Vanhellemont, Quinten. 2019. “Adaptation of the Dark Spectrum Fitting Atmospheric Correction for Aquatic Applications of the Landsat and Sentinel-2 Archives.” *Remote Sensing of Environment*. http://agris.fao.org/agris-search/search.do?recordID=US201900181511.

Vannforskriften. 2018. “-Veileder 02:2018. Klassifisering Av Miljøtilstand i Vann; Økologisk Og Kjemisk Klassifiseringssystem for Kystvann, Grunnvann, Innsjøer Og Elver.” Veileder 02:2018. http://www.vannportalen.no/globalassets/nasjonalt/dokumenter/veiledere-direktoratsgruppa/Klassifisering-av-miljotilstand-i-vann-02-2018.pdf.

Zhang, Yuchao, Ronghua Ma, Hongtao Duan, Steven Loiselle, and Jinduo Xu. 2014. “A Spectral Decomposition Algorithm for Estimating Chlorophyll-a Concentrations in Lake Taihu, China.” *Remote Sensing* 6 (6): 5090–5106. https://doi.org/10.3390/rs6065090.

Appendix A

A.1 Apparent optical properties, AOPs

The reflectance and the light interactions with water are not only dependent on its constituents but also on both the incoming and outgoing light path. The variables describing the light conditions within the water are called apparent optical properties (AOP´s) and depend both on the medium (e.g. water and the constituents) as well as the light field within, i.e. the angular distribution and the ambient light field (Kirk 2011). Those are e.g. irradiance, radiance and reflectance. AOPs are detectable variations in reflectance at the sea surface (Harvey 2015; IOCCG 2000), and thus affect the reflectance detected by the sensor and are used for algorithm development.

Reflectance (R) is wavelength dependent and defined at any depth as;

$$R(\lambda, z) = E_u(\lambda,z)/E_d(\lambda,z) \quad \text{Eq. 3}$$

where $E_u(\lambda,z)$ is the upwelling irradiance (flux per unit surface area) in all directions at wavelength λ and depth z. The upwelling irradiance is a measure of all light that leaves the sea surface. $E_d(\lambda,z)$ is the downwelling irradiance at the same wavelength and depth as for $E_u(\lambda,z)$. In remote sensing, *remote sensing reflectance (R_{rs})* is used which is closely related to the sea surface reflectance (IOCCG 2000) (Figure 48).

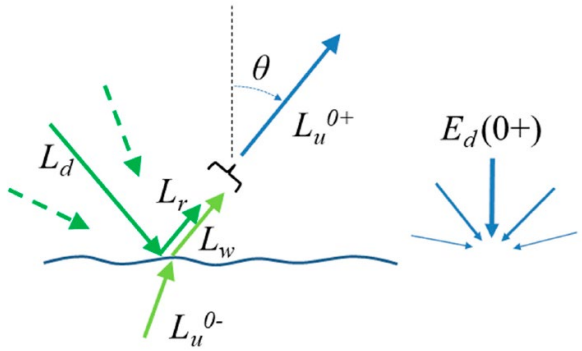

Figure 48. An illustration of water leaving radiance L_w and the downwelling irradiance E_d. The illustration show that the L_w is the above-water directional upwelling radiance (L0+u) after the removal of radiance (L_r) from the air-sea interface reflection called sky-glint and/or sun-glint (reflection from wave facets). The width of the $E_d(0+)$ arrows represent the weighting for the different angles. Figure from Ruddick et al. (2019).

However, R_{rs} makes use of the radiance (L_w) rather than the downwelling irradiance (E_u) and is defined as

$$R_{rs}(\theta,\phi,\lambda) = L_w(\theta,\phi,\lambda)/E_d(\lambda,0+) \quad \text{Eq. 4}$$

where $L_w(\theta,\phi,\lambda)$ is defined as water-leaving radiance (Ruddick et al. 2019) and Ed(λ,0+) as above-water irradiance. A remote detector with a narrow field of view does not receive all the water leaving irradiance since the shape of the detector and its viewing geometry limit the signal to a small fraction of this flux (IOCCG 2000). The description of the light field must include how fluxes varies a function of direction. The radiance provide this description and it measures flux per unit area and per unit solid angle. Remote sensing reflectance has dimensions of sr^{-1} (steradianer). The R_{rs} decomposes the reflectance into its component radiances of the viewing nadir angle θ (viewing angle downward from vertical axis) and viewing azimuth angle ϕ (viewing direction clockwise from north). The angel against the sun and the time of the day affects how much light that is reflected through the surface (for details see e.g. Ruddick et al. (2019).

Another apparent optical property is the diffuse attenuation coefficient for downwelling irradiance, k_d (IOOCG, 2000). This property defines the rate of decrease of downwelling irradiance with depth. The

K_d is often used as an index based on the diffuse attenuation at 490nm (K_d490) on the clarity of the water and is strongly related to the Secchi disc depth (Kirk 2011; Aas al. 2014).

$$dE_d(\lambda,z)/E_d(\lambda,z) = -K_d(\lambda)dz \qquad \text{Eq. 5}$$

A.2 Inherent optical properties, IOPs

Inherent optical properties are not dependent on any variation of the angular distribution of the incident light field but are determined by the of type of substances and the concentrations of these in the water (IOCCG 2006). The IOPs are defined by the three main optical components divided into phytoplankton pigments (dominated by Chl-a), the total suspended inorganic material and organic suspended materials coming from resuspension or river run-off, the colored part of the dissolved organic matter (cDOM) originating from the decomposition of both terrestrial and marine organic matter (Harvey et al. 2018 and references thein). The absorption and scattering of light are wavelength dependent, and therefore the composition and concentration of these substances will affect the light in the water column differently (Harvey 2015 and references thein).

The light absorption is dependent on the components in the water and the *total absorption coefficient* a(λ) is defined as the sum of the absorption coefficients of the different components present in the water, including the absorption coefficient of water itself:

$$a(\lambda) = a_w(\lambda) + a_{ph}(\lambda) + a_d(\lambda) + a_{cDOM}(\lambda) \qquad \text{(Kirk 2011)} \qquad \text{Eq. 6}$$

Where $a_w(\lambda)$ is the absorption coefficient for clear water, $a_{ph}(\lambda)$ is the absorption coefficient for photosynthetic pigments, $a_d(\lambda)$ is the absorption coefficient for detrital and suspended material (TSM) and $a_{cDOM}(\lambda)$ is the absorption coefficient for cDOM. For the photosynthetic pigments there are in addition to Chl-a also Chl-b, Chl-c, Carotenoids, Biliproteins (Cyanobacteria pigments), Phycoerythrin and Phycocyanin (Figure 49) which all can modify the reflectance in lakes particular. Chl-a will only be a proxy for these.

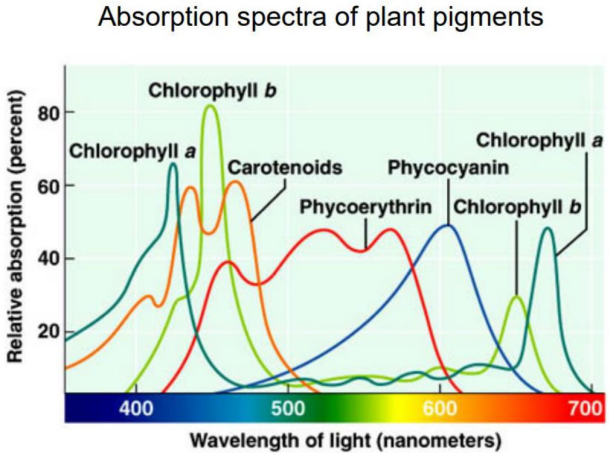

Figure 49. Relative absorption of Chl-a, Chl-b, Chl-c, Carotenoids, Biliproteins (Cyanobacteria pigments), Phycoerythrin and Phycocyanin. Adapted from Brockman (2019, Appendix G) and Stramski (IOCCG course 2018).

Absorption (*a*) removes photons from the light field, while scattering (scattering coefficient *b*) changes the direction and increases the path length of the photons (IOCCG 2000, Harvey 2015 and references there in). Scattering can be divided into elastic scattering where the scattered photon has the same wavelength as the incident photon and into elastic scattering which implies a change in the wavelength

of the scattered photon. The scattering by water molecules are wavelength dependent and scattering occurs across all angles. Sea water scatter around 30% more than pure water due to the salts (Kirk 2011). The absorption and scattering are illustrated in the bio-optical model in Figure 50a and Figure 50b below. As seen in Figure 50a, the difference in the absorption spectra are clearly seen, with the low absorption of water in the lower range of the visible light spectra, the typical Chl-a spectra with two peaks and the high absorption in the blue by cDOM.

Scatter is divided into forward scattering, b_f and backward scattering, b_b and the volume scattering function is the sum of those in all angels;

$$b = b_f + b_b \quad \text{Eq. 7}$$

Attenuation c is describing the loss of light due to absorption and scattering. Attenuation and absorption are both main optical variables that can be measured in situ.

$$c = a + b \quad \text{Eq. 8}$$

a)

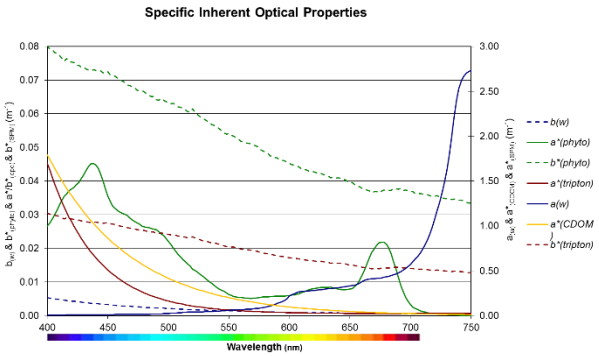

b)

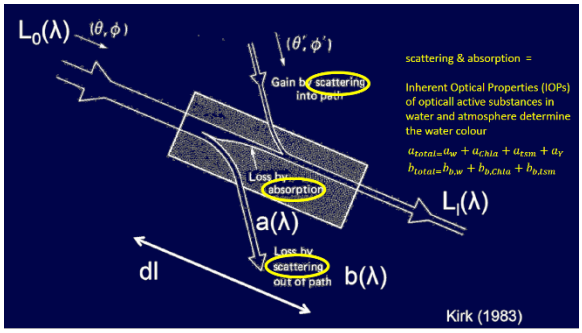

Figure 50. a) Graph showing the different spectra for absorption and scattering for the different bio-optical components in the visible wavelengths. The lines on the right y-axis represents the absorption per optical component and the dashed lines on the left y-axis corresponds to the scattering. a(w), a*(phyto), a(tripton) and a(cDOM) are the absorption of water, specific absorption of phytoplankton, tripton and cDOM and b(w), b*(phyto) and b*tripton) are the backscatter of water, specific backscatter of phytoplankton and tripton, (i.e. TSM). The graph is based on a simulation in BI-OPTI (Hoogenboom, 1996) for (Harvey 2015). b) Figure from Brockman (2019) illustrating how scattering and absorption affects a light beam entering and leaving a water body, e.g. the light from the sun and the remote sensing reflectance.

Appendix B Atmospheric correction

The effects from the atmosphere and the ocean surface needs to be removed from the signals measured by the satellite sensor at various spectral bands (IOCCG 2010). Therefore, atmospheric correction (AC) is performed when quantifying ocean properties by satellite remote sensing. From the ocean-atmosphere system, the top of the atmosphere (TOA) radiance $L_t(\lambda)$ can be divided linearly into the sum of distinct physical contributions:

$$L_t(\lambda) = L_r(\lambda) + L_a(\lambda) + L_{ra}(\lambda) + t(\lambda)L_{wc}(\lambda) + T(\lambda)L_g(\lambda) + t(\lambda)t_0(\lambda)\cos\theta_0[L_w(\lambda)]_N \quad \text{Eq. 9}$$

The important thing to note from this equation in this context is that the TOA ($L_t(\lambda)$, is made up by 1) an atmospheric part; scattering by air molecules $L_r(\lambda)$ (also Rayleigh scattering), scattering by aerosols $L_a(\lambda)$ and the interaction between them, $L_{ra}(\lambda)$; 2) white caps on the sea surface ($L_{wc}(\lambda)$) and the specular reflection of direct sunlight from the sea surface, called sun glitter ($L_g(\lambda)$); 3) the water signal, which is the normalized water leaving radiance (backscattered photons that has penetrated the sea surface), $[L_w(\lambda)]_N$. The two terms $t_0(\lambda)$ and $t(\lambda)$ are the diffuse transmittances of the atmosphere from the sun to the surface and from the surface to the sensor and $T(\lambda)$ is the direct transmittance from the water surface to the sensor. The determination of the radiance's origination from Rayleigh scattering is easily handled and can be accounted for. The other part originating from aerosols as much more challenging to estimate as both the distribution and the optical properties are variable and unknown when processing an ocean colour scene. Thus, the TOA atmospheric path radiance, is defined as:

$$L_{path}(\lambda) = L_r(\lambda) + L_a(\lambda) + L_{ra}(\lambda) \quad \text{Eq. 10}$$

The main challenge for AC is to remove L_{path} from L_t, which is the AC carried out by several types of algorithms (se Chp. 3 for). Applying an AC is the first step to retrieve a correct remote sensing reflectance that can be used to derive and distinguish between the water quality parameters and IOPs. For waters where the signal is only affected by water and Chl-a, it is easier to filter out the atmospheric signal than for waters containing other optical parameters as well. With increased complexity the signal-to-noise ratio increases and makes it more difficult to resolve the AC. For clear oceanic waters it is about 10% of the TOA reflectance that is carrying the water information whereas it is a little as less than 1% in optical complex waters with high cDOM (IOCCG 2000; 2010).

B.1 Free University Berlin/WeW Water Processor

The FUB processor consists of different algorithms and one is for the atmospheric correction of MERIS data, presented in this study from Mjøsa and Hemnessjøen. The algorithm makes use of MERIS Level 1 TOA radiances (i.e. the 'raw' data input to the sensor), and by using these bands the water-leaving reflectance and Case 2 water properties along with aerosol optical thickness (AOT) bands are retrieved. The retrieval procedure of the processor is based on four separate artificial neural networks (NN). These neural networks are trained based on the results from radiative transfer simulations (Hollstein et al., 2010).

B.2 Case 2 Regional CoastColour

The Case 2 Regional CoastColor (C2RCC) algorithm are developed for all three sensors presented in this study (MERIS, S-2 and S-3), but in this work the C2RCC processor is run on the S-2 and S-3 data. C2RCC consists of three different algorithms which deal with atmospheric corrected reflectance and water quality constituents (Brockmann et al., 2016). The atmospheric correction is based on a large database of radiative transfers simulations of water-leaving radiances as well as TOA radiances. The disadvantage is that a full bio-optical model for the water must be included, but the advantage is that

the extrapolation from the NIR bands is avoided. For the bio-optical model, two NNs is used, a forward (forwNN) and a backward (invNN). The input is water-leaving radiance reflectance from 8 bands which are outputs from the AC above. IOPs such as total scattering of particles bp (TSM), the absorption coefficient of phytoplankton pigments (a_pig), and the absorption of dissolved organic matter a_gelb (cDOM) are derived at 443 nm. An inverse model is used to get an estimate of the concentrations by R_{rs} and geometry data.

B.3 Acolite (S-2)

Acolite is a processor for atmospheric correction developed for Landsat-8 (L-8) and S-2 data. Acolite use the "dark spectrum fitting" by default which is used in this study. Acolite can be configured to use "exponential extrapolation" as briefly mentioned in Ch.3.2 . More details on this processor can be found in Vanhellemont et al. (2018) and Vanhellemont (2019).

B.4 Polymer (S-3)

For the Copernicus lake quality products, Polymer is the processor for the AC. This processor is developed to handle sun glint specifically. The processor uses a spectral matching method based in polynomial to model the spectral reflectance of the atmosphere and sun glint, a water reflectance model and it use all available spectral bands in the visible. More details on this processor can be found in Steinmetzet al. (2011).

B.5 OC-Smart (S-2 and S-3)

Although, not tested within this project the OC-SMART algorithm can be applied for lakes as well (Marty et al. 2018, 2019). It is applicable in both open ocean and coastal/inland waters and is based on comprehensive radiative transfer simulations and multilayer neural network (MLNN) methods. The MLNN AC algorithm is a spectral matching method that exploits the spectral similarity between Rayleigh corrected TOA radiances (Lrc) and water-leaving radiances (Lw). The algorithm uses a well-trained MLNN to retrieve the normalized remote sensing reflectance (nRrs = nLw=E0+d) directly from Lrc without estimating aerosol information. The keys to the success of the algorithm include:

- an extensive and accurate radiative transfer simulations using a coupled atmosphere-ocean RT model, AccuRT, that accurately accounts for multiple scattering and BRDF effects between the atmosphere and ocean.
- Multiple flexible water and aerosol IOP models are used in the RT simulations to create a comprehensive global dataset that is representative of most marine and aerosol conditions.
- Realistic input parameter distributions for the aerosol and water IOP models are obtained by analysing level-3 global ocean colour products derived from current ocean colour sensors data.

OC-SMART has been developed with a special emphasis on Norwegian waters retrievals. Its development has been co-funded by the Norwegian Space Agency, and NIVA has validated the algorithm performances in Norwegian marine water with data from the NorSOOP ship of opportunity program (Marty et al 2018, 2019).

Appendix C

C.1 Spectral signature with MERIS and S-2 data from Hemnessjøen and Mjøsa

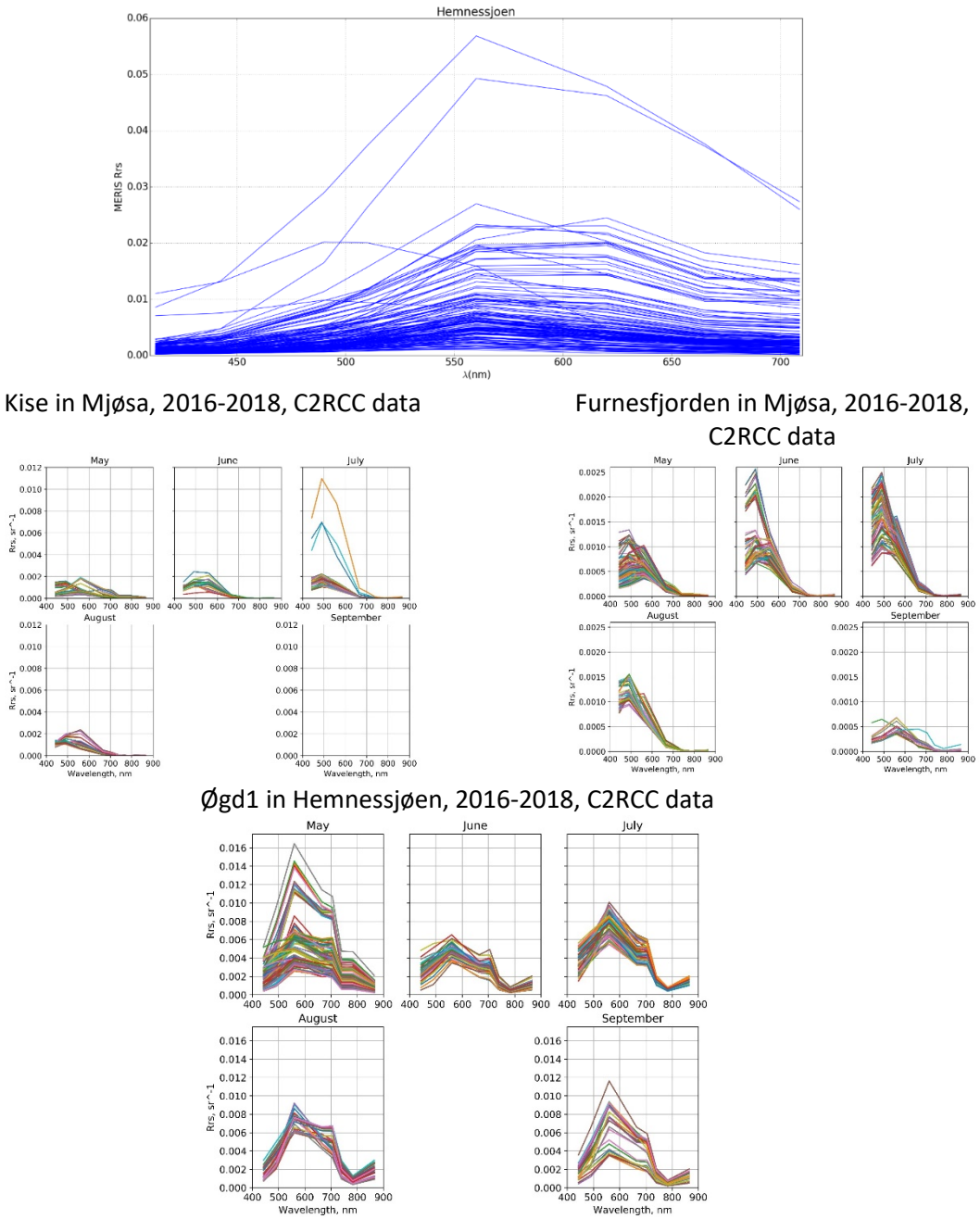

Figure 51. Remote sensing reflectance (R_{rs}). Top: FUB processed MERIS for Øgd1 in Hemnessjøen from 2002 to 2012. Middle and bottom: C2RCC processed S-2-data. Middle: Station Kise and Furnesfjorden in Mjøsa. Bottom: Station Øgd1 in Hemnessjøen. All data are clear sky scenes from 2016 to 2018.

Appendix D

D.2 Time series with MERIS and S-2 data from Mjøsa, Tyrifjorden and Vansjø

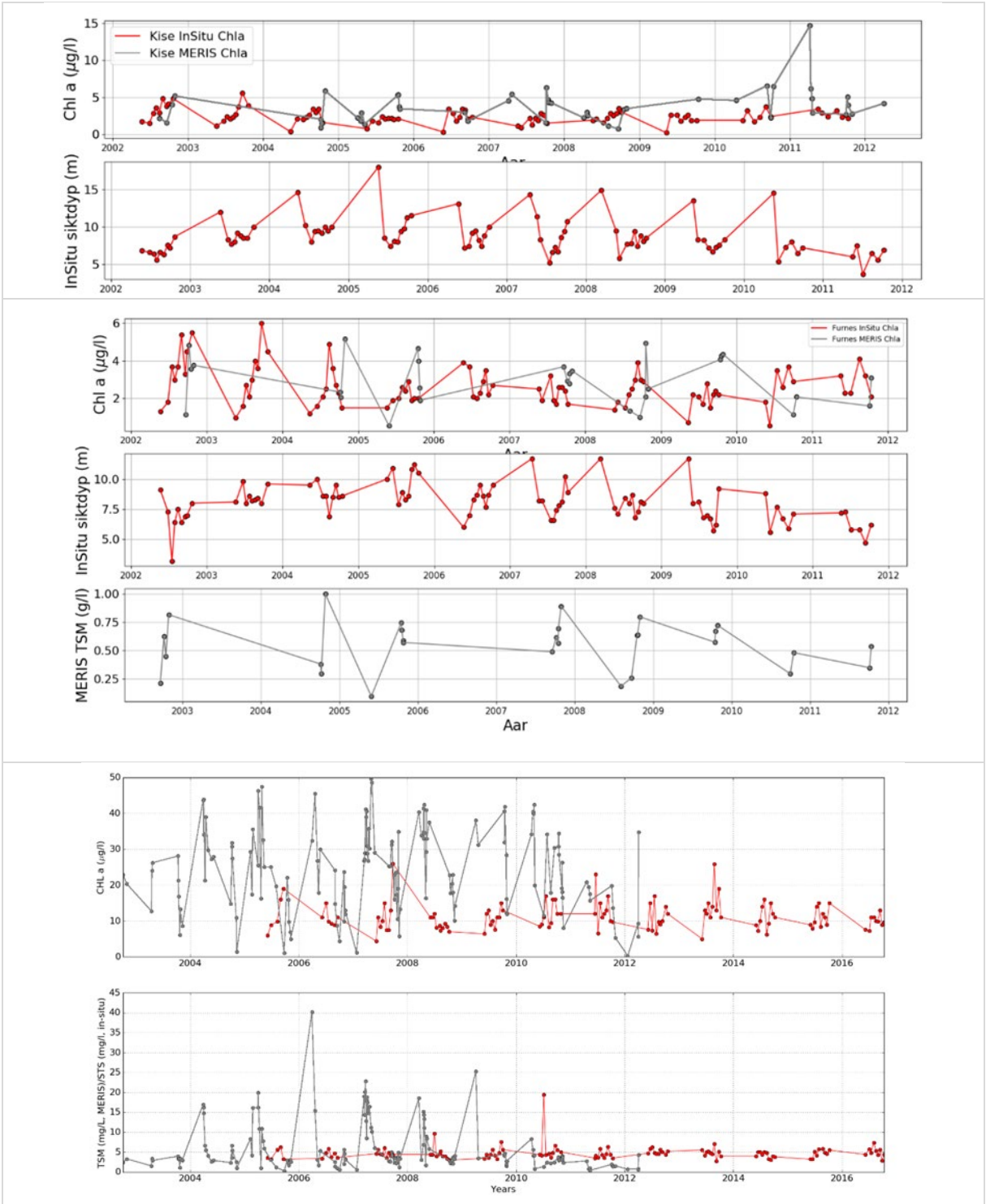

Figure 52. Remote sensing observations and in situ data from MERIS data. Top: Kise in Mjøsa, middle: Furnesfjorden in Mjøsa, bottom: Øgd1 in Hemnessjøen.

Data presented in Figure 53 show that Oc2_443, Oc2_490 and Oc3 using the C2RCC R_{rs} with coefficient from literature do not correspond very well with the in situ data. This is valid for all three lakes presented, and for all the stations within. The coefficients are not regional adapted.

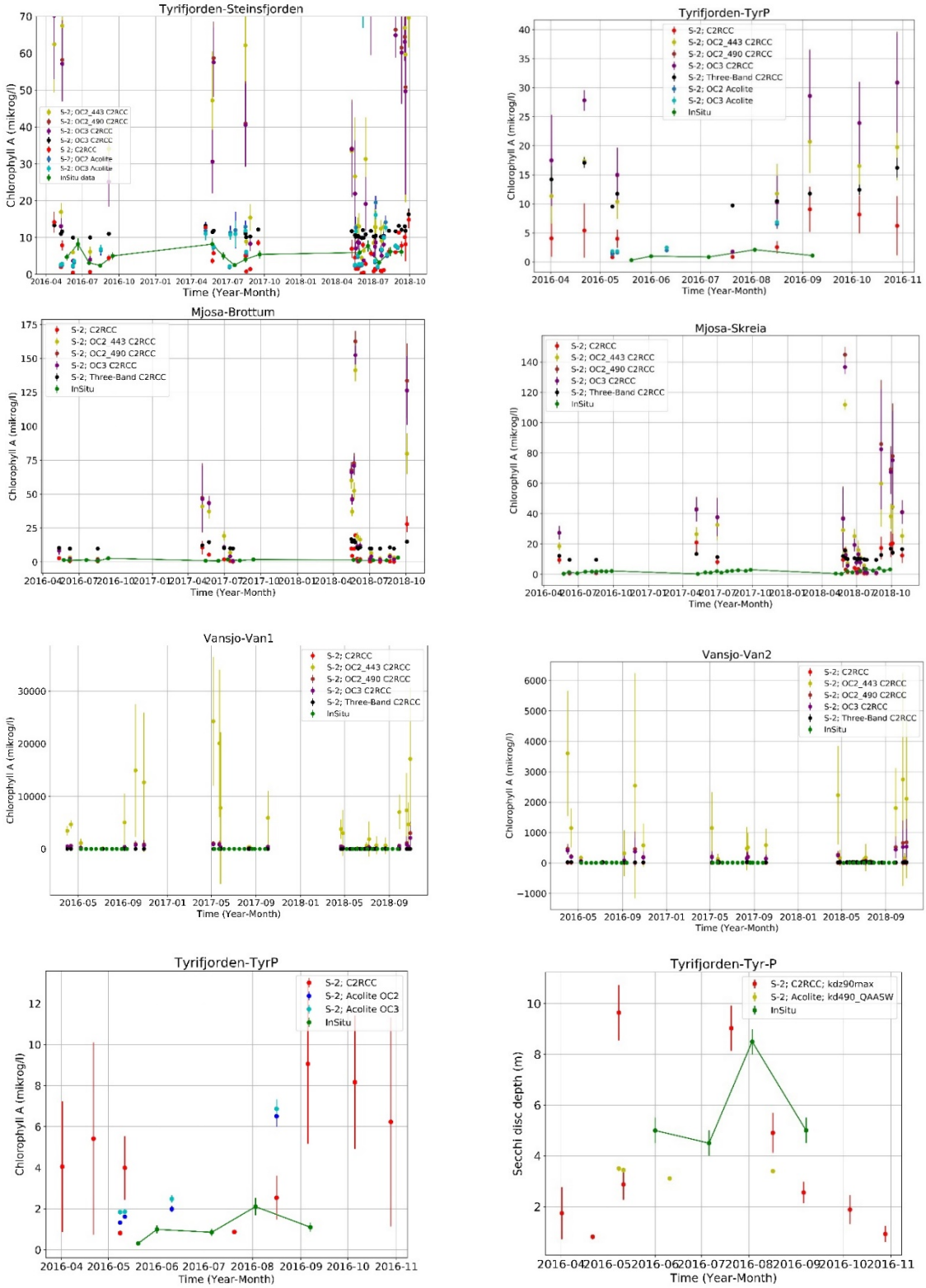

Figure 53. Time series with a comparison of algorithms for developing Chl-a products shown for stations with in situ data from 2016 to 2018. Top: Tyrifjorden, 2nd top: Mjøsa, 2nd bottom: Vansjø. Bottom: Time series of C2RCC processed S-2 data of Chl-a and Secchi disc depth from 2016, both from Tyr-P in Tyrifjorden.

Appendix E

E.1 Seasonal analysis from Mjøsa and Hemnessjøen

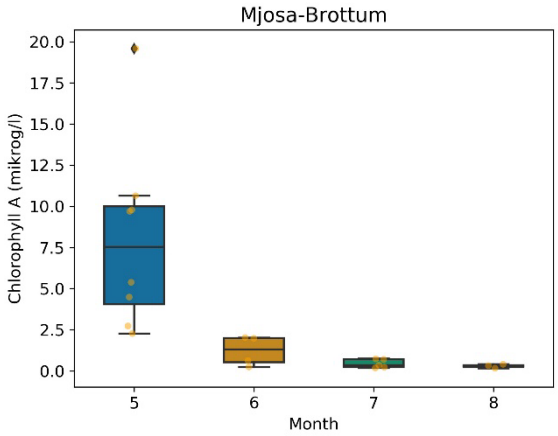

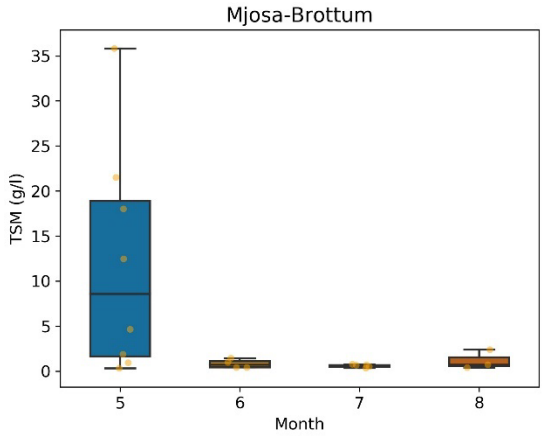

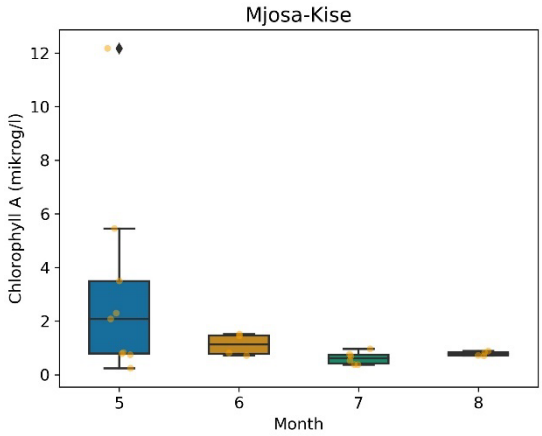

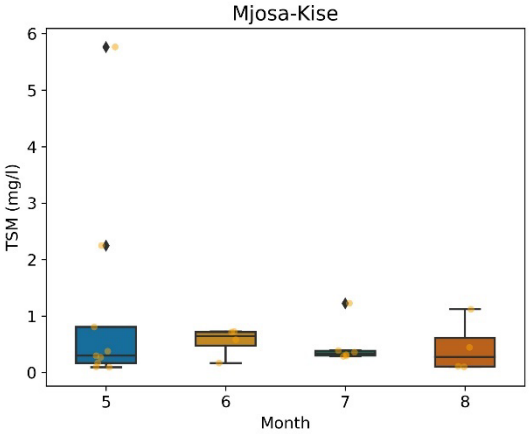

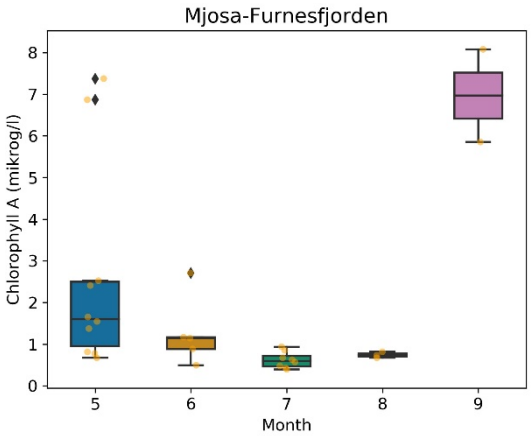

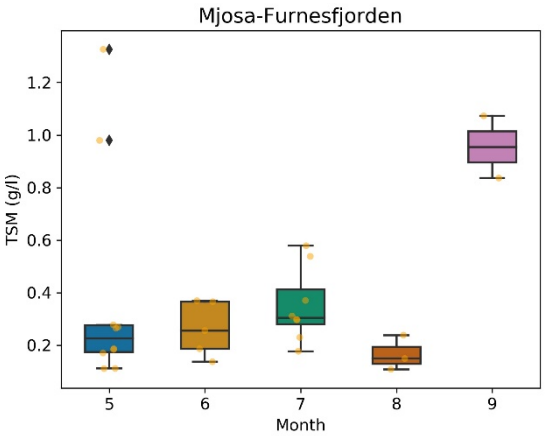

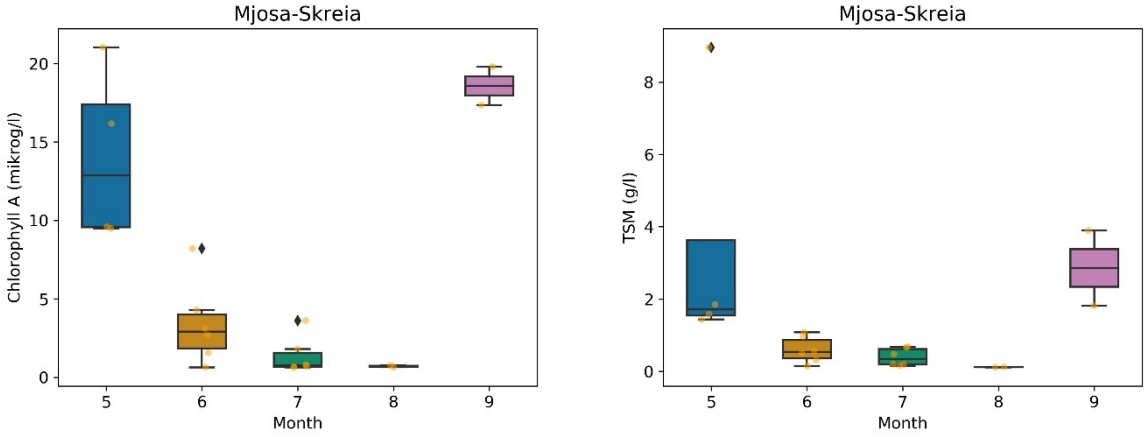

Figure 54. Remote sensing monthly Chl-a and TSM shown as boxplots. The boxes represent the 25th percentile (Q1). 50th percentile (median. Q2) and the 75th percentile (Q3) of the dataset. The outermost bar represents the "minimum" (Q1-1.5*interquartile range (IQR). lower bar) and the maximum (Q3+1.5*IQR. upper bar). The orange dots represent the remote sensing observations. The black diamond is defined as an outlier.

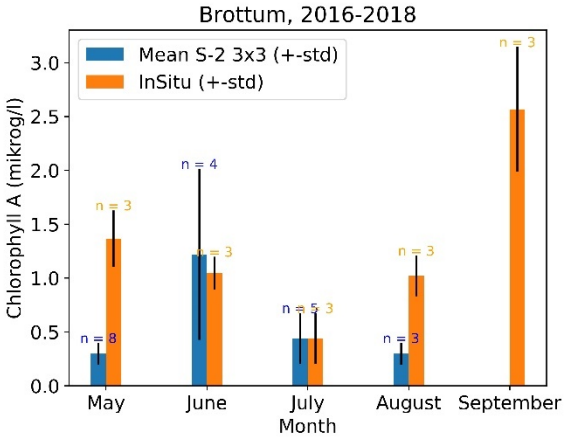

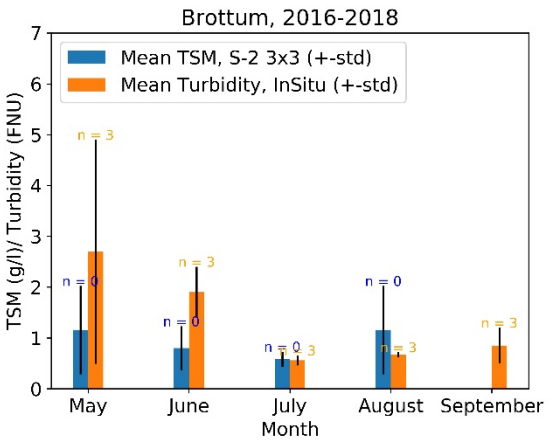

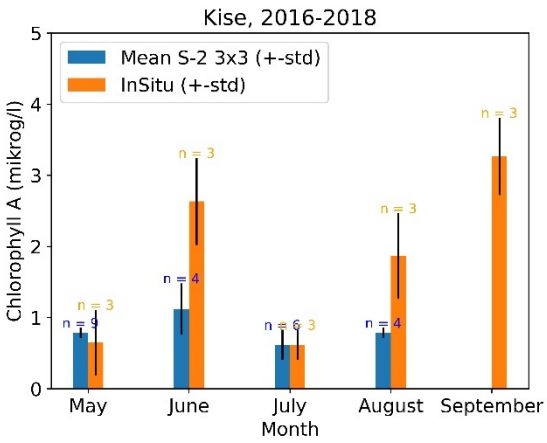

No turbidity data from Kise these years

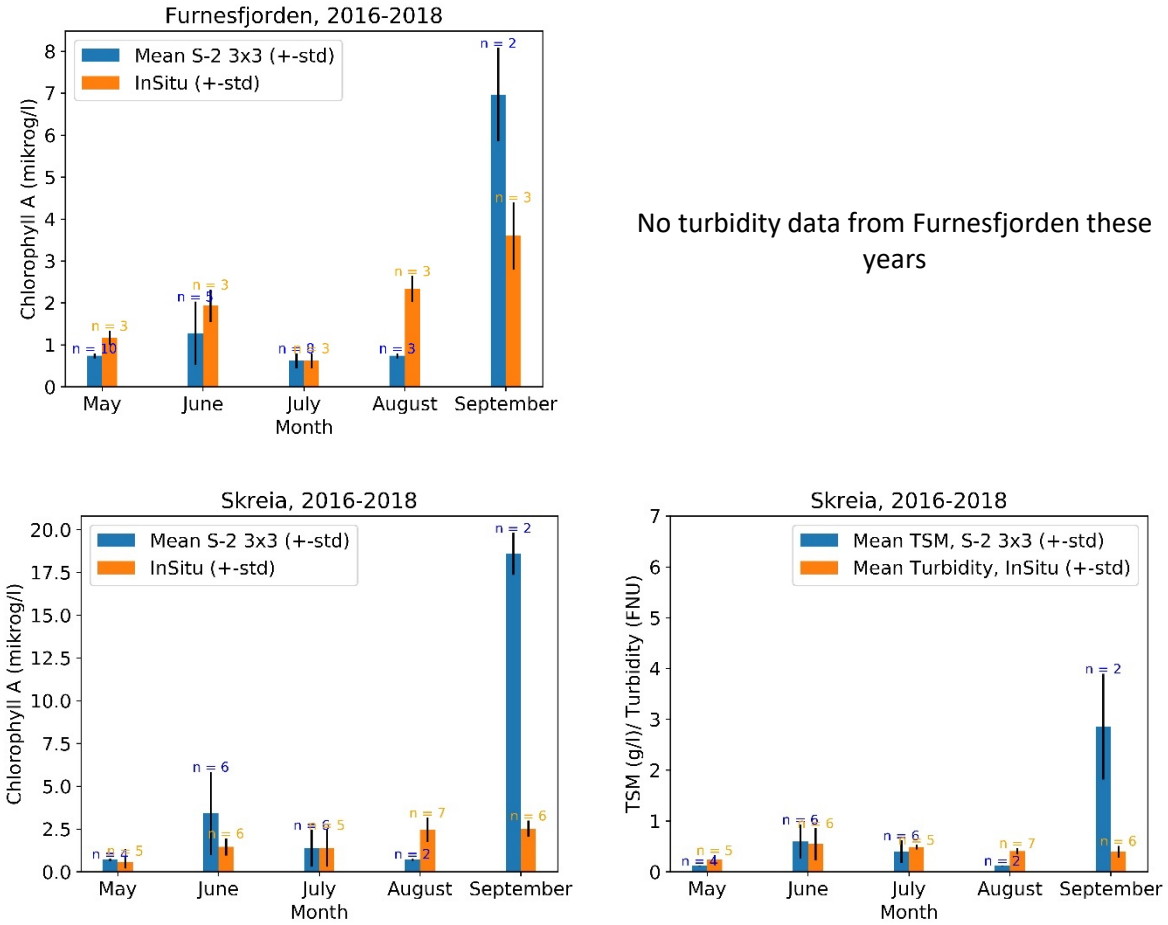

Figure 55. Monthly averages with standard deviation bars for remote sensing Chl-a and TSM data and in situ Chl-a and turbidity data. The remote sensing observations are CR2CC processed S-2 data.

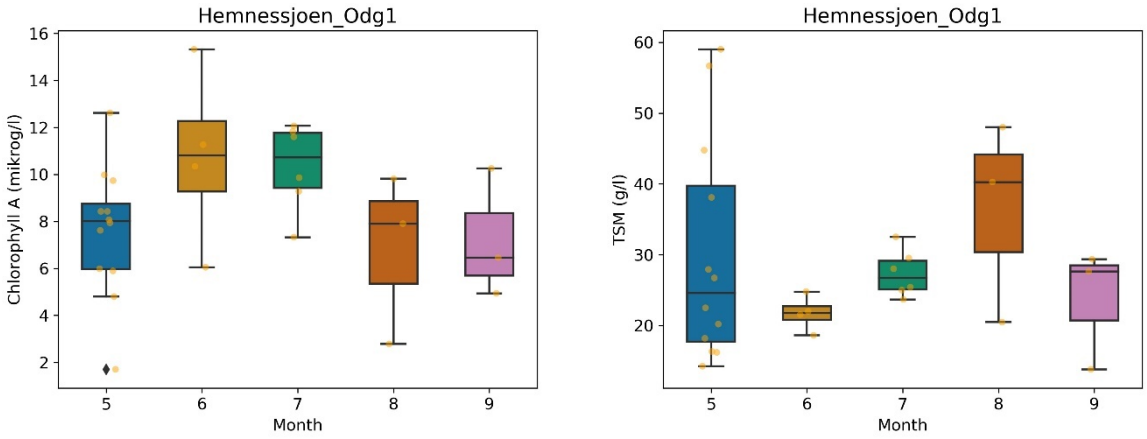

Figure 56. remote sensing monthly Chl-a and TSM shown as boxplots. The boxes represent the 25th percentile (Q1). 50th percentile (median. Q2) and the 75th percentile (Q3) of the dataset. The outermost bar represents the "minimum" (Q1-1.5*interquartile range (IQR). lower bar) and the maximum (Q3+1.5*IQR. upper bar). The orange dots represent the remote sensing observations. The black diamond is defined as an outlier.

Appendix F

F.1 Chl-a WFD status classification from Hemnessjøen

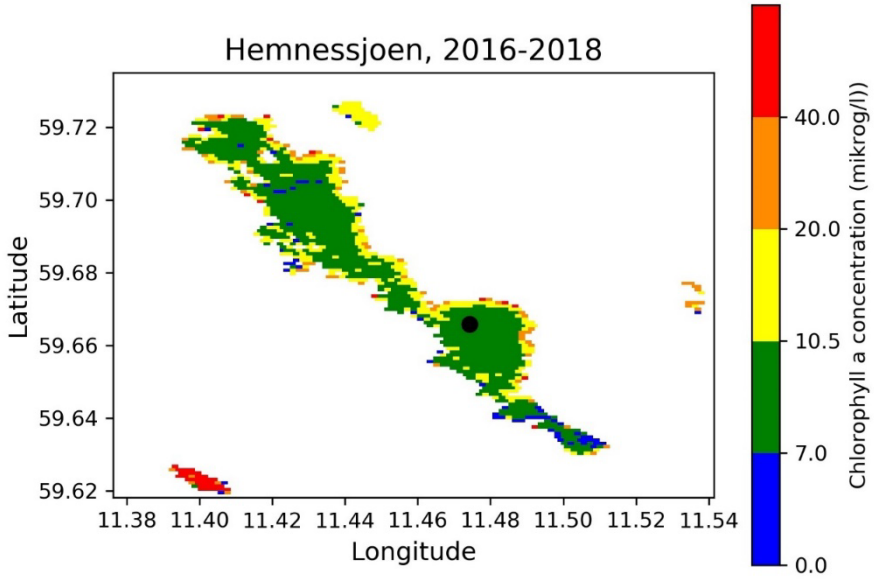

Figure 57. Classification per pixel for Hemnessjøen based on scenes from 2016 to 2018 for water type L108/L-N8. The station point used in as monitoring station is marked as black circle point.

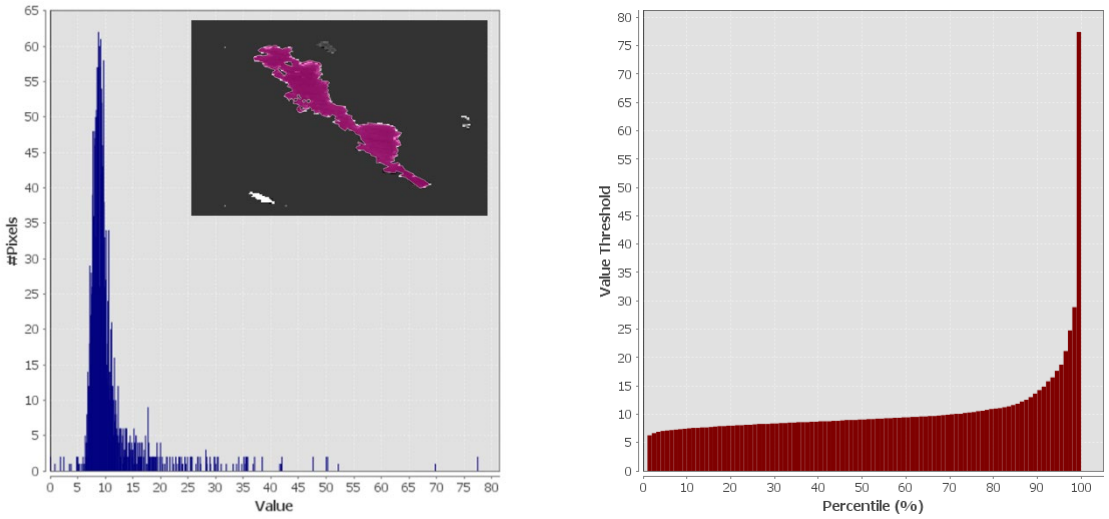

Figure 58. The mean Chl-a concentration distribution over the pixels and the percentile distribution of the pixels with value threshold of the mean Chl-a concentration in Hemnessjøen (shown as pink polygon).

Table 13. The mean Chl-a concentration distribution over the pixels and the percentile distribution of the pixels with value threshold of the mean Chl-a concentration in Steinsfjorden.

Number of considered pixels:	**2395**
Minimum:	0.001
Maximum:	77.4
Mean:	10.5
Sigma:	5.5
P10 treshold:	7.5
P25 tresholds:	8.2
P50 treshold:	9.1
P75 threshold:	10.4
P90 threshold:	14.3

Appendix G

Thursday 5th of September

09:00-09:05	In meeting room VIA at Oslo Science Park
09:05-09:10	Welcome, introduction and general information Kai Sørensen/Anna Birgitta Ledang, Norwegian Institute for Water Research (NIVA)
09:15-09:30	General background for the Workshop Steinar Sandøy/Agnes Moquet-Stenback Norwegian Environment Agency (NEA)
09:35-09:55	Optical remote sensing of water bodies Carsten Brockman, Brockmann Consult GmbH
10:00-10:20	Belgian experience with remote sensing: Marine water quality monitoring. Dimitry Van Der Zande, Royal Belgian Institute of Natural Sciences (RBINS)
10:25-10:45	Use of remote sensing for monitoring WFD water bodies in Finland Jenni Attila, Finnish Environmental Institue (SYKE)
10:50-11:15	Coffee break
11:20-11:40	Remote sensing for monitoring lakes and coastal waters in Sweden Petra Philipson, Brockman Geomatics Sweden AB
11:45-12:05	Remote sensing of inland waters for monitoring and reporting in Germany Carsten Brockman, Brockmann Consult GmbH
12:10-12:30	Norwegian examples from ongoing work using remote sensing in lakes Therese Harvey, Norwegian Institute for Water Research (NIVA)
12:35-12:55	Estonian experience on remote sensing applications for water quality Kristi Uudeberg, Tarty Observatory
13:00-14:00	Lunch
14:05-14:25	Experience from Flemish and Irish water monitoring with remote sensing Els Knaeps, VITO
14:30-14:50	DCS4COP Dimitry Van Der Zande, RBINS
14:55-15:15	Tentative presentation
15:20-17:00	Time for disposition
Starts at: 17:30/18:00	Workshop dinner Tapas with drinks served at the Top center at Oslo Science Park

Friday 6th of September

09:00-10:00	*Demonstration from Jenni Attila and Els Knaeps, in VIA*
10:00-10:45	Discussion: Future with remote sensing in water quality products. *Some questions we would like to have input/answers on* • What steps next would you suggest for NEA do for implementing an operational remote sensing system? • How can remote sensing fulfill/add important missing information to monitoring? • How can we make the development continuous and not project dependent? • What requirements do you see as essential for succeeding? • Other suggestions?
10:45-11:00	Coffee break
11.00-11:30	Wrap up, joint discussion
11:30-12:30	End of workshop with lunch

	Name	Institute
1	Carsten Brockmann	Brockman Consult
2	Dimitry Van Der Zande	RBINS
3	Petra Philipson	Brockman Geomatics
4	Jenni Attila	SYKE
5	Therese Harvey	NIVA-Denmark
6	Sabine Marty	NIVA
7	Kai Sørensen	NIVA
8	Anne Lyche Solheim	NIVA
9	Steinar Sandøy	Norwegian Environment Agency (NEA)
10	Agnes Moquet-Stenback	Norwegian Environment Agency (NEA)
11	Gunnar Skotte	Norwegian Environment Agency (NEA)
12	Solveig Havstad Winsvold	Norwegian Space Centre
13	Kristi Uudeberg	Tartu Observatory Tartu University
14	Anna Birgitta Ledang	NIVA
15	Els Knaeps	VITO
16	Kristoffer Kalbekken	NIVA
17	Ulrika Stensdotter Blomberg	Havs- och vattenmyndigheten i Sverige
18	Zofia Rudjord	NIVA
19	Jens Vedal	NIVA
20	Kasper Hancke	NIVA
21	Harry Simmons	NIVA
22	Johannes Grødem	NIVA
23	Francois Clayer	NIVA
24	Jan Karud	NIVA
25	Isabel Seifert-Dähnn	NIVA
26	Ailbhe Lisette Macken	NIVA
27	Øystein Rudjord	Norwegian Computing Center

NIVA: Norway's leading centre of competence in aquatic environments

NIVA provides government, business and the public with a basis for preferred water management through its contracted research, reports and development work. A characteristic of NIVA is its broad scope of professional disciplines and extensive contact network in Norway and abroad. Our solid professionalism, interdisciplinary working methods and holistic approach are key elements that make us an excellent advisor for government and society.

NIVA
Norwegian Institute for Water Research

Gaustadalléen 21 • NO-0349 Oslo, Norway
Telephone: +47 22 18 51 00 • Fax: 22 18 52 00
www.niva.no • post@niva.no